POLITECNICO DI TORINO

Master Degree Thesis

Simulation and modeling of Racetrack memories with VCMA synchronization

Supervisors
prof. Marco Vacca
prof. Maurizio Zamboni
Ph.D. Fabrizio Riente

Candidates
Pietro Diona
matricola: 274426

Anno accademico 2020-2021

Summary

This master thesis will concern the study and the application of the Voltage Controlled Magnetic Anisotropy (VCMA) effect on Racetrack Memory. The VCMA allows to locally modify the anisotropy of the material through an electric potential. This variation can be used to create potential barriers, or potential holes to favor the nucleation of the domains and to synchronize the movement of the bits, stored in form of domains, along the Racetrack. In the specific case of a Racetrack, being able to control the potential barrier through VCMA would allow to reduce the currents involved for the movement of the Domain Walls. This technique is an alternative to the creation of notches, which experimentally could be more difficult to realize. This thesis focuses on the study and physical modeling of the VCMA effect applied to Racetrack technology through the use of micromagnetic simulations and analytical models that describe the phenomenon. The aim of the study is to evaluate the benefits of the application of this phenomenon to Racetrack memories, and both the timing and the energetic performance of the resulting device.

Acknowledgement

At the end of this exciting experience, it is my duty to extend a great thanks to all the staff who validly and with great professionalism supported and guided me, in particular:

- Prof. Marco Vacca;
- Ph.D. Fabrizio Riente;
- Ph.D. Luca Gnoli;
- Prof. Maurizio Zamboni;

who I will remember for everything they taught me and allowed me to apply in this thesis. I cannot miss a thank you to my family who, as always, supported me even during these last final months of my master's career.
Finally, I have to thank the Eng. Leonardo Carpinteri, who six years ago introduced me to the world of physics. Thanks to him I developed the right passion and ability to face the entire university path, which in addition allowed me to develop a certain aptitude for physics and mathematical analysis.

Contents

Chapter 1

Introduction

Matter behaves in different ways when it interacts with an external magnetic field. The physics of magnetism is the branch of physics which explains magnetic phenomena, investigates the magnetic properties of matter and the interactions related to it. To describe magnetism within matter, it is fundamental to introduce the concept of magnetization or also called magnetic polarization. When an electric current passes through a coil it behaves like a magnetic dipole. In a semi-classical model, assuming a planetary model of the atom, electrons within matter orbit around the atomic nucleus generating a magnetic field just like that of a coil. Each electron therefore constitutes a microscopic coil which in the absence of external electromagnetic fields is randomly oriented. The presence of a local magnetic field involves a collective polarization of the coils. Therefore the concept of magnetic moment is born [1], and it can be conceptually represented as shown in Figure 1.1. The modulus of a magnetic moment is expressed by equation 1.1.

$$\mu = iS \tag{1.1}$$

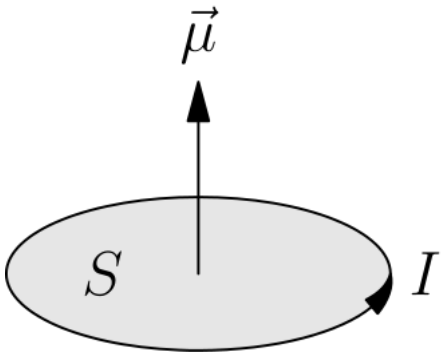

Figure 1.1: Concept of magnetic moment [2]

The microscopic magnetization currents can be traced back to a macroscopic quantity, in order to comprehensively describe the magnetic behavior of a material thanks to the magnetization intensity vector, also called magnetic polarization vector and denoted by $\vec{M}$. The magnetization intensity vector is defined as the average value of the proper magnetic moment of N particles contained in an infinitesimal volume dV [3]:

$$\vec{M} = \frac{\sum_{i=1}^{dN} \vec{\mu_i}}{dV} \tag{1.2}$$

The unit of measure of the magnetization vector is $\frac{A}{m}$.
Once the concept of magnetization is known, it is possible to classify the magnetic behavior of matter in the following way:

- Diamagnetism: property of matter which when subjected to the presence of an external magnetic field exhibits an internal magnetization, which has the opposite direction with respect to the external field;
- Paramagnetism: property of matter which when subjected to the presence of an external magnetic field exhibits an internal magnetization, which has the same direction of the external field;
- Ferromagnetism: property of matter which becomes magnetized under the action of an external magnetic field and which remains magnetized for a long time when the field is canceled out. This property is maintained only below a certain temperature, called the Curie temperature, above which the material behaves like a paramagnetic material;
- Antiferromagnetism: property of matter which is characterized by the

fact that it has an apparent neutral behavior under the action of an external magnetic field, at least up to a certain critical temperature, called Néel temperature, beyond which they exhibit a paramagnetic behavior;

- Ferrimagnetism: property of matter similar to antiferromagnetism with the difference that the antiparallel alignment of the atomic magnetic moments is not perfect and the external field is not canceled out, producing a behavior similar to that of ferromagnetism;

1.1 Ferromagnetism

As explained in the Introduction [1], the ferromagnetism is a property of matter which becomes magnetized under the action of an external magnetic field and which remains magnetized when the field is canceled out. A ferromagnetic material is characterized by an hysteresis loop as shown in Figure 1.2.

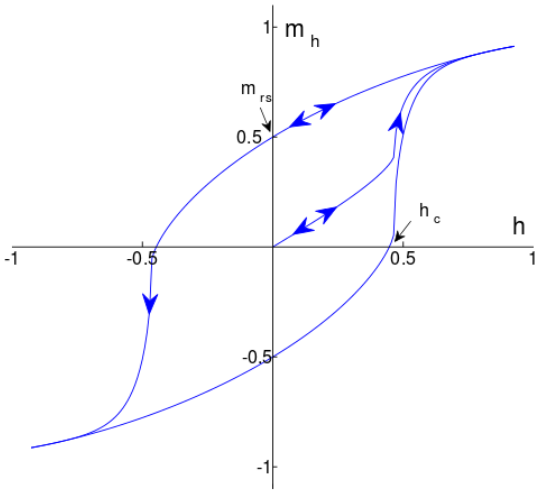

Figure 1.2: Magnetization $'m'$ against magnetic field $'h'$. Image extracted from [4].

The hysteresis loop shows how the magnetization is not equal to zero when the external magnetic field h is equal to zero.
In general, the magnetization varies (in direction, not in magnitude) across a magnet, but in sufficiently small magnets, it does not. Larger magnets are divided into regions called domains. Within each domain, the magnetization is constant; and between domains there are relatively thin domain walls

in which the direction of magnetization rotates from the direction of one domain to another. If the magnetic field changes, the walls move, changing the relative sizes of the domains. Because the domains are not magnetized in the same direction, the magnetic moment per unit volume is smaller than it would be in a single-domain magnet. The magnetization can also change by addition or subtraction of domains (called nucleation and denucleation respectively)[4]. The concept of domain wall, which is the main subject of this thesis, its physical description and its motion in ferromagnetic material will be studied in depth, starting from chapter 2.

1.2 Exchange interaction

The exchange interaction is a quantum mechanical effect that only occurs between identical particles. The effect is due to the wave function of indistinguishable particles being subjected to exchange symmetry, that is, either remaining unchanged (symmetric) or changing sign (antisymmetric) when two particles are exchanged. Both bosons and fermions can experience the exchange interaction. For fermions, this interaction is sometimes called Pauli repulsion and it is related to the Pauli exclusion principle. For bosons, the exchange interaction takes the form of an effective attraction that causes identical particles to be found closer together, as in Bose–Einstein condensation. The exchange interaction alters the expectation value of the distance when the wave functions of two or more indistinguishable particles overlap. This interaction increases (for fermions) or decreases (for bosons) the expectation value of the distance between identical particles (compared to distinguishable particles) [5]. The physical explanation which distinguishes a paramegnetic material from a ferromagnetic one is closely related to the physical concept of exchange interaction[6]:

- Paramagnetic material: The direct exchange interaction between the electron spins is smaller with respect to the thermal energy of the electrons involved. As a consequence the electron spins are not aligned and the magnetization is canceled out when the external magnetic field is switched off;
- Ferromagnetic material: The exchange interaction in ferromagnets is greater with respect to the thermal energy, therefore the magnetization is retained when the external magnetic field is switched off;

An analytical discussion of the magnetic field due to the exchange interaction

will be carried out in section 2.7.2.

1.3 Antisymmetric exchange: Dzyaloshinskii–Moriya interaction (DMI)

Antisymmetric exchange, also known as the Dzyaloshinskii–Moriya interaction (DMI), is a contribution to the total magnetic exchange interaction between two neighboring magnetic spins. Some antiferromagnetic materials exhibit a non-zero magnetic moment at a temperature near absolute zero. This effect is called spin canting, a phenomenon through which spins are tilted by a small angle about their axis rather than being exactly co-parallel. In magnetically ordered systems, DMI favors a spin canting of otherwise (anti)parallel aligned magnetic moments and thus, is a source of weak ferromagnetic behavior in an antiferromagnetic material [7]. DMI only exists in noncentrosymmetric systems. The most general equation of the modulus of the magnetic field due to DMI effect is the following:

$$H_{i,j}^{DMI} = \vec{D}_{i,j} \cdot (\vec{S}_i \times \vec{S}_j) \tag{1.3}$$

An analytical discussion will be carried out in section 2.8.

1.4 Magnetocrystalline anisotropy

A ferromagnetic material is characterized by magnetocrystalline anisotropy which is a phenomenon through which the ferromagnetic material itself takes more energy to magnetize it in certain directions than in others. These directions are usually related to the principal axes of its crystal lattice. The spin-orbit interaction is the primary source of magnetocrystalline anisotropy. Basically the orbital motion of the electrons, which couple with crystal electric field, gives rise to the first order contribution to magnetocrystalline anisotropy. The second order arises due to the mutual interaction of the magnetic dipoles [8]. Each crystal is characterized by a certain structural symmetry. Based on the crystalline structure of a material, the term of magnetocrystalline anisotropy changes. The most common magnetocrystalline anisotropies are the following:

- Uniaxial anisotropy: the crystal is characterized by a single axis of high symmetry, the energy density in this simplest and most common case is

expressed by the following formula:

$$\epsilon = \frac{E}{V} = K_u sin^2(\theta) \tag{1.4}$$

where K_u has units of energy density and depends on composition and temperature (it is a material constant), and θ is the angle in spherical coordinate shown in Figure 2.1a;

- Cubic anisotropy: the magnetocrystalline anisotropy energy density is described by a second order equation;

For more detail look at [8]. An analytical discussion of the uniaxial anisotropy energy will be carried out in section 2.7.3

1.5 Demagnetizing Energy

When a ferromagnetic material is placed in an external magnetic field, it develops a strong internal magnetization, therefore it behaves like a magnet. The edges of the ferromagnetic material become like north and south poles, and as a consequence a demagnetizing field is generated[9]. The demagnetization field physically arises because the internal magnetic field of the ferromagnetic material linked to the magnetization of the matter and the external field in which the ferromagnetic material is immersed must connect to the boundaries of the material itself. In other words, the magnetic field by definition must be a continuous physical quantity, therefore discontinuities cannot arise between the field inside the ferromagnet and the external field. The demagnetization field therefore arises spontaneously to create this condition of continuity:

$$\vec{H}_{int} = \vec{H}_{ext} + \vec{H}_d = \vec{H}_{ext} - \bar{N} \cdot \vec{M} \tag{1.5}$$

The demagnetizing field is expressed as the product between a tensor $\bar{N}$ which is strictly related to the geometrical structure of the ferromagnetic material, and the magnetization vector. The demagnetizing energy linked to the demagnetizing field is equal to:

$$E_{dem} = -\frac{1}{2}\mu_0 \vec{M} \cdot \vec{H}_{dem} V = -\frac{1}{2}\mu_0 \vec{M}(-\bar{N} \cdot \vec{M})V \tag{1.6}$$

where V is the volume of the sample. An analytical discussion of the demagnetizing will be carried out in section 2.7.4

1.6 Voltage Controlled Magnetic Anisotropy (VCMA)

The voltage controlled magnetic anisotropy is a physical phenomenon which consists in a correlation between a voltage applied to a magnetic material and its anisotropy. Assuming the uniaxial anisotropy property of a ferromagnetic plane explained in section 1.4, the ferromagnetic material is characterized by a certain anisotropy constant K_u. More exactly K_u is characterized by a volume anisotropy contribution and by a surface anisotropy contribution:

$$K_u = K_{vol} + \frac{K_i}{t_{FM}} \tag{1.7}$$

If the ferromagnetic layer is supposed to be extremely thin (like a plane), the volume anisotropy could be completely ignored, and the only contribution is related to the surface anisotropy. If a certain voltage is applied across a ferromagnetic material, it is possible to locally modify the anisotropy of the material which is characterized by a certain VCMA constant which correlates the applied voltage with the anisotropic variation of the material:

$$K_u = K_u(0) - \zeta_v \frac{V_{app}}{t_{ox}} \tag{1.8}$$

ζ_v is the VCMA constant, whose value depends on the ferromagnetic (FM) layer, while t_{ox} is the thickness of the oxide layer, which covers the FM layer. For a positive ζ_v value, when a positive voltage is applied, the interfacial anisotropy is lowered. For more details about Voltage Controlled Magnetic Anisotropy effect look at section 1.8.

1.7 Racetrack Memory

A Racetrack memory is a memory paradigm developed in 2008 by Stuart Parkin, with the aim of replacing Hard-Disk Drive and Solid State Drive [10][11][12]. The main idea upon which the concept of Racetrack Memory is based, is the domain wall motion induced by an applied current density. A Racetrack memory, simplistically, is nothing else than a "track" divided into a specific number of ferromagnetic domains, which can be moved along the track thanks to a certain current density or exploiting an external magnetic field. Each ferromagnetic domain works as a shift register which store '0' or '1' depending on the direction of the magnetization of the domain. Each

domain could be magnetized up or down in the case of "Perpendicular Magnetic Anisotropy" (PMA) of the layer, or it could be magnetized left or right in the case of "Parallel Magnetization" of the layer. The phenomenon related to the motion of a domain wall with a current density is called "Current Driver Domain Wall Motion" and microscopically it is related to an interaction between the electron spins of the layer and the current which applies a specific torque moment on the spins. The domains are shifted along the track with the aim of placing a specific domain in correspondence of the writing element or in correspondence of the reading element. Each domain has a specific address, therefore a specific current must be injected into the track to move a specific domain from its initial position to its final position. Different geometrical structures of the track or different dispositions of the domains along the track were proposed in the last years, but the three main elements are still the "track" with its ferromagnetic domains, the "writing component" through which it is possible to write '0' or '1' into a specific domain, and the "reading component" through which it is possible to read the stored bits[13]. Figure [1.3] shows the Racetrack memory idea in an abstract way. The blue and red zones are the domains of track and the two colors indicates the two different states of the magnetization ("0" and "1").

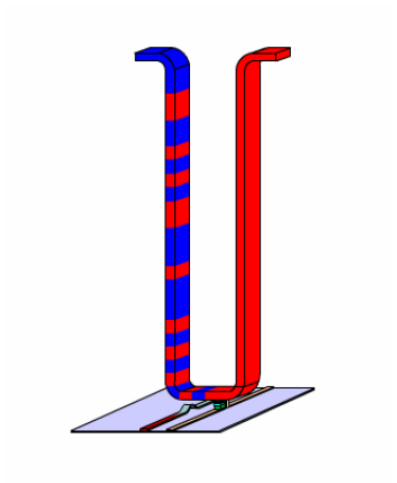

Figure 1.3: Racetrack Memory Idea[14]

The two elements in the lower part of the figure [1.3] are the reading element and the writing element. One of the methods that can be implemented to write a bit in a Racetrack memory is to exploit the fringing field of a domain wall. A domain wall naturally generates a magnetic field called

"fringing field". This magnetic field located just close to a specific domain of a Racetrack memory will switch the magnetization of the domain itself. There are some descriptive analytical models of the fringing field of a domain wall, for more information look at [15]. Concerning the writing element of a Racetrack memory, a good choice would be to read the magnetization of a domain using a magnetic tunnel junction (MTJ). For more details about MTJ structure look at section 1.7.2.

1.7.1 Division of the Racetrack in ferromagnetic domains

A Racetrack memory is "divided" into ferromagnetic domains, each one storing a bit information ('0' or '1'). Between two domains, there is a "wall" (a transition region) called domain wall, in which the magnetization gradually switches from "up" (or "right") state to "down" (or "left") state or viceversa. There are several methods to stably magnetize a specific region with a specific magnetization, and to create a stable domain wall in a specific site:

- Implementing different ferromagnetic domains;
- Using geometrical modification (notches); [16]
- Stepped nanowires for controlled pinning geometrical approach; [16]
- Local metal diffusion; [16]
- Ion implantation; [16]
- Tilted magnetization by exchange interaction; [16]
- Voltage Controlled Magnetic Anisotropy (VCMA) gate;

This thesis will concern the analysis of the VCMA gate approach. In other words periodical gates are put along the ferromagnetic track. When a voltage is applied across a gate the local anisotropy is modified and the domain wall could be blocked by the gate which behaves like a barrier when the anisotropy increases or like a hole when the anisotropy decreases. The concept is explained in more details in section 1.8.

1.7.2 Magnetic Tunnel Junction (MTJ)

Reading the magnetization of a specific domain of a ferromagnetic material (in other words reading a stored 'bit' in the track) is one of the three fundamental operation of a Racetrack memory. To accomplish this, a magnetic tunnel junction structure is exploited. The simplest model of a magnetic tunnel junction is made of three layer, two ferromagnetic layers and one insulating layer in the middle through which tunneling of electrons happens. The resistance of the structure depends on the relative orientation of the magnetization of the two ferromagnetic layers. The system is in high resistance state when the magnetizations of the two ferromagnetic layers are anti-parallel, while the system is in a low resistance state when the magnetizations are parallel as shown in Figure 1.4.

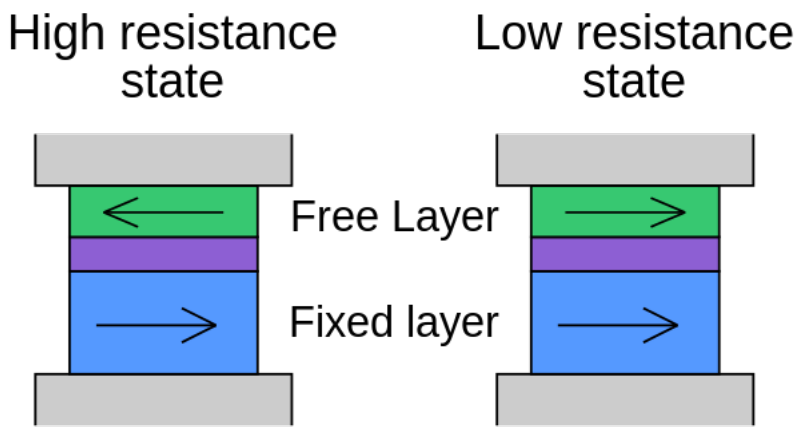

Figure 1.4: Picture of a Magnetic Tunnel Junction (MTJ)

Reading the resistance of the structure, composed by the ferromagnetic domain of the track, the insulating layer and the ferromagnetic layer of the substrate, it is possible to establish if a specific domain of the track "stores" a '0' or a '1'. Electrons tunnel through the insulating barrier from the fixed layer to the free layer or viceversa depending on the direction of the current. Three basic methods were formulated to describe the tunneling phenomenon in a magnetic tunnel junction:

- Free electron model;
- Julliere's model;

- Slonczewski's model;

Free electron model

Starting from the Schrodinger equation, it is possible to develop a basic model which describes the probability of electron tunneling through a potential barrier, and therefore the electric current of the structure related to the tunneling probability. From the electron current, it is simple to derive an expression of the conductance of the potential barrier, which explains how the resistance of the MTJ structure changes switching from the anti-parallel configuration to the parallel configuration. The final conductance formula evaluated with the free electron model is:

$$G = \frac{|e|I}{(E_{FL} - E_{FR})} = \frac{2e^2 M}{h} \int_{k_{//}} \frac{16 k_1^2 k_B^2 e^{2k_B l}}{[k_B(k_1 + k_2)(1 + e^{-2k_B l})]^2 + [(k_B^2 - k_1 k_2)(1 - e^{-2k_B l})]^2} dk_{//} \tag{1.9}$$

In the Appendix, section Free electron tunneling model, there is the complete demonstration of the conductance formula.

Julliere's model

In 1975 M. Julliere, with a phenomenological approach creates a basic model for the description of the conductance in a MTJ structure [17]. The model is based on the following assumptions [18]:

- The tunneling probability is proportional to the product of the Fermi energy density of states in the electrodes on either side of the barrier;
- Relates conductance change to spin polarization ratio of the magnetic layers;
- Tunneling conductance is independent from the tunneling junctions (therefore it is not a good model for amorphous barrier);
- Electrons that tunnel from the pinned layer to the free layer (or viceversa) are supposed to conserve their spin, so no spin-flip happens during tunneling through the oxide barrier;

For more details related to the mathematical expression of the Tunnel Magneto Resistance evaluated by Julliere, look at the Appendix, section Julliere's model.

Slonczewski's model

The model developed by Slonczewski was born as an extension of the Julliere's model which is the most basic model to analyze and describe tunneling phenomenon in MTJ and conductance state in MTJ. Slonczewski combines the simple free electron model, and the Julliere approach, understanding the imperfection of the Julliere's approach[19]. The model is based on the following main hyphothesis:

- Evaluate free electron model at the Γ point ($k_{||} = 0$);
- Free electron model in the limit of "thick" tunnel junctions;
- Tunneling conductance in Slonczewski's models depends on junction;

For more details look at the Appendix, section Slonczewski's model.

1.8 Voltage Controlled Magnetic Anisotropy (VCMA)

The main objectives related to the realization of a Racetrack memory are the control of the current which goes through the ferromagnetic layer and which "moves" the domains, and the power consumption involved during all the processes. Some strategies could be theoretically adopted to optimize the motion of the domain walls, for instance creating a gradient of anisotropy as shown in the article published by the department of Wuhan [20]. This section is dedicated to the analysis of the Voltage Controlled Magnetic Anisotropy effect. Practically the idea is to cover the ferromagnetic layer subdivided in different domains, with an oxide layer upon which a metallic layer is deposited in specific zones. In other words there will be some areas characterized by a metallic gate upon the ferromagnetic layer, through which it is possible to apply a specific voltage across the layers. The anisotropy constant of the ferromagnetic layer itself will change. The anisotropy constant $K_u = K_{vol} + \frac{K_i}{t_{FM}}$ is characterized by a volume contribution and a surface contribution, but since the ferromagnetic layer is extremely thin, the volume anisotropy could be completely ignored as explained in section 1.6. K_i varies around its constant value, when a voltage across the ferromagnetic layer is applied: higher is the applied voltage, higher will be the variation of the interfacial anisotropy constant. When the anisotropy constant increases, the gate behaves like a barrier through which the domain wall could pass or not.

When the anisotropy constant decreases, the gate behaves like a hole, therefore the domain wall usually enters inside the "hole" and then it could go out from the hole, or it could remain inside it. The region of different anisotropy is crossed when a specific value of the current is applied.
It is possible to synchronize the motion of the domain wall through a specific design of the track: when a specific current goes through the ferromagnetic layer a specific voltage value across the memory could block the domain walls.

1.8.1 VCMA constant

In this section, the most common values of the VCMA constant ζ_v are reported. In general, ζ_v could vary from few dozens of $\frac{fJ}{Vm}$, until few hundreds of $\frac{fJ}{Vm}$. A strong dependence of ζ_v from the temperature annealing of the structure is shown in figure 1.5, and figure 1.6. Temperature annealing is an important parameter that must be underlined to study the compatibility of magnetic memories with CMOS processes. For instance the low-k dielectrics used between interconnects in CMOS back-end-of-line processes, requires a thermal budget over $400°C$, and a MTJ structure made of $Ta/CoFeB/MgO$ shows an unstable PMA and TMR with a temperature annealing of $400°C$ making it incompatible with CMOS processes. Therefore more materials, more structures must be investigated to obtain a stable system, with good properties, high ζ_v, and great compatibility with CMOS processes [21].

Mo/CoFeB/MgO

$Mo/CoFeB/MgO$ structure shows discrete VCMA coefficient value and general properties with an annealing temperature of more than $400°C$, therefore good compatibility with CMOS processes. The thickness of Mo layer and of MgO layer are equal to 5 nm. ζ_v constant and K_i interfacial anisotropy constant of a $Mo/CoFeB/MgO$ structure show a dependence from the temperature annealing, while they are nearly independent from the thickness of the ferromagnetic layer of CoFeB. The following graph shows how ζ_v and K_i varies with CoFeB thickness [21]:

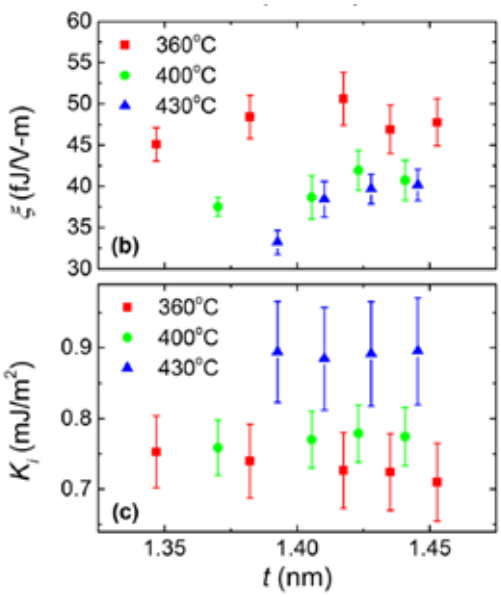

Figure 1.5: ζ_v and K_i in function of CoFeB thickness [21]

Averaging over CoFeB thickness values and expressing ζ_v and K_i in function of the temperature annealing:

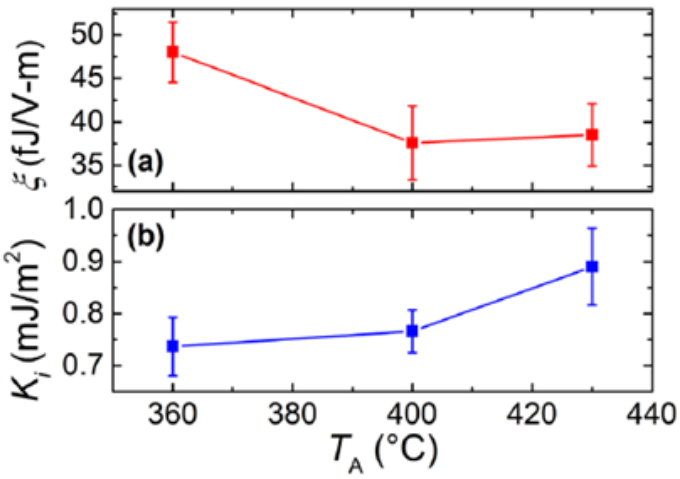

Figure 1.6: ζ_v and K_i in function of annealing temperature [21]

The graph shows that ζ_v value is equal to $40\frac{fJ}{Vm}$ when the annealing temperature is higher than $400°C$. Changing Mo with W, the structure $W/CoFeB/MgO$ shows a ζ_v value of $40 - 50\frac{fJ}{Vm}$ more or less similar to Mo structure.

Volatility and Non-Volatility Depending on the nature of the underlayer (UL) the VCMA behaviour will change between a volatile and a non-volatile behaviour. With an Underlayer (UL) of Ta or Pt, the structure exhibits a non volatile behaviour of VCMA, while with W the structure is characterized by a volatile VCMA[22]. The objective is to realize a volatile VCMA behaviour in a Racetrack, in this way when the voltage is turned off the interfacial anisotropy is recovered to the original one.

Double Oxide Structure

A strategy to improve the VCMA coefficient ζ_v is to realize a double oxide structure consisting of two oxides deposited on the ferromagnetic layer.
An example is $HM(2)/CoFeB(1.2)/MgO(2)/Ta(1)/SiO_2(63)$ where HM stays for heavy metal, the number in parenthesis indicates the thickness of the layer, and where Ta layer is a separator layer deposited between the two oxide [23]. Double oxide structure improves VCMA coefficient, but the trade-off is that the structure is thicker with respect to the structure described in the previous section. ζ_v values are:

- ζ_v for $Ta(2)/CoFeB(1.2)/MgO(2)/Ta(1)/SiO_2(63)$ is $163\frac{fJ}{Vm}$;
- ζ_v for $Hf(2)/CoFeB(1.2)/(MgO(2)/Ta(1)/SiO_2(63)$ is $174\frac{fJ}{Vm}$;

Thin Layer at CoFeB/MgO interface

A double oxide structure is not the only way to improve the value of the VCMA coefficient ζ_v. Depositing a thin layer of pure metal between $CoFeB$ layer and MgO gives the possibility to increase the ζ_v value.
An example of this kind of structure is: $Ta(5)/CoFeB(1)/Mg(0.2)/MgO(2.5)|Al_2O_3(5)$ where again the number in parenthesis indicates the thickness of the respective layer [24]. Mg layer could be replaced by Pt or by Ta, and depending on the metal deposited at the interface between $CoFeB$ and MgO, different values of saturation magnetization, interfacial anisotropy constant and VCMA coefficient are observed [24]:

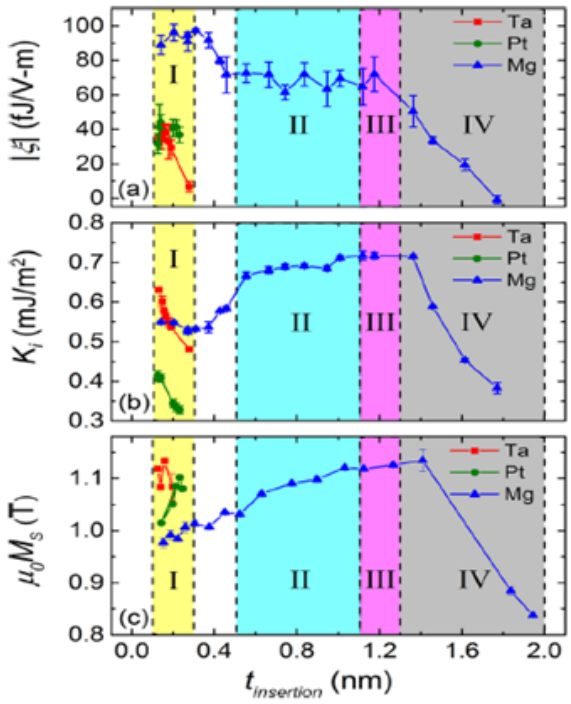

Figure 1.7: ζ_v, K_i and $\mu_0 M_s$ in function of the insertion layer thickness [24]

With Mg as the insertion layer, and with a thickness of 0.2 nm, the optimal value of ζ_v is obtained, equal to $100\frac{fJ}{Vm}$ about.

Chapter 2

Analytical modeling of domain Wall (DW) motion due to an applied current density and/or external magnetic field

2.1 Newtonian Approach

In the current chapter 2, an analytical model of the Domain Wall motion induced by Spin Transfer Torque (STT), by an external magnetic field and by Spin Orbit Torque (SOT) is derived. Finally the presence of a "gate" of different anisotropy along the ferromagnetic track, with the possible blocking of the Domain Wall due to this region of different anisotropy is analitically modeled in chapter 2.13. There are already analytical model, obtained with a Lagrangian approach which allow to describe the motion of a domain wall along the ferromagnetic track. In order to allow readers who do not know the Lagrangian concept, to fully understand how a domain wall moves due to STT effect, SOT effect or due to the presence of an external magnetic field, a purely mechanical Newtonian approach is adopted. The descriptive analytical model will be a two-coordinates model, i.e. a system

of two differential equations, one describing how the center of the domain wall moves over time, the other one describing how magnetization precedes around the perpendicular axis. In literature, models with two collective coordinates obtained with a Lagrangian approach have already been proposed [25][26][27][28]. Some modeling of pinning potentials have also been proposed as reported in [29][30][31]. Through the Lagrangian approach it is possible to obtain models with three collective coordinates, which is a system of three differential variables: the center of the domain wall $\dot{q}$, precession angle $\dot{\phi}$, and tilting angle of the domain wall $\dot{\Gamma}$, or instead of the latter the width of the domain wall $\dot{\Delta}$. Therefore, there are two distinct three-coordinates models: $\dot{q} - \dot{\phi} - \dot{\Gamma}$ model and $\dot{q} - \dot{\phi} - \dot{\Delta}$ model, as reported in [32][33][34][35]. A more complex model, obtained with the Lagrangian approach, would predict the presence of a four-coordinates system: $\dot{q} - \dot{\phi} - \dot{\Gamma} - \dot{\Delta}$ model as reported in [36][32]. These two additional collective coordinates, $\dot{\Delta} - \dot{\Gamma}$, add little precision to the results with respect to a two-collective coordinates because the width of the domain wall remains practically constant over time, and since the tilting profile of the domain wall usually stabilizes around a constant value. In the Appendix, section Four-Collective Coordinates system, the four-collective coordinates system is reported only for more details. The Newtonian model takes into account the tilting of the domain wall in the two differential equations. The tilting angle could be provided by code externally in fact, it is possible to observe and measure the tilting angle of a domain wall with a Moke microscope. Moreover the domain wall width, which depends on the magnetic anisotropy, is considered as a piecewise function in the case of the presence of gates that modify the local anisotropy during the solution of the differential system with Matlab. Therefore the innovative points of this thesis consist in the Newtonian approach, or in other words in deriving the differential system with two collective coordinates without using the Langrangian method; but above all in deriving an equation that allows to describe a pinning site due to the presence of a "gate" of different anisotropy due to VCMA effect. In conclusion, the main goal will be to find a function which at the same time is as close as possible to a profile of an anisotropic barrier/hole and which can be integrated for the anisotropic energy evaluation, and which can subsequently be differentiated with respect to the center of the domain wall as shown in chapter 2.13 to obtain a final expression of the effective pinning field. The validity of the equation which describes the effective pinning field generated by the VCMA gate will be confirmed with the analytical results of the two collective coordinates model.

2.2 Reference System

Figure 2.1a shows the reference system with respect to which, the motion of the domain wall and its possible crossing through the VCMA gate will be modeled.

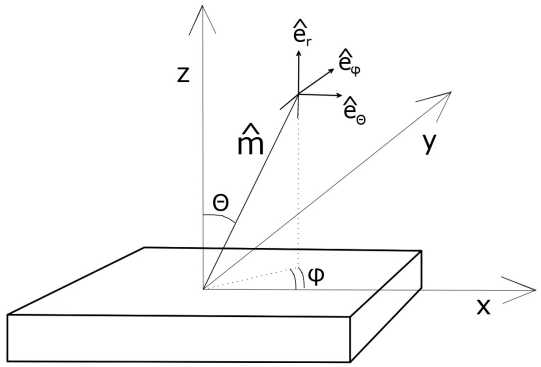

(a) Reference System

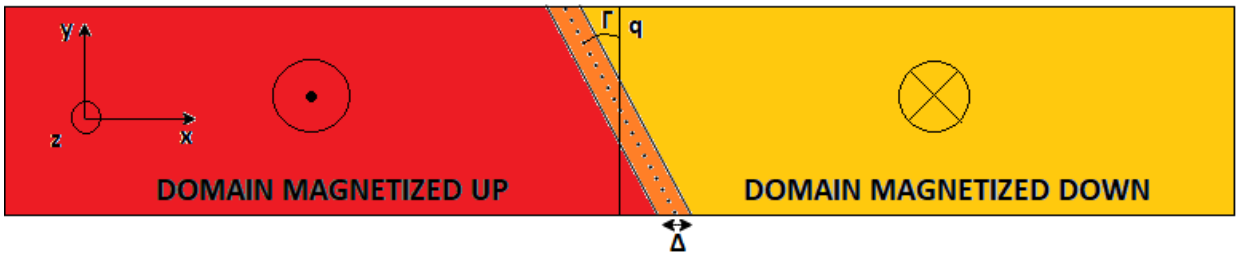

(b) Domain wall parameters: Δ is the domain wall width, Γ is the tilting angle of the domain wall, q is the center of the domain wall

Figure 2.1: Reference system and schematic of a domain wall

The tangent base vectors, trivially obtained from the derivative of the spherical coordinates are defined as:

$$\begin{cases} \hat{e}_r = (sin(\theta)cos(\phi); sin(\theta)sin(\phi); cos(\theta)) \\ \hat{e}_\theta = (cos(\theta)cos(\phi); cos(\theta)sin(\phi); -sin(\theta)) \\ \hat{e}_\phi = (-sin(\phi); cos(\phi); 0) \end{cases} \tag{2.1}$$

2.3 Angle profile of the magnetization

The profile of the θ angle of the magnetization could be described by the following function [37]:

$$\theta(x,y) = 2arctan[e^{\frac{(x-q)\cdot cos(\Gamma)+y\cdot sin(\Gamma)}{\Delta}}] \tag{2.2}$$

where Γ is the tilting angle of the domain wall in the 'xy' plane.

2.4 Domain Wall Width

In the current section 2.4 the equation of the Domain Wall width is demonstrated with a naive approach.
Neglecting the tilting profile of the domain wall, the θ function could be written in a simpler way, from which it will be easier to evaluate the infinitesimal angle variation:

$$\theta(x) = 2arctan[e^{\frac{x-q}{\Delta}}] \tag{2.3}$$

This function describes quite well the angle profile of the magnetization, and the counterexample is that in the middle of the profile, when $x = q$ its value is perfectly $\frac{\pi}{2}$ which means that our magnetization lies in the $'xy'$ plane. Another reasoning why this function is a good choice is due to the fact that the mathematical expression of the derivative could be rewritten in a easier form as it will be shown later. Now, to demonstrate the infinitesimal angle between two adjacent spins, the center of the domain wall profile is supposed for simplicity to be perfectly at the origin of the axis, therefore $q = 0$.

$$\theta(x) = 2arctan[e^{\frac{x}{\Delta}}] \tag{2.4}$$

The series of spins could be imagined far "a" from each other, with "a" the lattice parameter. The angle θ (which is the angle between the 'z' axis and 'xy' plane as illustrated in Figure 2.1a) varies really slow from 0° to +180°. In the domain wall there is a great number of electrons (assumed as an infinite number in the limit concept); it implies that the angle between one spin and its successive is practically infinitesimal. To calculate this infinitesimal variation of the angle, it could be simply defined as the difference between the angle in the middle of the wall ($\frac{\pi}{2}$) and the angle just one lattice space after. In the concept of the limit, this is the mathematical expression of the infinitesimal angle:

$$\theta_{inf} = lim_{x->0}[2arctan[e^{\frac{x+\Delta x}{\Delta}}] - 2arctan[e^{\frac{x}{\Delta}}]] = 2arctan[e^{\frac{a}{\Delta}}] - \frac{\pi}{2} \tag{2.5}$$

With a naive approach, the width of the domain wall could be defined as the product between the number of spins and the distance between each spin defined as the lattice space "a":

$$\Delta = N \cdot a \tag{2.6}$$

To evaluate the expression of the domain wall width, each energy quantity involved in the domain wall must be calculated in function of the number of spins N, and minimizing the total energy density with respect to N, the optimal N value is found, and therefore the final domain wall width equation is derived. In this basic model three energies are taken in consideration:

- Exchange energy;
- Uniaxial anisotropy energy;
- Demagnetizing energy;

Dzyaloshinskii–Moriya interaction (DMI) is not taken in consideration for the domain wall width demonstration.
Starting from the exchange energy, it is defined as follow:

$$E_{ex} = -2J_{12} \cdot S_1 \cdot S_2 = -2JS^2 \cdot cos(\theta_1 - \theta_2) \tag{2.7}$$

The exchange interaction is supposed to happen only between adjacent electrons. Since the angle difference between two successive spins is θ_{inf} just calculated before, the energy penalty of each electron couple is [38]:

$$\Delta E_{ex} = E_{ex} - E_{ex}^{\theta=0} = -2JS^2 \cdot cos(\theta_1 - \theta_2) + 2JS^2 = -2JS^2 \cdot cos(\theta_{inf}) + 2JS^2 \tag{2.8}$$

Substituting $\Delta = N \cdot a$, and in the limit of nearly infinite number of spins involved into the domain wall:

$$lim_{N->\infty}[-2JS^2 \cdot cos(2arctan[e^{\frac{1}{N}}] - \frac{\pi}{2}) + 2JS^2] = 1 - \frac{1}{2N^2} \tag{2.9}$$

Replacing the limit into the exchange energy equation [38]:

$$E_{ex} \approx -2JS^2 \cdot (1 - \frac{1}{2N^2}) + 2JS^2 = \frac{JS^2}{N^2} \tag{2.10}$$

The energy per unit area of an electron couple is expressed by the above equation divided by a^2, therefore considering that in this model there are (N-1) couples, the total exchange energy density is [38]:

$$\epsilon_{ex,tot} = lim_{N->\infty}[\frac{JS^2}{N^2a^2} \cdot (N-1)] \approx \frac{JS^2}{Na^2} \tag{2.11}$$

The uniaxial anisotropy energy and the demagnetizing energy could be assimilated both as anisotropy energy, both function of $\sum_{i=1}^{N}(sin(\theta_i))^2$. The total uniaxial anisotropy energy is:

$$E_a^{tot} = \sum_{i=1}^{N} K_u \cdot (sin(\theta_i))^2 \tag{2.12}$$

where θ_i are the various, almost infinite, angles from 0° to 180° in step of θ_{inf}. Concerning the demagnetizing energy, it is in general expressed as follow:

$$E_{dem} = -\frac{1}{2}\mu_0 \vec{M} \cdot \vec{H}_{dem} \tag{2.13}$$

but through an easy calculation, it can be rewritten as:

$$E_{dem} = \frac{\mu_0}{2} \cdot (sin(\theta_i))^2 \cdot [M_s^2 N_x (cos(\phi))^2 + M_s^2 N_y (sin(\phi))^2 - M_s^2 N_z] + \frac{\mu_0 M_s^2}{2} N_z \tag{2.14}$$

To rewrite E_{dem}, the definition of demagnetizing field $\vec{H}_{dem} = -\overleftrightarrow{N} \cdot \vec{M}$ is used, where $\overleftrightarrow{N}$ is the demagnetizing tensor. Joining the two energy quantities, the uniaxial one and the demagnetizing one, the total energy per unit of volume is:

$$E_{anis}^{tot} = \frac{\mu_0 M_s^2}{2} N_z + K_{eff} \sum_{i=1}^{N} (sin(\theta_i))^2 \tag{2.15}$$

with

$$K_{eff} = K_u + \frac{\mu_0 M_s^2}{2} (N_x (cos(\phi))^2 + N_y (sin(\phi))^2 - N_z) \tag{2.16}$$

Now the objective is to solve the series of $(sin(\theta_i))^2$. Practically each θ_i is a multiple of the infinitesimal angle θ_{inf}, from 0° to 180°:

$$\begin{cases} 1 \cdot 2arctan[e^{\frac{a}{\Delta}}] - \frac{\pi}{2} \\ 2 \cdot 2arctan[e^{\frac{a}{\Delta}}] - \frac{\pi}{2} \\ 3 \cdot 2arctan[e^{\frac{a}{\Delta}}] - \frac{\pi}{2} \\ ... \\ N \cdot 2arctan[e^{\frac{a}{\Delta}}] - \frac{\pi}{2} \end{cases} \tag{2.17}$$

Since the increment between one term of the series and its successive is practically infinitesimal, the series could be rewritten as an integral. We are

in the case in which a summation almost coincides with the integral concept:

$$\sum_{i=0}^{N}(sin(\theta_i))^2 = \sum_{i=0}^{N}(sin(i \cdot (2arctan[e^{\frac{a}{\Delta}}] - \frac{\pi}{2})))^2 \tag{2.18}$$

$$\sum_{i=0}^{N}(sin(\theta_i))^2 \approx \int_0^N (sin(N \cdot (2arctan[e^{\frac{a}{\Delta}}] - \frac{\pi}{2})))^2 dN \approx \frac{N}{2} \tag{2.19}$$

Replacing the result into the equation of the total anisotropy energy, and rewriting the total energy per unit of surface instead of per unit of volume [38]:

$$\epsilon_{anis}^{tot} = \frac{N}{2} \cdot K_{eff} a + \frac{\mu_0 M_s^2}{2} N_z a \tag{2.20}$$

The total energy per unit of surface is a function of N as expected [38]:

$$\epsilon^{tot} = \frac{JS^2}{Na^2} + \frac{N}{2} \cdot K_{eff} a + \frac{\mu_0 M_s^2}{2} N_z a \tag{2.21}$$

Now, as previously stated, minimizing the total energy in function of N [38]:

$$\frac{d\epsilon^{tot}}{dN} = 0 \tag{2.22}$$

It is possible to obtain the equilibrium expression of N:

$$N = \sqrt{\frac{2JS^2}{K_{eff} a^3}} \tag{2.23}$$

Replacing it into the equation of $\Delta = N \cdot a$, the final width is equal to [38]:

$$\begin{cases} \Delta = \sqrt{\frac{A_{bbc}}{\frac{K_i}{t} + \frac{\mu_0 M_s^2}{2}(N_x(cos(\phi))^2 + N_y(sin(\phi))^2 - N_z)}} \\ A_{bcc} = \frac{2JS^2}{a} \\ K_u = \frac{K_i}{t} + K_{vol} \approx \frac{K_i}{t} \end{cases} \tag{2.24}$$

where A_{bcc} is the exchange stiffness constant, which in the case of a body centered cubic lattice is equal to $A_{bbc} = \frac{2JS^2}{a}$ [39].

2.5 Landau-Lifshitz-Slonczewski equation & Spin Orbit Torque

Landau and Lifshitz described the motion of the magnetization taking in consideration its precession, Gilbert introduced the damping term of the magnetization, and finally Slonczewski and Zhang-Li added the STT terms, adiabatic and non-adiabatic one that are experimentally observed and formulated. The LLGS equation is equal to [40][37]:

$$\frac{d\vec{M}}{dt} = \gamma \vec{H}_{eff} \times \vec{M} + \frac{\alpha}{M_s}\vec{M} \times \frac{d\vec{M}}{dt} - u(\hat{j}_e \cdot \nabla)\vec{M} + \frac{\beta u}{M_s}\vec{M} \times (\hat{j}_e \cdot \nabla)\vec{M} \quad (2.25)$$

where β is the phenomenological non-adiabatic spin transfer parameter, γ is the gyromagnetic ratio and u has the following expression [40][37]:

$$u = \frac{g\mu_B P}{2eM_s} J_e \quad (2.26)$$

u has the dimension of velocity and it is directly proportional to the electrical current density.
The LLGS equation could be rewritten taking in consideration the Spin Orbit Torque (SOT) effect. Like the Spin Transfer Torque (STT) effect, the Spin Orbit Torque (SOT) effect also exerts two twisting moments on the magnetization, one of precession and one of damping. The authors of these articles [36], [41], [42], [43], [44], [45] propose an analytical expression of the Spin Orbit Torque effect; more exactly in [45], the analytical expression implemented in Mumax3 is illustrated and explained. The analytical expression of the SOT effect implemented in Mumax3 will be implemented in this thesis:

$$\begin{aligned}\frac{d\vec{M}}{dt} =& \gamma \vec{H}_{eff} \times \vec{M} + \frac{\alpha}{M_s}\vec{M} \times \frac{d\vec{M}}{dt} - u(\hat{j}_e \cdot \nabla)\vec{M} + \frac{\beta u}{M_s}\vec{M} \times (\hat{j}_e \cdot \nabla)\vec{M} \\ &+ \gamma M_s a_{FL}(\hat{m} \times \hat{\sigma}) + \gamma M_s b_{DL}\hat{m} \times (\hat{m} \times \hat{\sigma})\end{aligned} \quad (2.27)$$

where a_{FL} is the field like SOT constant, and b_{DL} is the damping like SOT constant:

$$\begin{cases} a_{FL} = \frac{\hbar \alpha_{h,FL} J_{SOT}}{2eM_s t_{FM}} \\ b_{DL} = \frac{\hbar \alpha_{h,DL} J_{SOT}}{2eM_s t_{FM}} \end{cases} \quad (2.28)$$

Before dealing with the equation of the domain wall motion, the last step is to remember the tangent base vector defined in the section 2.1a:

$$\begin{cases} \hat{e}_r = (sin(\theta)cos(\phi); sin(\theta)sin(\phi); cos(\theta)) \\ \hat{e}_\theta = (cos(\theta)cos(\phi); cos(\theta)sin(\phi); -sin(\theta)) \\ \hat{e}_\phi = (-sin(\phi); cos(\phi); 0) \end{cases} \tag{2.29}$$

From the infinitesimal displacement of the magnetization in spherical coordinate:

$$d\vec{M}(r,\theta,\phi) = dM\hat{e}_r + M_s d\theta\hat{e}_\theta + M_s sin(\theta)d\phi\hat{e}_\phi \tag{2.30}$$

The time derivative of the magnetization, supposing that the modulus of the magnetization does not change in time (it is a specific constant of the material), is therefore:

$$\frac{dM(r,\vec{\theta},\phi)}{dt} = \frac{dM}{dt}\hat{e}_r + M_s\frac{d\theta}{dt}\hat{e}_\theta + M_s sin(\theta)\frac{d\phi}{dt}\hat{e}_\phi = M_s\frac{d\theta}{dt}\hat{e}_\theta + M_s sin(\theta)\frac{d\phi}{dt}\hat{e}_\phi \tag{2.31}$$

Exploiting the last result and exploiting the general kinetic momentum theorem[37]:

$$\begin{cases} \dot{\theta} = \frac{\gamma}{M_s}\vec{\Gamma}_\theta\hat{e}_\theta \\ \dot{\phi}sin(\theta) = \frac{\gamma}{M_s}\vec{\Gamma}_\phi\hat{e}_\phi \\ \gamma = -\frac{e}{2m} \end{cases} \tag{2.32}$$

From the rewritten LLGS equation, it is easy to understand all the components of torque, acting on the magnetization[37]:

$$\begin{cases} \vec{\Gamma}_{H_{eff}} = \vec{M} \times \vec{H}_{eff} \\ \vec{\Gamma}_{H_\alpha} = \vec{M} \times \vec{H}_\alpha \\ \vec{\Gamma}_u = \frac{u}{\gamma}(\hat{j}_e \cdot \nabla)\vec{M} \\ \vec{\Gamma}_\beta = -\frac{\beta u}{\gamma M_s}\vec{M} \times (\hat{j}_e \cdot \nabla)\vec{M} \\ \vec{\tau}_{SOT,FL} = M_s a_{FL}(\hat{m} \times \hat{\sigma}) \\ \vec{\tau}_{SOT,DL} = M_s b_{DL}\hat{m} \times (\hat{m} \times \hat{\sigma}) \end{cases} \tag{2.33}$$

All the torque components are expressed in CGS system, therefore $\mu_0 = 1$. For each components, the approach consists to compute the vector products, and the gradient in spherical coordinate and then through an easy scalar product, translating or better projecting the result in the tangent base vector.

Concerning the first torque component, it is related to the effective field. The effective field is defined as follow:

$$\vec{H}_{eff} = \vec{H}_{ext} + \frac{2A_{ex}}{M_s}\nabla^2\hat{m} - \frac{2K_u}{M_s}m_z\hat{z} - \vec{H}_d - \frac{2D_0}{M_s}((\nabla\cdot\hat{m})\hat{z} - \nabla\hat{m}_z) \quad (2.34)$$

The field components of the effective fields are:

- The external applied field. For simplicity, the external field is supposed to be applied only along the $\hat{z}$ direction, but the demonstration could be extended taking in consideration also the other directions;
- The exchange field due to the exchange interaction between each spin;
- The uniaxial anisotropy field;
- The demagnetizing field;
- The Dzyaloshinskii-Moriya field due to DMI;

The sum of the uniaxial anisotropy field and the demagnetizing field component related to N_z are defined as the **Effective Anisotropy Field**. Exploiting this definition the remaining part of the demagnetizing field associated to N_x and N_y component of the demagnetizing field is called **Transverse Shape Anisotropy Field**. In conclusion the sum of the uniaxial anisotropy field with the demagnetizing field is equal to the sum of the effective field with the transverse shape anisotropy field. Making it explicit the $\vec{H}_{eff}$ could be rewritten as:

$$\vec{H}_{eff} = \vec{H}_{ext} + \frac{2A_{ex}}{M_s}\nabla^2\hat{m} + \frac{2K_{eff}}{M_s}m_z\hat{z} + \frac{2K_d}{M_s}m_y\hat{y} - \frac{2D_0}{M_s}((\nabla\cdot\hat{m})\hat{z} - \nabla\hat{m}_z) \quad (2.35)$$

where $K_{eff} = K_u - \frac{1}{2}\mu_0 M_s^2$. $K_d \approx \frac{\mu_0 N_x M_s^2}{2}$ because the structure of the ferromagnetic layer is planar.

2.6 Mathematical Properties

The function of the angle profile of the magnetization describes quite well the realistic angle profile of a domain wall. At the same time this function has some properties that allow to write the function itself and its derivative in a more simplistic way through algebraic manipulation. By exploiting this specific profile function, it will be possible to obtain final equations, which

describe the motion of the domain wall. The following equation shows an alternative way to write the function $sin(2arctan(x))$:

$$sin[2 \cdot arctan(x)] = 2 \cdot sin[arctan(x)]cos[arctan(x)] \tag{2.36}$$

$$sin[2 \cdot arctan(x)] = 2 \cdot \frac{x}{\sqrt{1+x^2}} \cdot \frac{1}{\sqrt{1+x^2}} = \frac{2x}{\sqrt{1+x^2}} \tag{2.37}$$

Substituting y with an exponential function:

$$sin[2 \cdot arctan(exp(x))] = \frac{2 \cdot e^x}{1+e^{2x}} = sech(x) \tag{2.38}$$

Now, making the derivative of the angle profile and exploiting the last relationship:

$$\frac{d}{dx}[2arctan[e^{\frac{(x-q)cos(\Gamma)+ysin(\Gamma)}{\Delta}}]] = \frac{cos(\Gamma)sech(\frac{(x-q)cos(\Gamma)+ysin(\Gamma)}{\Delta})}{\Delta} = \frac{cos(\Gamma)sin(\theta(x))}{\Delta} \tag{2.39}$$

In conclusion:

$$\frac{d\theta(x,y)}{dx} = \frac{cos(\Gamma)}{\Delta} sin(\theta(x,y)) \tag{2.40}$$

Another important property that will be exploited during the thesis is the following:

$$cos(2arctan(e^x)) = -tanh(x) \tag{2.41}$$

To demonstrate the equality, just start with:

$$cos(2arctan(e^x)) = \frac{1-tan^2(arctan(e^x))}{1+tan^2(arctan(e^x))} = \frac{1-e^{2x}}{1+e^{2x}} = \frac{1-e^{-(-2x)}}{1+e^{-(-2x)}} \tag{2.42}$$

$$cos(2arctan(e^x)) = tanh(-x) = -tanh(x) \tag{2.43}$$

therefore:

$$cos(\theta(x,y)) = -tanh(\frac{(x-q)cos(\Gamma)+ysin(\Gamma))}{\Delta}) \tag{2.44}$$

2.7 Effective Field

In section 2.5 all the effective torque components acting on the magnetization are expressed in the CGS system, therefore $\mu_0 = 1$. In the following subsection, each effective torque component and all the parameters will be expressed in the International System of Units (SI) for clarity.

2.7.1 External Field

Supposing that the external field is applied only along the $\hat{z}$ direction:

$$\vec{H}_{ext} = \begin{pmatrix} 0 \\ 0 \\ H_z \end{pmatrix} \cdot \begin{pmatrix} \hat{x} \\ \hat{y} \\ \hat{z} \end{pmatrix} \tag{2.45}$$

The external torque is equal to:

$$\vec{\Gamma}_{ext} = \mu_0 \vec{M} \times \vec{H}_{ext} = \begin{pmatrix} M_s \cdot sin(\theta)cos(\phi) \\ M_s \cdot sin(\theta)sin(\phi) \\ M_s \cdot cos(\theta) \end{pmatrix} \times \begin{pmatrix} 0 \\ 0 \\ \mu_0 H_z \end{pmatrix} \tag{2.46}$$

$$\vec{\Gamma}_{ext} = \begin{pmatrix} \mu_0 M_s \cdot H_z \cdot sin(\theta) \cdot sin(\phi) \\ -\mu_0 M_s \cdot H_z \cdot sin(\theta) \cdot cos(\phi) \\ 0 \end{pmatrix} \cdot \begin{pmatrix} \hat{x} \\ \hat{y} \\ \hat{z} \end{pmatrix} \tag{2.47}$$

Now through the scalar product with the tangent base vector, the final expression for the external torque is: [37]:

$$\vec{\Gamma}_{H_{ext}} = \begin{pmatrix} 0 \\ 0 \\ -\mu_0 \cdot M_s \cdot H_z \cdot sin(\theta) \end{pmatrix} \cdot \begin{pmatrix} \hat{e}_r \\ \hat{e}_\theta \\ \hat{e}_\phi \end{pmatrix} = -\mu_0 M_s \cdot H_z \cdot sin(\theta) \hat{e}_\phi \tag{2.48}$$

2.7.2 Exchange Field

The exchange field is strictly related to the profile angle of the magnetization. Its mathematical expression is:

$$\vec{H}_{ex} = \frac{2A_{ex}}{\mu_0 M_s} \nabla^2 \hat{m} = \frac{2A_{ex}}{\mu_0 M_s} (\frac{\partial^2 \hat{m}}{\partial x^2} + \frac{\partial^2 \hat{m}}{\partial y^2}) = \frac{2A_{ex}}{\mu_0 M_s^2} (\frac{\partial^2 \vec{M}}{\partial x^2} + \frac{\partial^2 \vec{M}}{\partial y^2}) \tag{2.49}$$

To evaluate the exchange torque, the vectorial product between the magnetization and the exchange field must be evaluated:

$$\vec{\Gamma}_{ex} = \mu_0 \frac{2A_{ex}}{\mu_0 M_s} (\vec{M} \times \nabla^2 \vec{m}) = \frac{2A_{ex}}{M_s} (\vec{M} \times (\frac{\partial^2 \vec{m}}{\partial x^2} + \frac{\partial^2 \vec{m}}{\partial y^2})) \tag{2.50}$$

The profile model of the magnetization is a one dimensional function, therefore the ∇ operator could be written simply with a one dimensional derivative. The second derivative of $\vec{m}$ could be calculated deriving each spherical

component:

$$\nabla^2\hat{m} = (\frac{\partial^2}{\partial x^2} + \frac{\partial^2}{\partial y^2}) \begin{pmatrix} cos(\phi)sin(2atan(e^{\frac{(x-q)cos(\Gamma)+ysin(\Gamma)}{\Delta}})) \\ sin(\phi)sin(2atan(e^{\frac{(x-q)cos(\Gamma)+ysin(\Gamma)}{\Delta}})) \\ cos(2atan(e^{\frac{(x-q)cos(\Gamma)+ysin(\Gamma)}{\Delta}})) \end{pmatrix} \tag{2.51}$$

$$\nabla^2\hat{m} = \begin{pmatrix} cos(\phi)(\frac{\partial^2 sin(2atan(e^{\frac{(x-q)cos(\Gamma)+ysin(\Gamma)}{\Delta}}))}{\partial x^2} + \frac{\partial^2 sin(2atan(e^{\frac{(x-q)cos(\Gamma)+ysin(\Gamma)}{\Delta}}))}{\partial y^2} \\ sin(\phi)(\frac{\partial^2 sin(2atan(e^{\frac{(x-q)cos(\Gamma)+ysin(\Gamma)}{\Delta}}))}{\partial x^2} + \frac{\partial^2 sin(2atan(e^{\frac{(x-q)cos(\Gamma)+ysin(\Gamma)}{\Delta}}))}{\partial y^2}) \\ \frac{\partial^2 cos(2atan(e^{\frac{(x-q)cos(\Gamma)+ysin(\Gamma)}{\Delta}}))}{\partial x^2} + \frac{\partial^2 cos(2atan(e^{\frac{(x-q)cos(\Gamma)+ysin(\Gamma)}{\Delta}}))}{\partial y^2} \end{pmatrix} \tag{2.52}$$

The second derivative of the sine function with respect to x could be rewritten as:

$$\frac{\partial^2 sin(2atan(e^{\frac{(x-q)cos(\Gamma)+ysin(\Gamma)}{\Delta}}))}{\partial x^2} = \frac{\partial^2 sech(\frac{(x-q)cos(\Gamma)+ysin(\Gamma)}{\Delta})}{\partial x^2} \tag{2.53}$$

The result of the derivation is:

$$\frac{cos(\Gamma)^2}{\Delta^2}[tanh^2(\frac{(x-q)cos(\Gamma)+ysin(\Gamma)}{\Delta})sech(\frac{(x-q)cos(\Gamma)+ysin(\Gamma)}{\Delta})]+ \\ -\frac{cos(\Gamma)^2}{\Delta^2}[sech^3(\frac{(x-q)cos(\Gamma)+ysin(\Gamma)}{\Delta})] \tag{2.54}$$

Through several algebraic manipulation the final result could be rewritten as:

$$\frac{\partial^2 sin(\theta(x,y))}{\partial x^2} = \frac{cos^2(\Gamma)}{\Delta^2}(sin(\theta) - 2sin^3(\theta)) \tag{2.55}$$

Similarly:

$$\frac{\partial^2 sin(\theta(x,y))}{\partial y^2} = \frac{sin^2(\Gamma)}{\Delta^2}(sin(\theta) - 2sin^3(\theta)) \tag{2.56}$$

Concerning the second derivative of the cosine function with respect to x:

$$\frac{\partial^2 cos(2atan(e^{\frac{(x-q)cos(\Gamma)+ysin(\Gamma)}{\Delta}}))}{\partial x^2} = \frac{\partial^2 tanh(-\frac{(x-q)cos(\Gamma)+ysin(\Gamma)}{\Delta})}{\partial x^2} \tag{2.57}$$

therefore:

$$\frac{\partial^2 cos(2atan(e^{\frac{(x-q)cos(\Gamma)+ysin(\Gamma)}{\Delta}}))}{\partial x^2} = -cos^2(\Gamma)\frac{2cos(\theta(x,y))sin^2(\theta(x,y))}{\Delta^2} \tag{2.58}$$

Similarly:

$$\frac{\partial^2 cos(\theta(x,y))}{\partial y^2} = -cos^2(\Gamma)\frac{2cos(\theta(x,y))sin^2(\theta(x,y))}{\Delta^2} \tag{2.59}$$

Therefore:

$$\nabla^2\vec{m} = \frac{\partial^2\vec{m}}{\partial x^2} + \frac{\partial^2\vec{m}}{\partial y^2} = \begin{pmatrix} cos(\phi)(\frac{sin(\theta)-2sin^3(\theta)}{\Delta^2}) \\ sin(\phi)(\frac{sin(\theta)-2sin^3(\theta)}{\Delta^2}) \\ -\frac{2cos(\theta)sin^2(\theta)}{\Delta^2} \end{pmatrix} \cdot \begin{pmatrix} \hat{x} \\ \hat{y} \\ \hat{z} \end{pmatrix} \tag{2.60}$$

Knowing the mathematical expression of $\nabla^2\vec{m}$, the vectorial product must be computed to obtain the final expression of the exchange torque:

$$\vec{M} \times \nabla^2\vec{m} = M_s \begin{pmatrix} -\frac{sin(\theta)cos(\theta)sin(\phi)}{\Delta^2} \\ -\frac{sin(\theta)cos(\theta)cos(\phi)}{\Delta^2} \\ 0 \end{pmatrix} \cdot \begin{pmatrix} \hat{x} \\ \hat{y} \\ \hat{z} \end{pmatrix} \tag{2.61}$$

Now making the scalar product with the tangent base vector, it is possible to obtain the final expression of the exchange torque in tangent base system:

$$\vec{\Gamma}_{ex} = \frac{2A_{ex}}{M_s}(\vec{M} \times \nabla^2\hat{m}) = \begin{pmatrix} 0 \\ 0 \\ 2A_{ex}\frac{sin(\theta)cos(\theta)}{\Delta^2} \end{pmatrix} \cdot \begin{pmatrix} \hat{e}_r \\ \hat{e}_\theta \\ \hat{e}_\phi \end{pmatrix} \tag{2.62}$$

2.7.3 Uniaxial Anisotropy Field

The uniaxial anisotropy is defined as:

$$\vec{H}_{ani} = -\frac{2K_u}{\mu_0 M_s} m_z \hat{z} = \begin{pmatrix} 0 \\ 0 \\ -\frac{2K_u}{M_s} \cdot cos(\theta) \end{pmatrix} \cdot \begin{pmatrix} \hat{x} \\ \hat{y} \\ \hat{z} \end{pmatrix} \tag{2.63}$$

The anisotropy field exerts a torque moment on the magnetization defined as:

$$\vec{\Gamma}_{ani} = -\mu_0\vec{M} \times \vec{H}_{ani} = -\mu_0 \begin{pmatrix} M_s \cdot sin(\theta)cos(\phi) \\ M_s \cdot sin(\theta)sin(\phi) \\ M_s \cdot cos(\theta) \end{pmatrix} \times \begin{pmatrix} 0 \\ 0 \\ \frac{2K_u}{\mu_0 M_s} \cdot cos(\theta) \end{pmatrix} \tag{2.64}$$

The result of the vectorial product is:

$$\vec{\Gamma}_{ani} = \begin{pmatrix} -2K_u sin(\theta)cos(\theta)sin(\phi) \\ 2K_u sin(\theta)cos(\theta)cos(\phi) \\ 0 \end{pmatrix} \cdot \begin{pmatrix} \hat{x} \\ \hat{y} \\ \hat{z} \end{pmatrix} \tag{2.65}$$

Transposing in the tangent base vector:

$$\vec{\Gamma}_{ani} = \begin{pmatrix} 0 \\ 0 \\ 2K_u sin(\theta)cos(\theta) \end{pmatrix} \cdot \begin{pmatrix} \hat{e}_r \\ \hat{e}_\theta \\ \hat{e}_\phi \end{pmatrix} \tag{2.66}$$

2.7.4 Demagnetizing Field

The demagnetizing torque is defined as:

$$\vec{\Gamma}_{H_d} = -\mu_0 \vec{M} \times \vec{H}_d = -\mu_0 \vec{M} \times (-\bar{N} \cdot \vec{M}) \tag{2.67}$$

$$\vec{\Gamma}_{H_d} = \mu_0 \begin{pmatrix} M_s \cdot sin(\theta)cos(\phi) \\ M_s \cdot sin(\theta)sin(\phi) \\ M_s \cdot cos(\theta) \end{pmatrix} \times \begin{pmatrix} M_s \cdot N_x sin(\theta)cos(\phi) \\ M_s \cdot N_y sin(\theta)sin(\phi) \\ M_s \cdot N_z cos(\theta) \end{pmatrix} \cdot \begin{pmatrix} \hat{x} \\ \hat{y} \\ \hat{z} \end{pmatrix} \tag{2.68}$$

Developing the vectorial product in the equation above:

$$\vec{\Gamma}_{H_d} = -\mu_0 M_s^2 \begin{pmatrix} (N_y - N_z) \cdot sin(\theta)cos(\theta)sin(\phi) \\ (N_z - N_x) \cdot sin(\theta)cos(\theta)cos(\phi) \\ (N_x - N_y) \cdot (sin(\theta))^2 sin(\phi)cos(\phi) \end{pmatrix} \cdot \begin{pmatrix} \hat{x} \\ \hat{y} \\ \hat{z} \end{pmatrix} \tag{2.69}$$

Making the scalar product with the tangent base vector, the final expression for the demagnetizing torque is:

$$\vec{\Gamma}_{H_d} = -\mu_0 M_s^2 \begin{pmatrix} 0 \\ (N_y - N_x) \cdot sin(\theta)sin(\phi)cos(\phi) \\ (N_z - N_y(sin(\phi))^2 - N_x(cos(\phi))^2) \cdot (sin(\theta))cos(\theta)) \end{pmatrix} \cdot \begin{pmatrix} \hat{e}_r \\ \hat{e}_\theta \\ \hat{e}_\phi \end{pmatrix} \tag{2.70}$$

In the presence of a certain tilting profile, the torque must be accurately modified. The approach is to change the coordinate system, supposing that there is a certain tilting angle Γ, and in this way a general expression can be found as done for the DMI torque. An easier method is to replace ϕ with $\phi - \Gamma$, because intuitively the in-plane angle ϕ changes a bit because of the presence of the tilting angle Γ. In conclusion the demagnetizing torque is equal to:

$$\vec{\Gamma}_{H_d} = -\mu_0 M_s^2 \begin{pmatrix} 0 \\ (N_y - N_x)sin(\theta)sin(\phi - \Gamma)cos(\phi - \Gamma) \\ (N_z - N_y(sin(\phi - \Gamma))^2 - N_x(cos(\phi - \Gamma))^2)sin(\theta)cos(\theta) \end{pmatrix} \cdot \begin{pmatrix} \hat{e}_r \\ \hat{e}_\theta \\ \hat{e}_\phi \end{pmatrix} \tag{2.71}$$

2.7.5 Effective Anisotropy Field

The Effective Anisotropy Field as explained before is the sum of the uniaxial anisotropy field with the N_z component of the Demagnetizing Field, therefore neglecting N_x and N_y , and since $N_z \approx 1$ the Effective Anisotropy Torque is equal to:

$$\vec{\Gamma}_{K_{eff}} = \vec{\Gamma}_{H_d} + \vec{\Gamma}_{ani,N_z} = \begin{pmatrix} 0 \\ 0 \\ 2K_u sin(\theta)cos(\theta) - \mu_0 M_s^2 sin(\theta)cos(\theta) \end{pmatrix} \cdot \begin{pmatrix} \hat{e}_r \\ \hat{e}_\theta \\ \hat{e}_\phi \end{pmatrix} \tag{2.72}$$

K_{eff} is defined as:

$$K_{eff} = K_u - \frac{1}{2}\mu_0 M_s^2 \tag{2.73}$$

Therefore the final expression of $\vec{\Gamma}_{K_{eff}}$ is:

$$\vec{\Gamma}_{K_{eff}} = 2K_{eff} sin(\theta)cos(\theta)\hat{e}_\phi \tag{2.74}$$

2.7.6 Transverse Shape Anisotropy

The transverse shape anisotropy energy is associated to the domain wall, and it differentiates the energetic state of a Bloch domain wall with respect to a Néel domain wall. The effective field due the transverse shape anisotropy energy is [20]:

$$\vec{H}_{K_d} = \frac{2K_d}{\mu_0 M_s} m_x \hat{x} \tag{2.75}$$

The K_d parameter is equal to:

$$K_d = \frac{\mu_0 N_x M_s^2}{2} \tag{2.76}$$

Where N_x could be evaluated with the following formula [20]:

$$N_x = \frac{ln(2)t_{FM}}{\pi\Delta} \tag{2.77}$$

where t_{FM} is equal to the thickness of the ferromagnetic layer. The torque associated to the effective field component $\vec{K}_d$ is:

$$\vec{\Gamma}_{K_d} = \frac{2K_d m_x}{\mu_0 M_s}\vec{M} \times \hat{x} = \frac{2K_d}{\mu_0} m_x \hat{m} \times \hat{x} \tag{2.78}$$

where m_x is equal to $sin(\theta)cos(\phi)$. The torque $\hat{m} \times \hat{x}$ is equal to:

$$\hat{m} \times \hat{x} = \begin{pmatrix} sin(\theta)cos(\phi) \\ sin(\theta)sin(\phi) \\ cos(\theta) \end{pmatrix} \times \begin{pmatrix} 1 \\ 0 \\ 0 \end{pmatrix} = \begin{pmatrix} 0 \\ cos(\theta) \\ -sin(\theta)sin(\phi) \end{pmatrix} \cdot \begin{pmatrix} \hat{x} \\ \hat{y} \\ \hat{z} \end{pmatrix} \tag{2.79}$$

Through the scalar product with the tangent base vector:

$$\hat{m} \times \hat{x} = \begin{pmatrix} 0 \\ sin(\phi) \\ cos(\theta)cos(\phi) \end{pmatrix} \cdot \begin{pmatrix} \hat{e}_r \\ \hat{e}_\theta \\ \hat{e}_\phi \end{pmatrix} \tag{2.80}$$

The final expression of the transverse anisotropic torque is:

$$\vec{\Gamma}_{K_d} = 2K_d \begin{pmatrix} 0 \\ sin(\theta)sin(\phi)cos(\phi) \\ sin(\theta)cos(\theta)cos^2(\phi) \end{pmatrix} \cdot \begin{pmatrix} \hat{e}_r \\ \hat{e}_\theta \\ \hat{e}_\phi \end{pmatrix} \tag{2.81}$$

The expression of the transverse shape torque reported in equation 2.81 is valid for a non tilted domain wall. In the presence of a certain tilting profile, the torque must be accurately modified. The approach is to change the coordinate system, supposing that there is a certain tilting angle Γ, and in this way a general expression can be found as done for the DMI torque. An easier method is to replace ϕ with $\phi - \Gamma$, because intuitively the in-plane angle ϕ changes because of the presence of the tilting angle Γ. In conclusion the expression of the transverse shape anisotropy is:

$$\vec{\Gamma}_{K_d} = 2K_d \begin{pmatrix} 0 \\ sin(\theta)sin(\phi - \Gamma)cos(\phi - \Gamma) \\ sin(\theta)cos(\theta)cos^2(\phi - \Gamma) \end{pmatrix} \cdot \begin{pmatrix} \hat{e}_r \\ \hat{e}_\theta \\ \hat{e}_\phi \end{pmatrix} \tag{2.82}$$

This final equation coincides with equation 2.70 supposing N_y equal to 0 and N_x equal to $\frac{ln(2)t_{FM}}{\pi\Delta}$. The domain wall in the initial state can be in the Néel configuration or in the Bloch configuration, and the sign of K_d determines which of the two configurations is energetically preferred.

2.7.7 Final expression of the effective field torque

The effective field will be expressed in function of the sum of the effective anisotropy field with the transverse shape anisotropy field instead of the

sum of the uniaxial anisotropy field with the demagnetizing field. The final expression of the effective field is therefore:

$$\begin{aligned}\vec{\Gamma}_{H_{eff}} =& -\mu_0 M_s * H_z * sin(\theta)\hat{e}_\phi + 2A_{ex}\frac{sin(\theta)cos(\theta)}{\Delta^2}\hat{e}_\phi + 2K_u sin(\theta)cos(\theta)\hat{e}_\phi + \\ &- \mu_0 M_s^2 sin(\theta)cos(\theta)\hat{e}_\phi + 2K_d sin(\theta)sin(\phi-\Gamma)cos(\phi-\Gamma)\hat{e}_\theta + \\ &+ 2K_d sin(\theta)cos(\theta)cos^2(\phi-\Gamma)\hat{e}_\phi\end{aligned} \tag{2.83}$$

2.8 DMI Field

Dzyaloshinskii–Moriya interaction field is equal to:

$$H_{DMI} = -\frac{2D_0}{\mu_0 M_s}((\nabla\cdot\hat{m})\hat{z} - \nabla\hat{m}_z) \tag{2.84}$$

The divergence of $\hat{m}$ could be easily evaluated:

$$\nabla\cdot\hat{m} = \frac{\partial\hat{m}_x}{\partial x} + \frac{\partial\hat{m}_y}{\partial y} + \frac{\partial\hat{m}_z}{\partial z} = cos(\phi)\frac{\partial sin(\theta(x,y))}{\partial x} + sin(\phi)\frac{\partial sin(\theta(x,y))}{\partial y} \tag{2.85}$$

Evaluating firstly the derivative of the sine function:

$$\frac{\partial sin(2atan(e^{\frac{(x-q)cos(\Gamma)+ysin(\Gamma)}{\Delta}}))}{\partial x} = -\frac{cos(\Gamma)tanh(\frac{(x-q)cos(\Gamma)+ysin(\Gamma)}{\Delta})sech(\frac{(x-q)cos(\Gamma)+ysin(\Gamma)}{\Delta})}{\Delta} \tag{2.86}$$

$$\frac{\partial sin(2atan(e^{\frac{(x-q)cos(\Gamma)+ysin(\Gamma)}{\Delta}}))}{\partial x} = cos(\Gamma)\frac{sin(\theta)cos(\theta)}{\Delta} \tag{2.87}$$

Similarly the derivative of the sine function with respect to y:

$$\frac{\partial sin(2atan(e^{\frac{(x-q)cos(\Gamma)+ysin(\Gamma)}{\Delta}}))}{\partial y} = sin(\Gamma)\frac{sin(\theta)cos(\theta)}{\Delta} \tag{2.88}$$

Finally:

$$\nabla\cdot\hat{m} = [\frac{cos(\Gamma)cos(\phi) + sin(\Gamma)sin(\phi)}{\Delta}]sin(\theta)cos(\theta) \tag{2.89}$$

For what concern the gradient of $\hat{m}_z$:

$$\nabla\hat{m}_z = \frac{\partial m_z}{\partial x}\hat{x} + \frac{\partial m_z}{\partial y}\hat{y} + \frac{\partial m_z}{\partial z}\hat{z} = \frac{\partial cos(\theta)}{\partial x}\hat{x} + \frac{\partial cos(\theta)}{\partial y}\hat{y} \tag{2.90}$$

The derivative of the cosine function with respect to x is:

$$\frac{\partial cos(2atan(e^{\frac{(x-q)cos(\Gamma)+ysin(\Gamma)}{\Delta}}))}{\partial x} = -cos(\Gamma)\frac{sech^2(\frac{(x-q)cos(\Gamma)+ysin(\Gamma)}{\Delta})}{\Delta} \tag{2.91}$$

$$\frac{\partial cos(2atan(e^{\frac{(x-q)cos(\Gamma)+ysin(\Gamma)}{\Delta}}))}{\partial x} = -\frac{cos(\Gamma)sin^2(\theta)}{\Delta} \tag{2.92}$$

while similarly:

$$\frac{\partial cos(2atan(e^{\frac{(x-q)cos(\Gamma)+ysin(\Gamma)}{\Delta}}))}{\partial y} = -\frac{sin(\Gamma)sin^2(\theta)}{\Delta} \tag{2.93}$$

The final expression of $\nabla\hat{m}_z$ is:

$$\nabla\hat{m}_z = -\frac{cos(\Gamma)sin^2(\theta)}{\Delta}\hat{x} - \frac{sin(\Gamma)sin^2(\theta)}{\Delta}\hat{y} \tag{2.94}$$

The DMI torque is equal to:

$$\vec{\Gamma_{DMI}} = -\mu_0\frac{2D_0}{\mu_0 M_s}\vec{M}\times((\nabla\cdot\hat{m})\hat{z}-\nabla\hat{m}_z) = -2D_0\vec{m}\times((\nabla\cdot\hat{m})\hat{z}-\nabla\hat{m}_z) \tag{2.95}$$

therefore to evaluate the final expression of $\vec{\Gamma_{DMI}}$, the vectorial product must be calculated:

$$\begin{aligned}&\vec{m}\times((\nabla\cdot\hat{m})\hat{z}-\nabla\hat{m}_z) = \\ &= \begin{pmatrix} sin(\theta)cos(\phi) \\ sin(\theta)sin(\phi) \\ cos(\theta)\end{pmatrix} \times \begin{pmatrix} \frac{cos(\Gamma)sin^2(\theta)}{\Delta} \\ \frac{sin(\Gamma)sin^2(\theta)}{\Delta} \\ \frac{cos(\Gamma)sin(\theta)cos(\theta)cos(\phi)}{\Delta} + \frac{sin(\Gamma)sin(\theta)cos(\theta)sin(\phi)}{\Delta}\end{pmatrix} \cdot \begin{pmatrix}\hat{x}\\ \hat{y}\\ \hat{z}\end{pmatrix}\end{aligned} \tag{2.96}$$

$$\begin{aligned}&\vec{m}\times((\nabla\cdot\hat{m})\hat{z}-\nabla\hat{m}_z) = \\ &= \begin{pmatrix} \frac{cos(\Gamma)sin^2(\theta)cos(\theta)sin(\phi)cos(\phi)}{\Delta} - \frac{sin(\Gamma)sin^2(\theta)cos(\theta)cos^2(\phi)}{\Delta} \\ \frac{cos(\Gamma)sin^2(\theta)cos(\theta)}{\Delta} - \frac{cos(\Gamma)sin^2(\theta)cos(\theta)cos^2(\phi)}{\Delta} - \frac{sin(\Gamma)sin^2(\theta)cos(\theta)sin(\phi)cos(\phi)}{\Delta} \\ \frac{sin(\Gamma)sin^3(\theta)cos(\phi)}{\Delta} - \frac{cos(\Gamma)sin^3(\theta)sin(\phi)}{\Delta}\end{pmatrix} \cdot \begin{pmatrix}\hat{x}\\ \hat{y}\\ \hat{z}\end{pmatrix}\end{aligned} \tag{2.97}$$

Now translating equation 2.97 in the tangent base vector:

$$\vec{m} \times ((\nabla \cdot \hat{m})\hat{z} - \nabla \hat{m}_z) = \begin{pmatrix} 0 \\ \frac{sin^2(\theta)}{\Delta}(cos(\Gamma)sin(\phi) - sin(\Gamma)cos(\phi)) \\ 0 \end{pmatrix} \cdot \begin{pmatrix} \hat{e}_r \\ \hat{e}_\theta \\ \hat{e}_\phi \end{pmatrix} \tag{2.98}$$

Final DMI torque moment is:

$$\vec{\Gamma}_{DMI} = -2D_0 \frac{sin^2(\theta)}{\Delta}(cos(\Gamma)sin(\phi) - sin(\Gamma)cos(\phi))\hat{e}_\theta \tag{2.99}$$

2.9 Damping Field

The explicit equation of the damping field was found by Gilbert, as stated before [37]:

$$H_\alpha = \frac{\alpha}{\gamma M_s}\frac{d\vec{M}}{dt} \tag{2.100}$$

The damping torque is defined as:

$$\vec{\Gamma}_{H_\alpha} = \vec{M} \times (\frac{\alpha}{\gamma M_s}\frac{d\vec{M}}{dt}) = \frac{\alpha}{\gamma M_s}(\vec{M} \times \frac{d\vec{M}}{dt}) \tag{2.101}$$

To evaluate the time derivative of the magnetization, it is sufficient to derive over time each component of the magnetization vector as follow:

$$\frac{d\vec{M}}{dt} = \frac{d}{dt}\begin{pmatrix} M_s \cdot sin(\theta(t))cos(\phi(t)) \\ M_s \cdot sin(\theta(t))sin(\phi(t)) \\ M_s \cdot cos(\theta(t)) \end{pmatrix} \tag{2.102}$$

$$\frac{d\vec{M}}{dt} = \begin{pmatrix} M_s(cos(\theta(t))cos(\phi(t))\dot{\theta(t)} - sin(\theta(t))sin(\phi(t))\dot{\phi(t)}) \\ M_s(cos(\theta(t))sin(\phi(t))\dot{\theta(t)} + sin(\theta(t))cos(\phi(t))\dot{\phi(t)}) \\ -M_s sin(\theta(t))\dot{\theta(t)} \end{pmatrix} \tag{2.103}$$

Performing the vectorial product $\vec{M} \times \frac{d\vec{M}}{dt}$:

$$\vec{\Gamma}_{H_\alpha} = \frac{\alpha M_s}{\gamma}\begin{pmatrix} -sin(\phi)\dot{\theta} - sin(\theta)cos(\theta)cos(\phi)\dot{\phi} \\ cos(\phi)\dot{\theta} - sin(\theta)cos(\theta)sin(\phi)\dot{\phi} \\ sin(\theta)^2\dot{\phi} \end{pmatrix} \cdot \begin{pmatrix} \hat{x} \\ \hat{y} \\ \hat{z} \end{pmatrix} \tag{2.104}$$

Transposing $\vec{\Gamma}_\alpha$ in the coordinate base system and dealing with all the calculations, the result is [37]:

$$\vec{\Gamma}_{H_\alpha} = \frac{\alpha M_s}{\gamma} \begin{pmatrix} 0 \\ -\dot{\phi} sin(\theta) \\ \dot{\theta} \end{pmatrix} \cdot \begin{pmatrix} \hat{e}_r \\ \hat{e}_\theta \\ \hat{e}_\phi \end{pmatrix} \tag{2.105}$$

2.10 Adiabatic Spin Transfer Torque (A-STT)

This is the mathematical expression of the adiabatic spin transfer torque (STT) [37]:

$$\vec{\Gamma}_u = -\frac{u}{\gamma}(\hat{j}_e \cdot \nabla)\vec{M} \tag{2.106}$$

There are two approaches to derive the expression of the adiabatic STT: the first one is to calculate the gradient of the vector $\vec{M}$ which is a tensor, and then evaluating the scalar product with $\hat{j}_e$, the second one is to calculate the scalar product between the current vector $\hat{j}_e$ and the ∇ operator. Avoiding the tensor notation will simplify a bit the notation and the calculation. Generalizing the direction of $\hat{j}_e$:

$$\vec{\Gamma}_u = -\frac{u}{\gamma}((\hat{x} + \hat{y} + \hat{z}) \cdot (\frac{\partial}{\partial x}\hat{x} + \frac{\partial}{\partial y}\hat{y} + \frac{\partial}{\partial z}\hat{z}))\vec{M} \tag{2.107}$$

Supposing that the current through the ferromagnetic layer is applied only along the $\hat{x}$ direction:

$$\vec{\Gamma}_u = -\frac{u}{\gamma}((\hat{x}) \cdot (\frac{\partial}{\partial x}\hat{x} + \frac{\partial}{\partial y}\hat{y} + \frac{\partial}{\partial z}\hat{z}))\vec{M} = -\frac{u}{\gamma}\frac{\partial}{\partial x}\vec{M} = -\frac{u}{\gamma}\frac{\partial \vec{M}}{\partial \theta}\frac{\partial \theta}{\partial x} \tag{2.108}$$

The derivative of $\vec{M}$ with respect to θ is equal to:

$$\frac{\partial \vec{M}}{\partial \theta} = M_s \frac{\partial}{\partial \theta} \begin{pmatrix} sin(\theta)cos(\phi) \\ sin(\theta)sin(\phi) \\ cos(\theta) \end{pmatrix} = M_s \begin{pmatrix} cos(\theta)cos(\phi) \\ cos(\theta)sin(\phi) \\ -sin(\theta) \end{pmatrix} = M_s \hat{e}_\theta \tag{2.109}$$

The derivatives of the θ profile with respect to x and y directions are:

$$\begin{cases} \frac{\partial \theta}{\partial x} = \frac{cos(\Gamma)sin(\theta)}{\Delta} \\ \frac{\partial \theta}{\partial y} = \frac{sin(\Gamma)sin(\theta)}{\Delta} \end{cases} \tag{2.110}$$

The final expression of $\vec{\Gamma}_u$ is:

$$\vec{\Gamma}_u = -\frac{uM_s cos(\Gamma)}{\gamma\Delta} sin(\theta)\hat{e}_\theta \tag{2.111}$$

Using the second approach, it is possible to evaluate the general tensor associated to the gradient of the magnetization vector $\vec{M}$. The gradient of a field is defined as the gradient of each component:

$$\nabla\vec{M} = \begin{pmatrix} \nabla sin(\theta(x,y))cos(\phi) \\ \nabla sin(\theta(x,y))sin(\phi) \\ \nabla cos(\theta(x,y)) \end{pmatrix} = \begin{pmatrix} cos(\phi)\nabla sinh(\frac{(x-q)cos(\Gamma)+ysin(\Gamma))}{\Delta} \\ sin(\phi)\nabla sinh(\frac{(x-q)cos(\Gamma)+ysin(\Gamma))}{\Delta} \\ -\nabla tanh(\frac{(x-q)cos(\Gamma)+ysin(\Gamma)}{\Delta}) \end{pmatrix} \tag{2.112}$$

Since $\nabla\vec{M}$ is a tensor each component of the gradient of the magnetization is a vector:

$$\nabla\vec{M} = \begin{pmatrix} cos(\phi)(\frac{cos(\Gamma)sin(\theta)cos(\theta)}{\Delta}\hat{x} + \frac{sin(\Gamma)sin(\theta)cos(\theta)}{\Delta}\hat{y} + 0\hat{z}) \\ sin(\phi)(\frac{cos(\Gamma)sin(\theta)cos(\theta)}{\Delta}\hat{x} + \frac{sin(\Gamma)sin(\theta)cos(\theta)}{\Delta}\hat{y} + 0\hat{z}) \\ -\frac{cos(\Gamma)sin^2(\theta)}{\Delta}\hat{x} - \frac{sin(\Gamma)sin^2(\theta)}{\Delta}\hat{y} + 0\hat{z} \end{pmatrix} \tag{2.113}$$

Writing in tensor notation:

$$\nabla\vec{M} = \bar{D} = \begin{bmatrix} cos(\phi)\frac{cos(\Gamma)sin(\theta)cos(\theta)}{\Delta} & cos(\phi)\frac{sin(\Gamma)sin(\theta)cos(\theta)}{\Delta} & 0 \\ sin(\phi)\frac{cos(\Gamma)sin(\theta)cos(\theta)}{\Delta} & sin(\phi)\frac{sin(\Gamma)sin(\theta)cos(\theta)}{\Delta} & 0 \\ -\frac{cos(\Gamma)sin^2(\theta)}{\Delta} & -\frac{sin(\Gamma)sin^2(\theta)}{\Delta} & 0 \end{bmatrix} \tag{2.114}$$

Making the scalar product of each component with $\hat{j}_e = \hat{x}$ the tensor becomes a vector and through the scalar product with the tangent base vector, the same result of the adiabatic torque evaluated before is obtained. If the current has also a component along $\hat{y}$ direction $\hat{j}_e = \hat{x} + \hat{y}$, the final torque expression will become:

$$\vec{\Gamma}_u = -\frac{uM_s[cos(\Gamma) + sin(\Gamma)]}{\gamma\Delta} sin(\theta)\hat{e}_\theta \tag{2.115}$$

2.11 Non-Adiabatic Spin Transfer Torque (NA-STT)

This is the mathematical expression of the non-adiabatic STT term [37]:

$$\vec{\Gamma}_\beta = \frac{\beta u}{\gamma M_s}\vec{M} \times (\hat{j}_e \cdot \nabla\vec{M}) = \frac{\beta u}{\gamma M_s}\vec{M} \times (\frac{\partial\vec{M}}{\partial\theta}\frac{\partial\theta}{\partial x}) \tag{2.116}$$

$\frac{\partial \vec{M}}{\partial \theta}\frac{\partial \theta}{\partial x}$ is calculated in the previous section A-STT, therefore only the vectorial product and the scalar product with the tangent base vector must be made explicit:

$$\vec{M}\times\frac{\partial \vec{M}}{\partial \theta}\frac{\partial \theta}{\partial x} = M_s\begin{pmatrix} sin(\theta)cos(\phi) \\ sin(\theta)sin(\phi) \\ cos(\theta) \end{pmatrix}\times\begin{pmatrix} 0 \\ \frac{M_s cos(\Gamma)}{\Delta} sin(\theta) \\ 0 \end{pmatrix} = \begin{pmatrix} 0 \\ 0 \\ \frac{M_s^2 cos(\Gamma) sin(\theta)}{\Delta} \end{pmatrix}\cdot\begin{pmatrix} \hat{e}_r \\ \hat{e}_\theta \\ \hat{e}_\phi \end{pmatrix} \tag{2.117}$$

The final expression of the non-adiabatic STT torque is:

$$\vec{\Gamma}_\beta = \frac{\beta u M_s cos(\Gamma) sin(\theta)}{\gamma\Delta}\hat{e}_\phi \tag{2.118}$$

2.12 Spin Orbit Torque

In section 2.5 the Spin Orbit Torque is expressed in the CGS system, therefore $\mu_0 = 1$. In the following subsection, it will be expressed in the International System of Units (SI) for clarity. The torque exerted on the domain wall due to the spin orbit torque effect is therefore equal to:

$$\vec{\tau}_{SOT} = \mu_0 M_s a_{FL}(\hat{m}\times\hat{\sigma}) + \mu_0 M_s b_{DL}\hat{m}\times(\hat{m}\times\hat{\sigma}) \tag{2.119}$$

where $\hat{\sigma}$ is:

$$\hat{\sigma} = \hat{J}_{SOT}\times\hat{n} \tag{2.120}$$

$\hat{n}$ is the normal unit vector with respect to the ferromagnetic layer, while $\hat{J}_{SOT}$ is the direction of the current flowing through the heavy metal layer. $\hat{\sigma}$ direction could be generalized as a combination of sine and cosine function, but usually, especially in the case of thin layers, it is parallel to $\hat{y}$ direction. Therefore $\hat{\sigma} = \hat{y}$.

2.12.1 Field Like Torque

Field like torque component is expressed by the following equation:

$$\vec{\tau}_{FL} = \mu_0 M_s a_{FL}(\hat{m}\times\hat{\sigma}) \tag{2.121}$$

Starting with the vectorial product calculation:

$$\hat{m}\times\hat{\sigma} = \begin{pmatrix} sin(\theta)cos(\phi) \\ sin(\theta)sin(\phi) \\ cos(\theta) \end{pmatrix}\times\begin{pmatrix} 0 \\ 1 \\ 0 \end{pmatrix} = \begin{pmatrix} -cos(\theta) \\ 0 \\ sin(\theta)cos(\phi) \end{pmatrix}\cdot\begin{pmatrix} \hat{x} \\ \hat{y} \\ \hat{z} \end{pmatrix} \tag{2.122}$$

projecting on the tangent base system:

$$\hat{m} \times \hat{\sigma} = \begin{pmatrix} 0 \\ -cos(\phi) \\ cos(\theta)sin(\phi) \end{pmatrix} \cdot \begin{pmatrix} \hat{e}_r \\ \hat{e}_\theta \\ \hat{e}_\phi \end{pmatrix} \tag{2.123}$$

Therefore:

$$\vec{\tau}_{FL} = \mu_0 M_s a_{FL}(\hat{m} \times \hat{\sigma}) = -\mu_0 M_s a_{FL} \begin{pmatrix} 0 \\ cos(\phi) \\ -cos(\theta)sin(\phi) \end{pmatrix} \cdot \begin{pmatrix} \hat{e}_r \\ \hat{e}_\theta \\ \hat{e}_\phi \end{pmatrix} \tag{2.124}$$

the parameter a_{FL} in SI is equal to:

$$a_{FL} = \frac{\hbar \alpha_{h,FL} J_{SOT}}{2\mu_0 e M_s t_{FM}} \tag{2.125}$$

where $\hbar$ is the Planck constant divided by 2π, α_h is a factor of intensity related to the Damping Like Torque (it is the ratio between the Spin Current and the Current that goes through the heavy metal), e is the electron charge, and t_{FM} is the thickness of the ferromagnetic layer.

2.12.2 Damping Like Torque

Slonczewski like torque or damping like torque component is expressed by the following equation:

$$\vec{\tau}_{DL} = \mu_0 M_s b_{DL} \hat{m} \times (\hat{m} \times \hat{\sigma}) \tag{2.126}$$

$\hat{m} \times \hat{\sigma}$ is calculated in the previous section, and it can be exploited to evaluate $\hat{m} \times (\hat{m} \times \hat{\sigma})$:

$$\hat{m} \times (\hat{m} \times \hat{\sigma}) = \begin{pmatrix} sin(\theta)cos(\phi) \\ sin(\theta)sin(\phi) \\ cos(\theta) \end{pmatrix} \times \begin{pmatrix} -cos(\theta) \\ 0 \\ sin(\theta)cos(\phi) \end{pmatrix} \tag{2.127}$$

$$\hat{m} \times (\hat{m} \times \hat{\sigma}) = \begin{pmatrix} sin^2(\theta)sin(\phi)cos(\phi) \\ -sin^2(\theta)cos^2(\phi) - cos^2(\theta) \\ sin(\theta)cos(\theta)sin(\phi) \end{pmatrix} \cdot \begin{pmatrix} \hat{x} \\ \hat{y} \\ \hat{z} \end{pmatrix} \tag{2.128}$$

Projecting on the tangent base system:

$$\hat{m} \times (\hat{m} \times \hat{\sigma}) = \begin{pmatrix} 0 \\ -cos(\theta)sin(\phi) \\ -cos(\phi) \end{pmatrix} \cdot \begin{pmatrix} \hat{e}_r \\ \hat{e}_\theta \\ \hat{e}_\phi \end{pmatrix} \tag{2.129}$$

The final expression of the Damping Like Torque is:

$$\vec{\tau}_{DL} = \mu_0 M_s b_{DL} \begin{pmatrix} 0 \\ -cos(\theta)sin(\phi) \\ -cos(\phi) \end{pmatrix} \cdot \begin{pmatrix} \hat{e}_r \\ \hat{e}_\theta \\ \hat{e}_\phi \end{pmatrix} = -\mu_0 M_s b_{DL} \begin{pmatrix} 0 \\ cos(\theta)sin(\phi) \\ cos(\phi) \end{pmatrix} \cdot \begin{pmatrix} \hat{e}_r \\ \hat{e}_\theta \\ \hat{e}_\phi \end{pmatrix} \tag{2.130}$$

the expression of b_{DL} in SI is:

$$b_{DL} = \frac{\hbar \alpha_{h,DL} J_{SOT}}{2\mu_0 e M_s t_{FM}} \tag{2.131}$$

where $\hbar$ is the Planck constant divided by 2π, α_h is a factor of intensity related to the Damping Like Torque (it is the ratio between the Spin Current and the Current that goes through the heavy metal layer), e is the electron charge, and t_{FM} is the thickness of the ferromagnetic layer.

2.13 Modelling of a Gate of different anisotropy

In this section an analytical description of a "Gate" of different anisotropy is proposed. As previously explained the motion of the Domain Walls (DWs) along the track can be synchronized thanks to the presence of periodical gates through which a specific voltage is applied to locally change the anisotropy value. Practically periodical potential barrier of anisotropy are created, and in this way the DWs are blocked if the strength of the torque exerted on the DWs themselves is not sufficiently high, in other words it is possible to establish a threshold current, above which the DW crosses the gate. The idea consists in modelling the presence of a gate as an effective field that acts on the DW as an external field along the perpendicular direction ("z" direction). To find an analytical expression of the effective field, we must start by defining the energy density of a domain wall:

$$\begin{aligned}\sigma_{DW}(q) = \int_{-\infty}^{+\infty} A|\nabla m|^2 dx + \int_{-\infty}^{+\infty} D(m_z \nabla \vec{m} - (\vec{m}\cdot\nabla)m_z)dx + \\ + \int_{-\infty}^{+\infty} [K_u(x) + k_d sin^2(\phi - \Gamma)] sin^2(\theta(x))dx\end{aligned} \tag{2.132}$$

Dealing with all the integrals:

$$\begin{aligned}\sigma_{DW}(q) = \frac{2A}{\Delta}[\frac{1}{cos(\Gamma)} + 2sin(\Gamma)] + \frac{\pi D}{cos(\Gamma)} cos(\phi - \Gamma) + \\ + \frac{2\Delta}{cos(\Gamma)} k_d sin^2(\phi - \Gamma) + \int_{-\infty}^{+\infty} K_u(x) sin^2(\theta(x))dx\end{aligned} \tag{2.133}$$

The objective is to find a function which describes the behaviour of an anisotropy barrier profile, and which at the same time is integrable when multiplied by $sin^2(\theta(x))$ with a final analytical expression. θ is supposed to be only a function of $'x'$, therefore the tilting profile of the domain wall is not taken in consideration also because it is negligible for the integral computation. The expression of θ is therefore:

$$\theta = 2arctan(e^{\frac{x-q}{\Delta}}) \tag{2.134}$$

The integral of the anisotropy energy density can be rewritten as follow:

$$\int_{-\infty}^{+\infty} K_u(x) sech^2(\frac{x-q}{\Delta})dx \tag{2.135}$$

A function that describes in a very satisfactory way the anisotropic profile of a VCMA gate and that can be integrated when multiplied by the $sech^2(\frac{x-q}{\Delta})$

giving back a closed analytical form is the following:

$$K_u(x) = K_u + \frac{\Delta K_u}{2}[tanh(\frac{x + c + \frac{w}{2}}{\delta}) - tanh(\frac{x + c - \frac{w}{2}}{\delta})] \qquad (2.136)$$

In the above equation ΔK_u is the anisotropy variation of the gate with respect to the anisotropy of the track, or in other words $\Delta K_u = K_{u,gate} - K_{u,track}$, $'c'$ is the center of the "Gate", $'w'$ is the width of the gate, while δ is the parameter which establishes the sharpness of the anisotropy barrier profile. δ will establish how abrupt is the rising and falling edges of the anisotropy barrier, it is nothing else that a submultiple of the "gradient length" of the edge profile. Since the edge profile of a *tanh* function behaves like an exponential one, after more or less 2δ starting from the center $'c'$ of the edge (which corresponds to the 50% of the quote) the *tanh* function reaches more or less the 90% of the quote of the barrier (approximately evaluated as $\approx (1 - e^{-2})$), therefore starting from the 10% of the quote 4δ are necessary to reach the 90% of the quote. 4δ is therefore the value of the gradient length which normally is evaluated as the abscissa difference between the two points associated respectively to the 90% and to the 10% of the quote of the rising or falling edge.

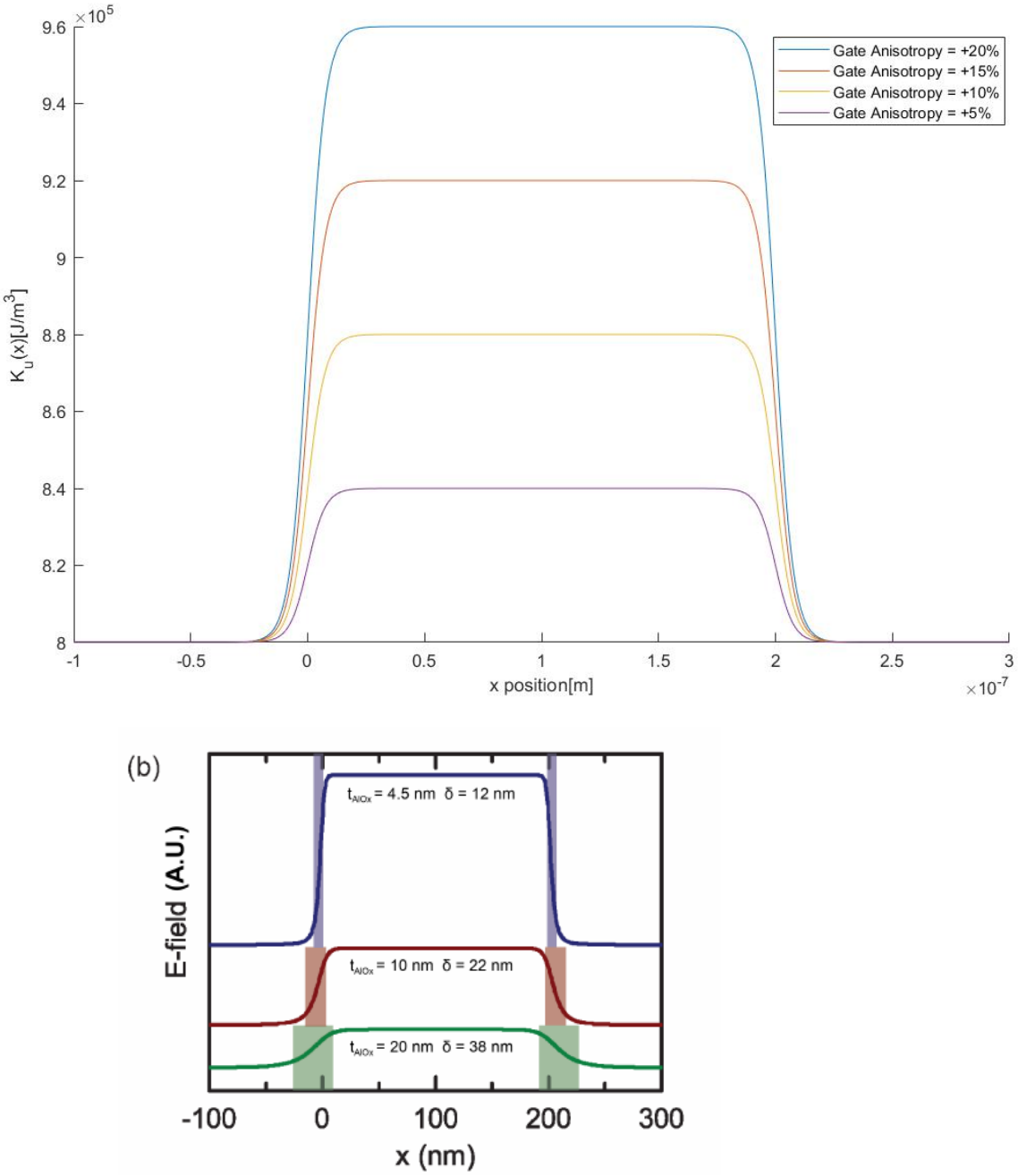

Figure 2.2: On the top side the plot of equation 2.136, on the lower side the plot of a typical experimental profile of the Electric Field across the Gate evaluated by COMSOL, as reported in [29]. The anisotropy profile and the electric field profile can be compared indistinguishably because they differ only by a multiplicative constant

Whichever δ is chosen, the integral is solvable, but to obtain an easy final analytical expression it is convenient to choose δ equal to the width of the domain wall: $\delta = \Delta$.
This choice is very smart because in addition to simplify the final analytical expression, it establishes a gradient length compatible with the most common experimental gradient lengths. Usually the experimental gradient lengths are in the range between few nanometers until 40-50 nm depending on the quality of the oxide and on the width of the gate. Being Δ equal to more or less 5 nm, 4Δ correspond to more or less 20 nm which is a very satisfactory value. The analytical expression of the anisotropy profile could be rewritten as follow:

$$K_u(x) = K_u + \frac{\Delta K_u}{2}[tanh(\frac{x+c+\frac{w}{2}}{\Delta}) - tanh(\frac{x+c-\frac{w}{2}}{\Delta})] \tag{2.137}$$

The integral of the anisotropy energy density is therefore equal to:

$$\sigma_{DW_{K_u}}(q) = \int_{-\infty}^{+\infty}(K_u+\frac{\Delta K_u}{2}[tanh(\frac{x+c+\frac{w}{2}}{\Delta})-tanh(\frac{x+c-\frac{w}{2}}{\Delta})])sech^2(\frac{x-q}{\Delta})dx \tag{2.138}$$

The integral can be splitted in the sum of two integrals:

$$\begin{aligned}\sigma_{DW_{K_u}}(q) = &\int_{-\infty}^{+\infty} K_u sech^2(\frac{x-q}{\Delta})+ \\ &+ \int_{-\infty}^{+\infty} \frac{\Delta K_u}{2}[tanh(\frac{x+c+\frac{w}{2}}{\Delta}) - tanh(\frac{x+c-\frac{w}{2}}{\Delta})]sech^2(\frac{x-q}{\Delta})dx\end{aligned} \tag{2.139}$$

$$\sigma_{DW_{K_u}}(q) = \frac{2\Delta}{cos(\Gamma)}K_u+\int_{-\infty}^{+\infty} \frac{\Delta K_u}{2}[tanh(\frac{x+c+\frac{w}{2}}{\Delta})-tanh(\frac{x+c-\frac{w}{2}}{\Delta})]sech^2(\frac{x-q}{\Delta})dx \tag{2.140}$$

Now dealing with the integral:

$$\begin{aligned}&\int_{-\infty}^{+\infty} \frac{\Delta K_u}{2}[tanh(\frac{x+c+\frac{w}{2}}{\Delta}) - tanh(\frac{x+c-\frac{w}{2}}{\Delta})]sech^2(\frac{x-q}{\Delta})dx = \\ &= \int_{-\infty}^{+\infty} \frac{\Delta K_u}{2}tanh(\frac{x+c+\frac{w}{2}}{\Delta})sech^2(\frac{x-q}{\Delta})dx+ \\ &- \int_{-\infty}^{+\infty} \frac{\Delta K_u}{2}tanh(\frac{x+c-\frac{w}{2}}{\Delta})]sech^2(\frac{x-q}{\Delta})dx\end{aligned} \tag{2.141}$$

The following parameters are defined to simplify the integral:

$$\begin{cases} c' \coloneqq \frac{c+\frac{w}{2}}{\Delta} \\ c'' \coloneqq \frac{c-\frac{w}{2}}{\Delta} \\ q' \coloneqq \frac{q}{\Delta} \end{cases} \tag{2.142}$$

The general solution of the indefinite integral is:

$$\begin{aligned}
&\int \frac{\Delta K_u}{2} tanh(\frac{x}{\Delta}+c')sech^2(\frac{x}{\Delta}-q')dx - \int \frac{\Delta K_u}{2} tanh(\frac{x}{\Delta}+c'')sech^2(\frac{x}{\Delta}-q')dx = \\
&= \Delta[csch^2(c'+q')(log(cosh(q'-\frac{x}{\Delta}))-log(cosh(c'+\frac{x}{\Delta}))]+ \\
&+ \Delta[sech(q')cotanh(c'+q')sinh(\frac{x}{\Delta})sech(q'-\frac{x}{\Delta})]+ \\
&- \Delta[csch^2(c''+q')(log(cosh(q'-\frac{x}{\Delta}))-log(cosh(c''+\frac{x}{\Delta}))]+ \\
&- \Delta[sech(q')cotanh(c''+q')sinh(\frac{x}{\Delta})sech(q'-\frac{x}{\Delta})]
\end{aligned} \tag{2.143}$$

Studying the integral from $-\infty$ to $+\infty$:

$$\begin{aligned}
\sigma_{DW_{K_u}}(q) = &\frac{\Delta K_u}{2}\Delta[-2(c'+\frac{q}{\Delta})csch^2(c'+\frac{q}{\Delta})+2cotanh(c'+\frac{q}{\Delta})]+ \\
&-\frac{\Delta K_u}{2}\Delta[-2(c''+\frac{q}{\Delta})csch^2(c''+\frac{q}{\Delta})+2cotanh(c''+\frac{q}{\Delta})]
\end{aligned} \tag{2.144}$$

Therefore the final expression of the energy density of the domain wall in the presence of an anisotropy barrier is:

$$\begin{aligned}
\sigma_{DW}(q) = &\frac{2A}{\Delta}[\frac{1}{cos(\Gamma)}+2sin(\Gamma)]+\frac{\pi D}{cos(\Gamma)}cos(\phi-\Gamma)+\frac{2\Delta}{cos(\Gamma)}k_d sin^2(\phi-\Gamma)+ \\
&+\frac{\Delta K_u}{2}\Delta[-2(c'+\frac{q}{\Delta})csch^2(c'+\frac{q}{\Delta})+2cotanh(c'+\frac{q}{\Delta})]+ \\
&-\frac{\Delta K_u}{2}\Delta[-2(c''+\frac{q}{\Delta})csch^2(c''+\frac{q}{\Delta})+2cotanh(c''+\frac{q}{\Delta})]
\end{aligned} \tag{2.145}$$

The effective field associated to the anisotropy barrier is a pinning field. We must start from the hypothesis that the depinning of the DW takes place as soon as the energy barrier is canceled out by the Zeeman energy, therefore by setting the following expression to zero it will be possible to obtain a final analytical expression for the pinning field [29]:

$$\frac{d}{dq}[\sigma_{DW}(q)+2\mu_0 M_s H q] \tag{2.146}$$

Therefore [29]:

$$H_{pin} = \frac{-\frac{d}{dq}\sigma_{DW}}{2\mu_0 M_s} \tag{2.147}$$

The derivative of the energy density of the domain wall with respect to $'q'$ (which is a function of time: $q(t)$) which is the position of the center of the domain wall is equal to:

$$\begin{aligned}\frac{d\sigma_{DW}(q)}{dq} &= \frac{d}{dq}(\frac{\Delta K_u}{2}\Delta[-2(c'+\frac{q}{\Delta})csch^2(c'+\frac{q}{\Delta})+2cotanh(c'+\frac{q}{\Delta})])+\\ &-\frac{d}{dq}(\frac{\Delta K_u}{2}\Delta[-2(c''+\frac{q}{\Delta})csch^2(c''+\frac{q}{\Delta})+2cotanh(c''+\frac{q}{\Delta})]) =\\ &\frac{\Delta K_u}{2}[4csch^2(c'+\frac{q}{\Delta})((c'+\frac{q}{\Delta})coth(c'+\frac{q}{\Delta})-1)]+\\ &-\frac{\Delta K_u}{2}[4csch^2(c''+\frac{q}{\Delta})((c''+\frac{q}{\Delta})coth(c''+\frac{q}{\Delta})-1)]\end{aligned} \tag{2.148}$$

The final expression of the pinning field is therefore:

$$H_{pin} = \frac{\Delta K_u}{2}\frac{4csch^2(c''+\frac{q}{\Delta})((c''+\frac{q}{\Delta})coth(c''+\frac{q}{\Delta})-1)-4csch^2(c'+\frac{q}{\Delta})((c'+\frac{q}{\Delta})coth(c'+\frac{q}{\Delta})-1)}{2\mu_0 M_s} \tag{2.149}$$

with $c' = \frac{c+\frac{w}{2}}{\Delta}$ and $c'' = \frac{c-\frac{w}{2}}{\Delta}$.

2.14 Final differential equation

Exploiting the Kinetic Theorem:

$$\begin{cases} \dot{\theta} = \frac{\gamma}{M_s}\Gamma_\theta \\ \dot{\phi}sin(\theta) = \frac{\gamma}{M_s}\Gamma_\phi \\ \gamma = -\frac{e}{2m} \end{cases} \tag{2.150}$$

where e is the absolute value of the electron charge. These are all the torque components evaluated in chapter 2:

$$\begin{cases} \vec{\Gamma}_{ext} = -\mu_0 M_s H_{ext} sin(\theta)\hat{e}_\phi \\ \vec{\Gamma}_{ex} = \frac{2A_{ex}}{\Delta^2} sin(\theta)cos(\theta)\hat{e}_\phi \\ \vec{\Gamma}_{DMI} = -\frac{2D_0}{\Delta} sin^2(\theta)[cos(\Gamma)sin(\phi) - sin(\Gamma)cos(\phi)]\hat{e}_\theta \\ \vec{\Gamma}_{K_d} = 2K_d \begin{pmatrix} 0 \\ sin(\theta)sin(\phi-\Gamma)cos(\phi-\Gamma) \\ sin(\theta)cos(\theta)cos^2(\phi-\Gamma) \end{pmatrix} \cdot \begin{pmatrix} \hat{e}_r \\ \hat{e}_\theta \\ \hat{e}_\phi \end{pmatrix} \\ \vec{\Gamma}_{K_{eff}} = \begin{pmatrix} 0 \\ 0 \\ 2K_u sin(\theta)cos(\theta) - \mu_0 M_s^2 sin(\theta)cos(\theta) \end{pmatrix} \cdot \begin{pmatrix} \hat{e}_r \\ \hat{e}_\theta \\ \hat{e}_\phi \end{pmatrix} \\ \vec{\Gamma}_{H_\alpha} = \frac{\alpha M_s}{\gamma} \begin{pmatrix} 0 \\ -\dot{\phi}sin(\theta) \\ \dot{\theta} \end{pmatrix} \cdot \begin{pmatrix} \hat{e}_r \\ \hat{e}_\theta \\ \hat{e}_\phi \end{pmatrix} \\ \vec{\Gamma}_u = -\frac{uM_s cos(\Gamma)}{\gamma\Delta} sin(\theta)\hat{e}_\theta \\ \vec{\Gamma}_\beta = \frac{\beta u M_s cos(\Gamma)}{\gamma\Delta} sin(\theta)\hat{e}_\phi \\ \vec{\tau}_{FL} = -\mu_0 M_s a_{FL} \begin{pmatrix} 0 \\ cos(\phi) \\ -cos(\theta)sin(\phi) \end{pmatrix} \cdot \begin{pmatrix} \hat{e}_r \\ \hat{e}_\theta \\ \hat{e}_\phi \end{pmatrix} \\ \vec{\tau}_{DL} = -\mu_0 M_s b_{DL} \begin{pmatrix} 0 \\ cos(\theta)sin(\phi) \\ cos(\phi) \end{pmatrix} \cdot \begin{pmatrix} \hat{e}_r \\ \hat{e}_\theta \\ \hat{e}_\phi \end{pmatrix} \end{cases} \tag{2.151}$$

Dividing all the torque terms in $\hat{e}_\theta$ and $\hat{e}_\phi$ components:

$$\begin{cases} \Gamma_\theta = -\frac{2D_0}{\Delta} sin^2(\theta)[cos(\Gamma)sin(\phi) - sin(\Gamma)cos(\phi)] + \\ \quad + 2K_d sin(\theta)sin(\phi-\Gamma)cos(\phi-\Gamma) - \frac{\alpha M_s}{\gamma}\dot{\phi}sin(\theta) + \\ \quad - \frac{uM_s cos(\Gamma)}{\gamma\Delta} sin(\theta) - \mu_0 M_s a_{FL} cos(\phi) - \mu_0 M_s b_{DL} cos(\theta) sin(\phi) \\ \Gamma_\phi = \frac{2A_{ex}}{\Delta^2} sin(\theta)cos(\theta) - \mu_0 M_s H_{ext} sin(\theta) + 2K_u sin(\theta)cos(\theta) + \\ \quad + 2K_d sin(\theta)cos(\theta)cos^2(\phi-\Gamma) - \mu_0 M_s^2 N_z sin(\theta)cos(\theta) + \\ \quad + \frac{\alpha M_s}{\gamma}\dot{\theta} + \frac{\beta u M_s cos(\Gamma)}{\gamma\Delta} sin(\theta) + \mu_0 M_s a_{FL} cos(\theta) sin(\phi) - \mu_0 M_s b_{DL} cos(\phi) \end{cases} \tag{2.152}$$

Exploiting the general Kinetic Theorem (2.150), the differential equation system becomes:

$$\begin{cases} \dot{\theta} = -\frac{2\gamma D_0}{M_s\Delta} sin^2(\theta)[cos(\Gamma)sin(\phi) - sin(\Gamma)cos(\phi)] + \\ \quad + \frac{2\gamma K_d}{M_s} sin(\theta)sin(\phi-\Gamma)cos(\phi-\Gamma) + \\ \quad - \alpha\dot{\phi}sin(\theta) - \frac{u\cdot cos(\Gamma)}{\Delta} sin(\theta) - \gamma\mu_0 a_{FL} cos(\phi) - \gamma\mu_0 b_{DL} cos(\theta) sin(\phi) \\ \dot{\phi}sin(\theta) = \frac{2\gamma A_{ex}}{M_s\Delta^2} sin(\theta)cos(\theta) - \mu_0\gamma H_{ext} sin(\theta) + \frac{2\gamma K_{eff}}{M_s} sin(\theta)cos(\theta) + \\ \quad + \frac{2\gamma K_d}{M_s} sin(\theta)cos(\theta)cos^2(\phi-\Gamma) + \alpha\dot{\theta} + \\ \quad + \frac{\beta u\cdot cos(\Gamma)}{\Delta} sin(\theta) + \gamma\mu_0 a_{FL} cos(\theta) sin(\phi) - \gamma\mu_0 b_{DL} cos(\phi) \end{cases} \tag{2.153}$$

Then $\dot{\theta}$ is replaced with:

$$\dot{\theta} = (-\frac{cos(\Gamma)}{\Delta}\dot{q} + \frac{(q-x)sin(\Gamma) + ycos(\Gamma)}{\Delta}\dot{\Gamma} - \frac{(x-q)cos(\Gamma) + ysin(\Gamma)}{\Delta^2}\dot{\Delta})sin(\theta) \tag{2.154}$$

$\dot{\theta}$ can be rewritten as follow:

$$\dot{\theta} = (-\frac{cos(\Gamma)}{\Delta}\dot{q} + \frac{y - \Delta sin(\Gamma) ln(tan(\frac{\theta}{2}))}{\Delta cos(\Gamma)}\dot{\Gamma} - \frac{ln(tan(\frac{\theta}{2}))}{\Delta}\dot{\Delta})sin(\theta) \tag{2.155}$$

In the differential equation system the anisotropy constant K_{eff} is equal to $K_u - \frac{1}{2}\mu_0 M_s^2$ as previously defined is section 2.7.5 and K_u is the sum of the

volume and of the surface contribution:

$$K_u = K_{vol} + \frac{K_i}{t_{FM}} \tag{2.156}$$

where t_{FM} is the thickness of the ferromagnetic layer. Considering that the thickness of the ferromagnetic layer is nanometric, the anisotropy constant is dominated by the interfacial component. To solve the differential equation system, the two differential equation must be integrated over θ and then over y. Initially $\dot{\theta}$ must be replaced with equation 2.155:

$$\begin{cases} -\frac{cos(\Gamma)}{\Delta}\dot{q}sin(\theta) = -\frac{y-\Delta sin(\Gamma)ln(tan(\frac{\theta}{2}))}{\Delta cos(\Gamma)}\dot{\Gamma}sin(\theta) + \frac{ln(tan(\frac{\theta}{2}))}{\Delta}\dot{\Delta}sin(\theta) + \\ \qquad -\frac{2\gamma D_0}{M_s\Delta}sin^2(\theta)[cos(\Gamma)sin(\phi) - sin(\Gamma)cos(\phi)] + \\ \qquad +\frac{\gamma K_d}{M_s}sin(\theta)sin(2(\phi-\Gamma)) - \alpha\dot{\phi}sin(\theta) + \\ \qquad -\frac{u\cdot cos(\Gamma)}{\Delta}sin(\theta) - \gamma\mu_0 a_{FL}cos(\phi) - \gamma\mu_0 b_{DL}cos(\theta)sin(\phi) \\ \dot{\phi}sin(\theta) = \frac{2\gamma A_{ex}}{M_s\Delta^2}sin(\theta)cos(\theta) - \mu_0\gamma H_{ext}sin(\theta) + \frac{2\gamma K_{eff}}{M_s}sin(\theta)cos(\theta) + \\ \qquad +\frac{2\gamma K_d}{M_s}sin(\theta)cos(\theta)cos^2(\phi-\Gamma) + \\ \qquad +\alpha(-\frac{cos(\Gamma)}{\Delta}\dot{q} + \frac{y-\Delta sin(\Gamma)ln(tan(\frac{\theta}{2}))}{\Delta cos(\Gamma)}\dot{\Gamma} - \frac{ln(tan(\frac{\theta}{2}))}{\Delta}\dot{\Delta})sin(\theta) + \\ \qquad +\frac{\beta u\cdot cos(\Gamma)}{\Delta}sin(\theta) + \gamma\mu_0 a_{FL}cos(\theta)sin(\phi) - \gamma\mu_0 b_{DL}cos(\phi) \end{cases} \tag{2.157}$$

Integrating both member of each differential equation with respect to θ:

$$\begin{cases} -\int_0^\pi \frac{cos(\Gamma)}{\Delta}\dot{q}sin(\theta)\,d\theta = -\int_0^\pi \frac{y-\Delta sin(\Gamma)ln(tan(\frac{\theta}{2}))}{\Delta cos(\Gamma)}\dot{\Gamma}sin(\theta)\,d\theta + \\ \qquad + \int_0^\pi \frac{ln(tan(\frac{\theta}{2}))}{\Delta}\dot{\Delta}sin(\theta)\,d\theta + \\ \qquad - \int_0^\pi \frac{2\gamma D_0}{M_s\Delta}sin^2(\theta)[cos(\Gamma)sin(\phi)-sin(\Gamma)cos(\phi)]\,d\theta + \\ \qquad + \int_0^\pi \frac{\gamma K_d}{M_s}sin(\theta)sin(2(\phi-\Gamma))\,d\theta + \\ \qquad - \int_0^\pi \alpha\dot{\phi}sin(\theta)\,d\theta - \int_0^\pi \frac{u\cdot cos(\Gamma)}{\Delta}sin(\theta)\,d\theta + \\ \qquad - \int_0^\pi \gamma\mu_0 a_{FL}cos(\phi)\,d\theta - \int_0^\pi \gamma\mu_0 b_{DL}cos(\theta)sin(\phi)\,d\theta \\ \int_0^\pi \dot{\phi}sin(\theta)\,d\theta = \int_0^\pi \frac{2\gamma A_{ex}}{M_s\Delta^2}sin(\theta)cos(\theta)\,d\theta - \int_0^\pi \mu_0\gamma H_{ext}sin(\theta)\,d\theta + \\ \qquad + \int_0^\pi \frac{2\gamma K_{eff}}{M_s}sin(\theta)cos(\theta)\,d\theta + \\ \qquad + \int_0^\pi \frac{2\gamma K_d}{M_s}sin(\theta)cos(\theta)cos^2(\phi-\Gamma)\,d\theta + \\ \qquad + \int_0^\pi \alpha(-\frac{cos(\Gamma)}{\Delta}\dot{q} + \frac{y-\Delta sin(\Gamma)ln(tan(\frac{\theta}{2}))}{\Delta cos(\Gamma)}\dot{\Gamma})sin(\theta)\,d\theta + \\ \qquad - \int_0^\pi \alpha\frac{ln(tan(\frac{\theta}{2}))}{\Delta}sin(\theta)\dot{\Delta}\,d\theta + \int_0^\pi \frac{\beta u\cdot cos(\Gamma)}{\Delta}sin(\theta)\,d\theta + \\ \qquad + \int_0^\pi \gamma\mu_0 a_{FL}cos(\theta)sin(\phi)\,d\theta - \int_0^\pi \gamma\mu_0 b_{DL}cos(\phi)\,d\theta \end{cases} \tag{2.158}$$

Exploiting the results of the following integrals:

$$\begin{cases} \int_0^\pi cos(\theta)\,d\theta = 0; \\ \int_0^\pi sin(\theta)\,d\theta = 2; \\ \int_0^\pi sin(\theta)cos(\theta)\,d\theta = 0; \\ \int_0^\pi sin^2(\theta)\,d\theta = \pi; \\ \int_0^\pi ln(tan(\frac{\theta}{2}))sin(\theta)\,d\theta = 0; \end{cases} \tag{2.159}$$

The differential equation system could be rewritten:

$$\begin{cases} \dfrac{cos(\Gamma)}{\Delta}\dot{q} = \dfrac{y}{\Delta cos(\Gamma)}\dot{\Gamma} + \dfrac{\pi\gamma D_0}{2M_s\Delta}sin(\phi-\Gamma) - \dfrac{\gamma K_d}{M_s}sin(2(\phi-\Gamma)) + \alpha\dot{\phi} + \\ \qquad\qquad + \dfrac{u\cdot cos(\Gamma)}{\Delta} + \gamma\dfrac{\pi}{2}\mu_0 a_{FL}cos(\phi) \\ \dot{\phi} = -\mu_0\gamma H_{ext} - \alpha\dfrac{cos(\Gamma)}{\Delta}\dot{q} + \alpha\dfrac{y}{\Delta cos(\Gamma)}\dot{\Gamma} + \dfrac{\beta u\cdot cos(\Gamma)}{\Delta} - \dfrac{\pi}{2}\gamma\mu_0 b_{DL}cos(\phi) \end{cases} \tag{2.160}$$

To obtain the final differential system, the two differential equation must be integrated along "y" direction:

$$\begin{cases} \displaystyle\int_0^w \frac{cos(\Gamma)}{\Delta}\dot{q}\,dy = \int_0^w \frac{y}{\Delta cos(\Gamma)}\dot{\Gamma}\,dy + \int_0^w \frac{\pi\gamma D_0}{2M_s\Delta}sin(\phi-\Gamma)\,dy + \\ \qquad\qquad - \displaystyle\int_0^w \frac{\gamma K_d}{M_s}sin(2(\phi-\Gamma))\,dy + \int_0^w \alpha\dot{\phi}\,dy + \int_0^w \frac{u\cdot cos(\Gamma)}{\Delta}\,dy + \\ \qquad\qquad + \displaystyle\int_0^w \gamma\frac{\pi}{2}\mu_0 a_{FL}cos(\phi)\,dy \\ \displaystyle\int_0^w \dot{\phi}\,dy = -\int_0^w \mu_0\gamma H_{ext}\,dy - \int_0^w \alpha\frac{cos(\Gamma)}{\Delta}\dot{q}\,dy + \int_0^w \alpha\frac{y}{\Delta cos(\Gamma)}\dot{\Gamma}\,dy + \\ \qquad\qquad + \displaystyle\int_0^w \frac{\beta u\cdot cos(\Gamma)}{\Delta}\,dy - \int_0^w \gamma\frac{\pi}{2}\mu_0 b_{DL}cos(\phi)\,dy \end{cases} \tag{2.161}$$

Now replacing $\int_0^w dy = w$ and $\int_0^w y\,dy = \frac{w^2}{2}$, and dividing both member by w:

$$\begin{cases} \dfrac{cos(\Gamma)}{\Delta}\dot{q} = \dfrac{w}{2\Delta cos(\Gamma)}\dot{\Gamma} + \dfrac{\pi\gamma D_0}{2M_s\Delta}sin(\phi-\Gamma) - \dfrac{\gamma K_d}{M_s}sin(2(\phi-\Gamma)) + \alpha\dot{\phi} + \\ \qquad\qquad + \dfrac{u\cdot cos(\Gamma)}{\Delta} + \gamma\dfrac{\pi}{2}\mu_0 a_{FL}cos(\phi) \\ \dot{\phi} = -\mu_0\gamma H_{ext} - \alpha\dfrac{cos(\Gamma)}{\Delta}\dot{q} + \alpha\dfrac{w}{2\Delta cos(\Gamma)}\dot{\Gamma} + \dfrac{\beta u\cdot cos(\Gamma)}{\Delta} - \gamma\dfrac{\pi}{2}\mu_0 b_{DL}cos(\phi) \end{cases} \tag{2.162}$$

The differential equation system is composed by two coupled differential equations. Replacing the second differential equation inside the first one

and viceversa:

$$\begin{cases} \dot{q} = \frac{\frac{w}{2\Delta cos(\Gamma)}(1+\alpha^2)\dot{\Gamma} + \frac{\pi\gamma D_0}{2M_s\Delta}sin(\phi-\Gamma) - \frac{\gamma K_d}{M_s}sin(2(\phi-\Gamma)) + \frac{u\cdot cos(\Gamma)}{\Delta}}{\frac{cos(\Gamma)}{\Delta}(1+\alpha^2)} + \\ \quad + \frac{\gamma\frac{\pi}{2}\mu_0 a_{FL}cos(\phi) + \frac{\alpha\beta u}{\Delta}cos(\Gamma) - \alpha\mu_0\gamma H_{ext} - \alpha\gamma\frac{\pi}{2}\mu_0 b_{DL}cos(\phi)}{\frac{cos(\Gamma)}{\Delta}(1+\alpha^2)} \\ \dot{\phi} = -\mu_0\gamma H_{ext} + \alpha\frac{w}{2\Delta cos(\Gamma)}\dot{\Gamma} + \frac{\beta u\cdot cos(\Gamma)}{\Delta} - \gamma\frac{\pi}{2}\mu_0 b_{DL}cos(\phi) + \\ \quad - \alpha\frac{cos(\Gamma)}{\Delta}[\frac{\frac{w}{2\Delta cos(\Gamma)}(1+\alpha^2)\dot{\Gamma} + \frac{\pi\gamma D_0}{2M_s\Delta}sin(\phi-\Gamma) - \frac{\gamma K_d}{M_s}sin(2(\phi-\Gamma))}{\frac{cos(\Gamma)}{\Delta}(1+\alpha^2)} + \\ \quad + \frac{\frac{u\cdot cos(\Gamma)}{\Delta} + \gamma\frac{\pi}{2}\mu_0 a_{FL}cos(\phi) + \frac{\alpha\beta u}{\Delta}cos(\Gamma) - \alpha\mu_0\gamma H_{ext} - \alpha\gamma\frac{\pi}{2}\mu_0 b_{DL}cos(\phi)}{\frac{cos(\Gamma)}{\Delta}(1+\alpha^2)}] \end{cases} \tag{2.163}$$

The value of Δ is supposed to be equal to:

$$\Delta = \sqrt{\frac{A}{\frac{K_i}{t} + \frac{\mu_0 M_s^2}{2}(N_x(cos(\phi))^2 + N_y(sin(\phi))^2 - N_z)}} \tag{2.164}$$

2.15 Final differential equation with VCMA pinning field

The aim of this section consists in the description of the pinning field due to the presence of a region of different anisotropy created by the VCMA effect. The pinning field is supposed to be applied along "z" direction like the external one, already considered within the differential equation system, therefore $\vec{H}_{ext}$ must be substituted with $\vec{H'}_{ext} = \vec{H}_{ext} + \vec{H}_{pin}$:

$$
\begin{cases}
\dot{q} = \dfrac{\frac{w}{2\Delta cos(\Gamma)}(1+\alpha^2)\dot{\Gamma} + \frac{\pi\gamma D_0}{2M_s\Delta}sin(\phi-\Gamma) - \frac{\gamma K_d}{M_s}sin(2(\phi-\Gamma)) + \frac{u\cdot cos(\Gamma)}{\Delta}}{\frac{cos(\Gamma)}{\Delta}(1+\alpha^2)} + \\
\quad + \dfrac{\gamma\frac{\pi}{2}\mu_0 a_{FL}cos(\phi) + \frac{\alpha\beta u}{\Delta}cos(\Gamma) - \alpha\mu_0\gamma(H_{ext}+H_{pin}) - \alpha\gamma\frac{\pi}{2}\mu_0 b_{DL}cos(\phi)}{\frac{cos(\Gamma)}{\Delta}(1+\alpha^2)} \\
\dot{\phi} = -\mu_0\gamma(H_{ext}+H_{pin}) + \alpha\dfrac{w}{2\Delta cos(\Gamma)}\dot{\Gamma} + \dfrac{\beta u\cdot cos(\Gamma)}{\Delta} - \gamma\dfrac{\pi}{2}\mu_0 b_{DL}cos(\phi) + \\
\quad - \alpha\dfrac{cos(\Gamma)}{\Delta}\Big[\dfrac{\frac{w}{2\Delta cos(\Gamma)}(1+\alpha^2)\dot{\Gamma} + \frac{\pi\gamma D_0}{2M_s\Delta}sin(\phi-\Gamma) - \frac{\gamma K_d}{M_s}sin(2(\phi-\Gamma))}{\frac{cos(\Gamma)}{\Delta}(1+\alpha^2)} + \\
\quad + \dfrac{\frac{u\cdot cos(\Gamma)}{\Delta} + \gamma\frac{\pi}{2}\mu_0 a_{FL}cos(\phi) + \frac{\alpha\beta u}{\Delta}cos(\Gamma) - \alpha\mu_0\gamma(H_{ext}+H_{pin}) - \alpha\gamma\frac{\pi}{2}\mu_0 b_{DL}cos(\phi)}{\frac{cos(\Gamma)}{\Delta}(1+\alpha^2)}\Big]
\end{cases}
\tag{2.165}
$$

Substituting the analytical expression of H_{pin}:

$$\begin{cases} \dot{q} = \frac{\frac{w}{2\Delta cos(\Gamma)}(1+\alpha^2)\dot{\Gamma} + \frac{\pi\gamma D_0}{2M_s\Delta}sin(\phi-\Gamma) - \frac{\gamma K_d}{M_s}sin(2(\phi-\Gamma)) + \frac{u\cdot cos(\Gamma)}{\Delta}}{\frac{cos(\Gamma)}{\Delta}(1+\alpha^2)} + \\ \quad + \frac{\gamma\frac{\pi}{2}\mu_0 a_{FL}cos(\phi) + \frac{\alpha\beta u}{\Delta}cos(\Gamma) - \alpha\mu_0\gamma H_{ext} - \alpha\gamma\frac{\pi}{2}\mu_0 b_{DL}cos(\phi)}{\frac{cos(\Gamma)}{\Delta}(1+\alpha^2)} + \\ \quad - \alpha\mu_0\gamma\frac{\frac{\frac{\Delta K_u}{2}}{2\mu_0 M_s}[4csch^2(c''+\frac{q}{\Delta})((c''+\frac{q}{\Delta})coth(c''+\frac{q}{\Delta})-1)]}{\frac{cos(\Gamma)}{\Delta}(1+\alpha^2)} + \\ \quad + \alpha\mu_0\gamma\frac{\frac{\frac{\Delta K_u}{2}}{2\mu_0 M_s}[4csch^2(c'+\frac{q}{\Delta})((c'+\frac{q}{\Delta})coth(c'+\frac{q}{\Delta})-1)]}{\frac{cos(\Gamma)}{\Delta}(1+\alpha^2)} \\ \dot{\phi} = -\mu_0\gamma H_{ext} + \alpha\frac{w}{2\Delta cos(\Gamma)}\dot{\Gamma} + \frac{\beta u\cdot cos(\Gamma)}{\Delta} - \gamma\frac{\pi}{2}\mu_0 b_{DL}cos(\phi) + \\ \quad - \mu_0\gamma\frac{\frac{\Delta K_u}{2}}{2\mu_0 M_s}[4csch^2(c''+\frac{q}{\Delta})((c''+\frac{q}{\Delta})coth(c''+\frac{q}{\Delta})-1)] + \\ \quad + \mu_0\gamma\frac{\frac{\Delta K_u}{2}}{2\mu_0 M_s}[4csch^2(c'+\frac{q}{\Delta})((c'+\frac{q}{\Delta})coth(c'+\frac{q}{\Delta})-1)] + \\ \quad - \alpha\frac{cos(\Gamma)}{\Delta}[\frac{\frac{w}{2\Delta cos(\Gamma)}(1+\alpha^2)\dot{\Gamma} + \frac{\pi\gamma D_0}{2M_s\Delta}sin(\phi-\Gamma) - \frac{\gamma K_d}{M_s}sin(2(\phi-\Gamma))}{\frac{cos(\Gamma)}{\Delta}(1+\alpha^2)} + \\ \quad + \frac{\frac{u\cdot cos(\Gamma)}{\Delta} + \gamma\frac{\pi}{2}\mu_0 a_{FL}cos(\phi) + \frac{\alpha\beta u}{\Delta}cos(\Gamma) - \alpha\mu_0\gamma H_{ext} - \alpha\gamma\frac{\pi}{2}\mu_0 b_{DL}cos(\phi)}{\frac{cos(\Gamma)}{\Delta}(1+\alpha^2)} + \\ \quad - \alpha\mu_0\gamma\frac{\frac{\frac{\Delta K_u}{2}}{2\mu_0 M_s}[4csch^2(c''+\frac{q}{\Delta})((c''+\frac{q}{\Delta})coth(c''+\frac{q}{\Delta})-1)]}{\frac{cos(\Gamma)}{\Delta}(1+\alpha^2)} + \\ \quad + \alpha\mu_0\gamma\frac{\frac{\frac{\Delta K_u}{2}}{2\mu_0 M_s}[4csch^2(c'+\frac{q}{\Delta})((c'+\frac{q}{\Delta})coth(c'+\frac{q}{\Delta})-1)]}{\frac{cos(\Gamma)}{\Delta}(1+\alpha^2)}] \end{cases} \tag{2.166}$$

If the VCMA effect is exploited, the anisotropy constant varies by a specific percentage proportional to the voltage applied across the structure:

$$K_u = K_u(0) - \zeta_v\frac{V_{app}}{t_{ox}} \tag{2.167}$$

Therefore, if a certain voltage is applied across the structure, the anisotropy

constant must be calculated and replaced inside Δ equation:

$$\Delta = \sqrt{\frac{A}{\frac{K_i(0)}{t_{FM}} - \zeta_v \frac{V_{app}}{t_{ox}} + \frac{\mu_0 M_s^2}{2}(N_x(cos(\phi))^2 + N_y(sin(\phi))^2 - N_z)}} \tag{2.168}$$

Chapter 3

Comparison of the analytical model with the micromagnetic simulations

In this chapter, the analytical model expressed in equation 2.166 is compared with the micromagnetic results of Mumax3. At first, the Spin Transfer Torque (STT) effect will be compared, then the Spin Orbit Torque (SOT) effect. Since the SOT effect is more efficient with respect to the STT effect (to reach the same domain speed, a current of about one order of magnitude lower is required exploiting SOT instead of STT as shown in Figures 3.1a and 3.3) for the motion of a magnetic domain, it will be analyzed together with VCMA technology. Therefore, the crossing of a domain wall through a VCMA gate of higher or lower anisotropy due to the SOT effect will be compared. The differential equation system 2.166 is solved with Runge-Kutta(4,5) method implemented in MatLab. The result of such method, is that the prediction error is of fifth order, and the total accumulated error is of fourth order, from which the name 45 [46]. A micromagnetic simulator like Mumax3 solves calculations with much more precision with respect to Matlab with the ODE45 method. At the same time, however, the computational effort required by Mumax3 is very high because it calculates the LLG equation 2.27 for each single magnetic moment into which the simulated

ferromagnetic material is divided. The tilting angle of the domain wall Γ provided to the differential equation system 2.166 with Matlab is extracted via magnetic simulation with Mumax3 with the command *ext_dwtilt*. It is not necessary to provide the tilting angle of the domain wall, but it can increase the accuracy of the result.

3.1 Simulation Parameters

In the following table all the simulation parameters are reported:

Table 3.1: Simulation Parameters

Parameter	Value
Anisotropy Constant K_u	$0.8 \cdot 10^6 \frac{J}{m^3}$
Exchange Stiffness A	$10^{-11} \frac{J}{m}$
Saturation Magnetization M_s	$10^6 \frac{A}{m}$
μ_0	$4\pi \cdot 10^{-7} \frac{H}{m}$
Heavy Metal (HM) thickness $'d'$	$1nm$
Damping Factor α	0.04
μ_b	$9.274 \cdot 10^{-24} \frac{J}{T}$
Gyromagnetic Ratio γ	$-1.7595 \cdot 10^{11} \frac{rad}{s \cdot T}$
DMI	$0.6 \cdot 10^{-3} \frac{J}{m^3}$
Landé Factor G	2
Current Polarization P	1
Non-Adiabatic STT β	0.2
Ferramagnetic Layer Width	$128nm$
Ferromagnetic Layer Thickness	$1nm$
$\alpha_{h,FL}$	-0.30
$\alpha_{h,DL}$	0.15
VCMA Gate width	$40nm, 60nm, 80nm$
VCMA Gate Center	$-128nm$

3.2 Spin Transfer Torque

This section concerns the comparison between the average speed of a domain wall due to Spin Transfer Torque (STT) effect estimated by the analytical

model in equation 2.166 and by the micromagnetic simulator Mumax3, shown in figure 3.1a. The parameters adopted for the comparison are reported in Table 3.1. The DMI effect in this case is ignored. The percentage of error for each current density value is shown in figure 3.1b. A lower error is obtained when an average tilting angle is passed to Matlab. In general, passing the angle instant by instant leads to divergences in Matlab due to the angle vector estimated by Mumax3 which has continuous steps, therefore an average tilting angle is evaluated. Since the angle is very small, there is no tangible difference between the two cases. The average error is the average of the error estimated point by point. The average error estimated in the case in which an average angle is passed to the theoretical model with Mumax3 is equal to $\approx -3.9\%$. If, on the other hand, the tilting angle and its time derivative are both assumed to be zero, the average error is equal to $\approx -4.34\%$, therefore better precision is obtained when the tilting profile of the domain wall is taken in consideration. For more details about Mumax3 code look at the Appendix, section STT code, while for more detail about Matlab code, look at the Appendix, section Matlab Code.

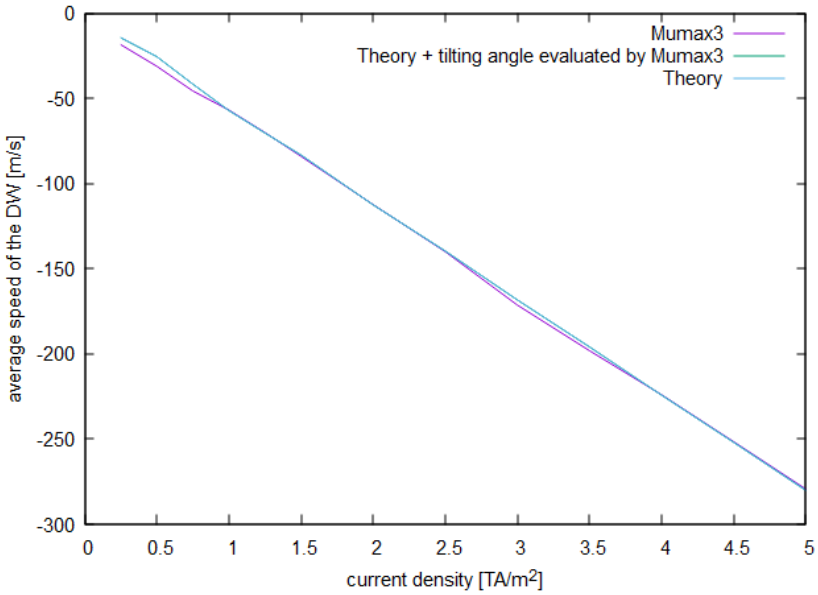

(a) Average Speed of the domain wall subjected to spin transfer torque (STT) in function of the applied current density

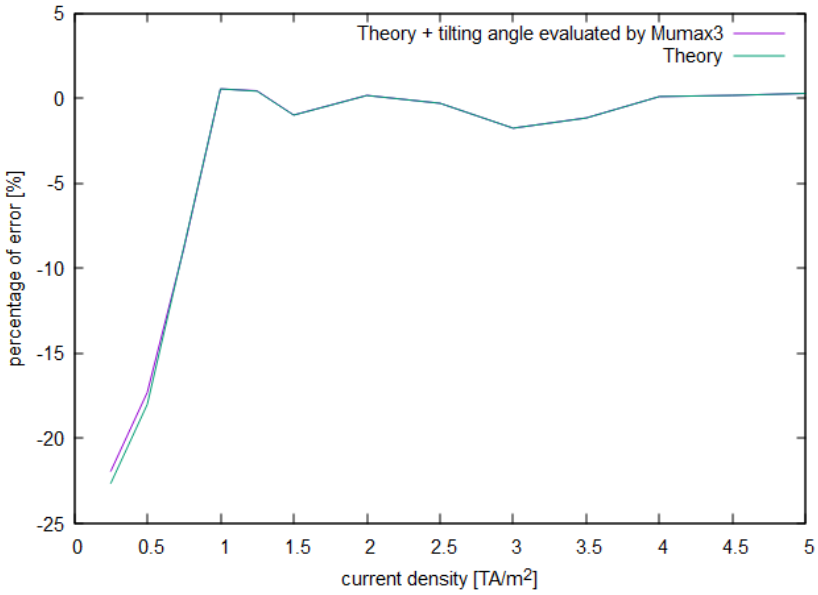

(b) Percentage of error with STT effect in function of the applied current density

Figure 3.1: Average speed of the domain wall due to STT effect in function of the applied current density. The average speed is evaluated by the analytical model of equation 2.166 and by Mumax3 simulation

3.3 Spin Orbit Torque

This section concerns the comparison between the speed of a domain wall due to the Spin Orbit Torque (SOT) effect estimated by the analytical model in equation 2.166 and by the micromagnetic simulator Mumax3. The parameters adopted for the comparison are reported in table 3.1. In figure 3.2 the initial state and the final state of Mumax3 simulation are shown. As expected the domain wall is tilted because of Dzyaloshinskii–Moriya interaction (DMI).

(a) Initial state of the simulation

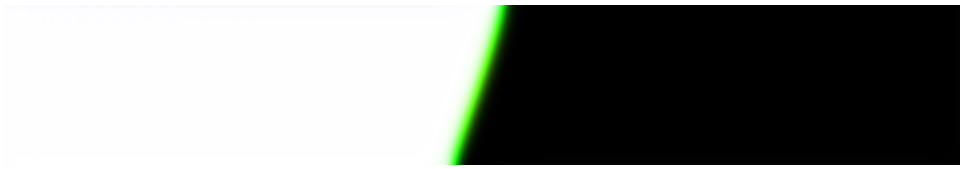

(b) Final state of the simulation after 8 ns with a DMI energy density equal to $0.6 \cdot 10^{-3} \frac{J}{m^3}$

Figure 3.2: Initial and final state of the domain wall subjected to Spin Orbit Torque. The white area symbolizes the up state of magnetization while the black area symbolizes the down state of the magnetization.The domain wall remains in the center of the simulation window because *ext_dwpos*, *ext_dwspeed* and *ext_dwtilt* command are used as shown in the Mumax3 code in section SOT code. These three commands allow to evaluate respectively the position, the speed and the tilting angle of the domain wall by fixing the domain wall itself in the center of the simulation window. The simulation window is 'moved' while the domain wall is fixed, therefore speed, position and tilting of the simulation window with respect to the domain wall are evaluated. The parameters adopted in the simulation are reported in table 3.1

In figure 3.3 the average speed of the domain wall subjected to spin orbit torque evaluated by the analytical model is compared with Mumax3 results. The analytical model of equation 2.166 is solved twice, in one case the tilting angle is ignored, while in the other one an average angle of the angle profile

is considered and passed to the analytical model directly by Mumax3 to Matlab.

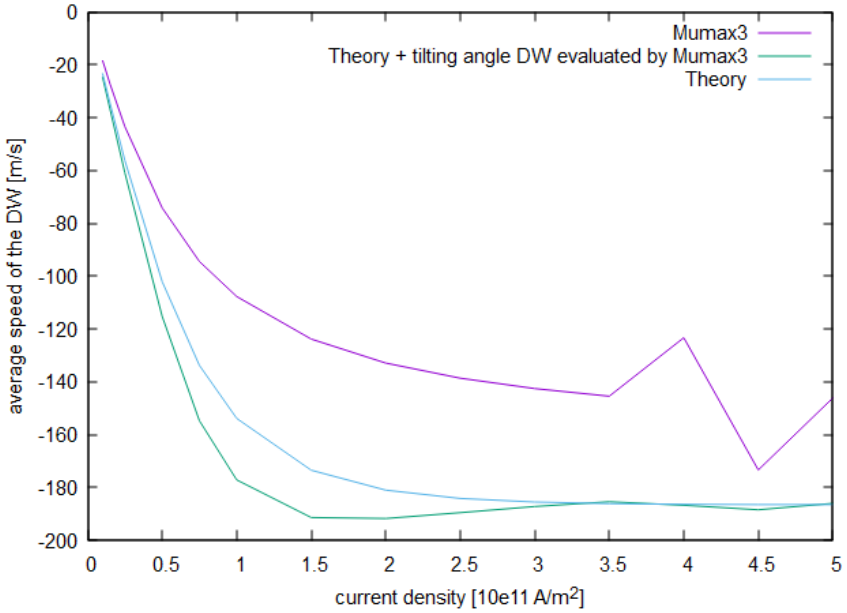

Figure 3.3: Average Speed of the domain wall subjected to Spin Orbit Torque in function of the applied current density evaluated by the analytical model and by Mumax3 simulation.

In Figure 3.4 the percentage of error of the analytical model with respect to Mumax3 simulation is shown. The percentage of error is evaluated both when the tilting angle of the domain wall is taken in consideration and when it is ignored. The error is evaluated for each current density value, and it can be noted that for higher current density values, the percentage of error decreases.

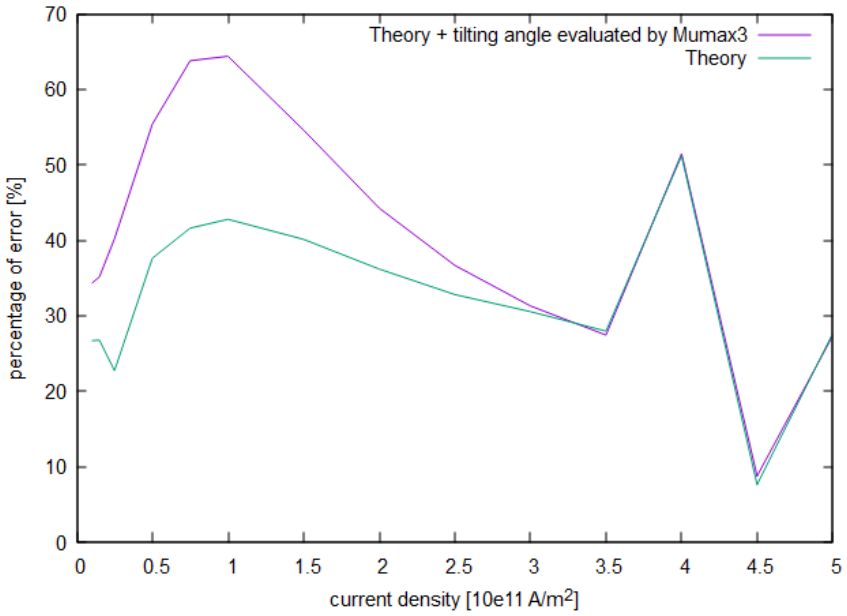

Figure 3.4: Percentage of error with SOT effect in function of the applied current density

A larger error is obtained when an average tilting angle is passed to Matlab. The average error estimated in the case in which an average angle is passed to the analytical model with Mumax3 is equal to $\approx$ 41.07%. If, on the other hand, the tilting angle and its time derivative are both assumed to be zero, the average error is equal to $\approx$ 32.3%, therefore $\approx$ 10% of better accuracy is obtained if the tilting angle of the domain wall is not taken in consideration. In the case of the presence of a VCMA gate, the tilting angle of the domain wall (DW) becomes more pronounced, therefore it is recommended to evaluate it. For more details about Mumax3 code, look at the Appendix, section SOT code.

3.4 Spin Orbit Torque with VCMA effect

This section is dedicated to the comparision between the results of the analytical model with Mumax3 results when a domain wall moves because of SOT effect going across a region (" VCMA gate") of higher anisotropy. The domain wall will cross the VCMA gate if the current is sufficiently high, otherwise the domain wall will be blocked by the presence of the VCMA gate.

60 nm is chosen as the gate width, and -128 nm as the gate center, and the anisotropy of the gate is varied from +5% until +20% in step of 5%. To establish if the domain wall crosses the gate or not, the average speed of the domain wall itself is evaluated: in a good approximation, if the average speed of the domain wall is really low the domain wall does not cross the gate, while if the average speed of the domain wall is sufficiently high the domain wall will cross the gate in an acceptable time. In other words, if the domain wall is blocked by the VCMA gate, its final velocity will be equal to zero, therefore the average speed of the domain wall will be almost zero, lower than $20\frac{m}{s}$. Therefore, the average speed of the domain wall, in the case in which the domain wall itself is blocked by the gate, is more or less an order of magnitude lower with respect to the average speed in the case in which the domain wall crosses the gate. The average speed estimated with the analytical model when the domain wall crosses the gate is a bit higher with respect to the value calculated by Mumax. As reported in the previous section, the expectation value of the average speed of the Domain Wall due to SOT effect in a 1D model is more or less 32% higher with respect to Mumax3 prediction. Mumax3 implements a numerical approach, with a more complex and more accurate algorithm which takes in consideration also the 3D structure of the material. Furthermore the analytical model is based on the assumption of a rigid domain wall, the transverse shape anisotropy is approximated and the tilting angle of the domain wall is supposed to be constant over time with an average value of tilting. These assumptions allow to create a simple model from the point of view of numerical computation, without excessive loss of precision, and with high processing speed. In fact, the objective is not to estimate the average speed of the domain wall, in an impeccable way, but rather its eventual passage through the VCMA gate, therefore the crossing threshold current.

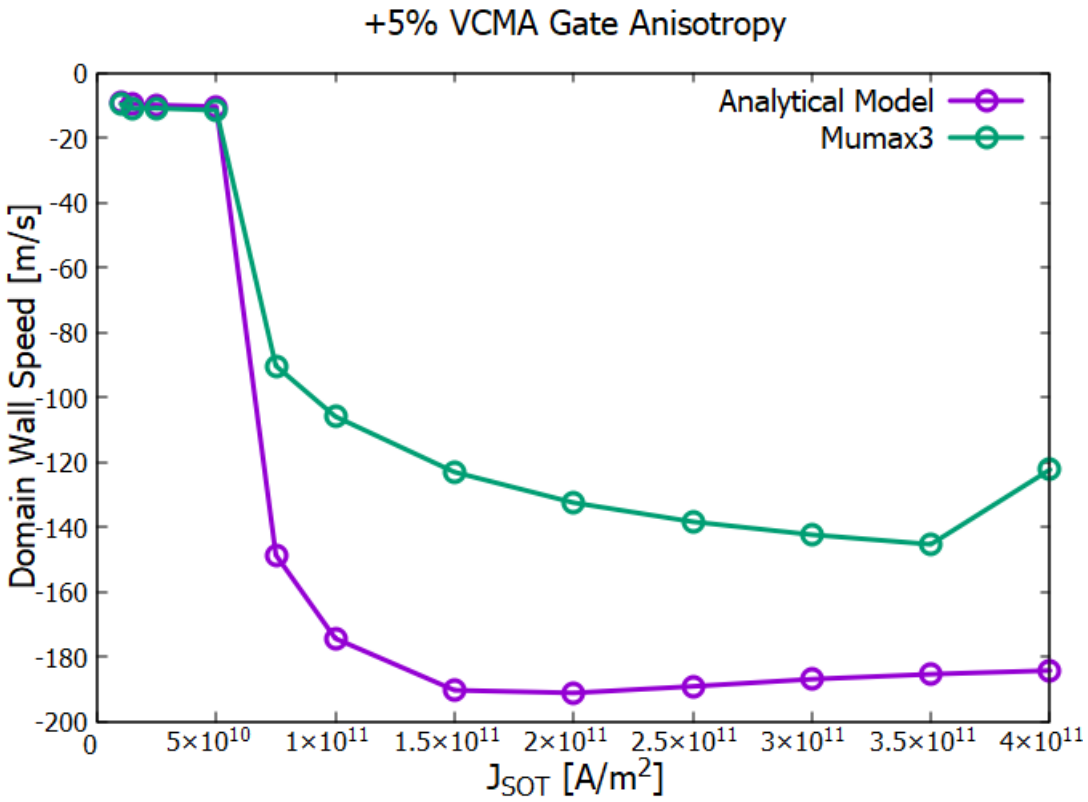

Figure 3.5: Average Speed of the Domain Wall in function of the applied current in the presence of a gate anisotropy 5% higher with respect to the anisotropy of the ferromagnetic layer

The analytical result fits with Mumax3 result, because the same threshold current is evaluated: $0.5e11\frac{A}{m^2}$. In other words, if the current is higher than $0.5e11\frac{A}{m^2}$ the domain wall crosses the VCMA gate.

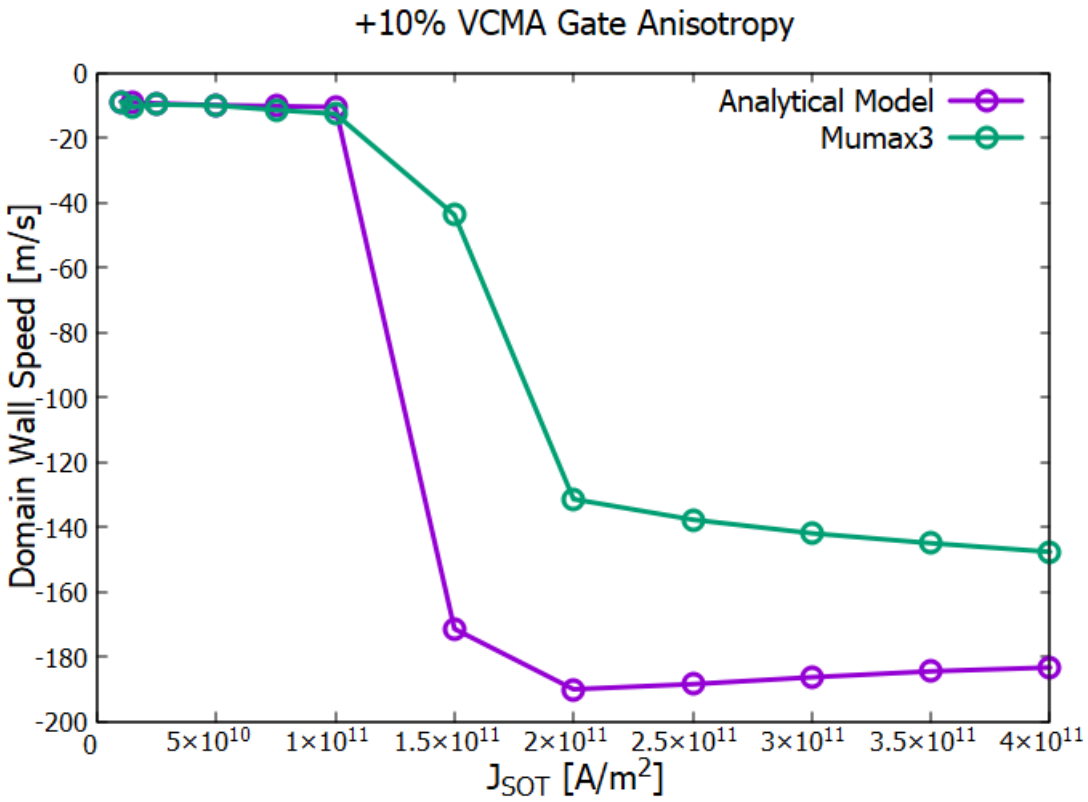

Figure 3.6: Average Speed of the Domain Wall in function of the applied current in the presence of a gate anisotropy 10% higher with respect to the anisotropy of the ferromagnetic layer

The analytical result fits with Mumax3 result, because the same threshold current is evaluated: $1e11\frac{A}{m^2}$. In other words, if the current is higher than $1e11\frac{A}{m^2}$ the domain wall crosses the VCMA gate.

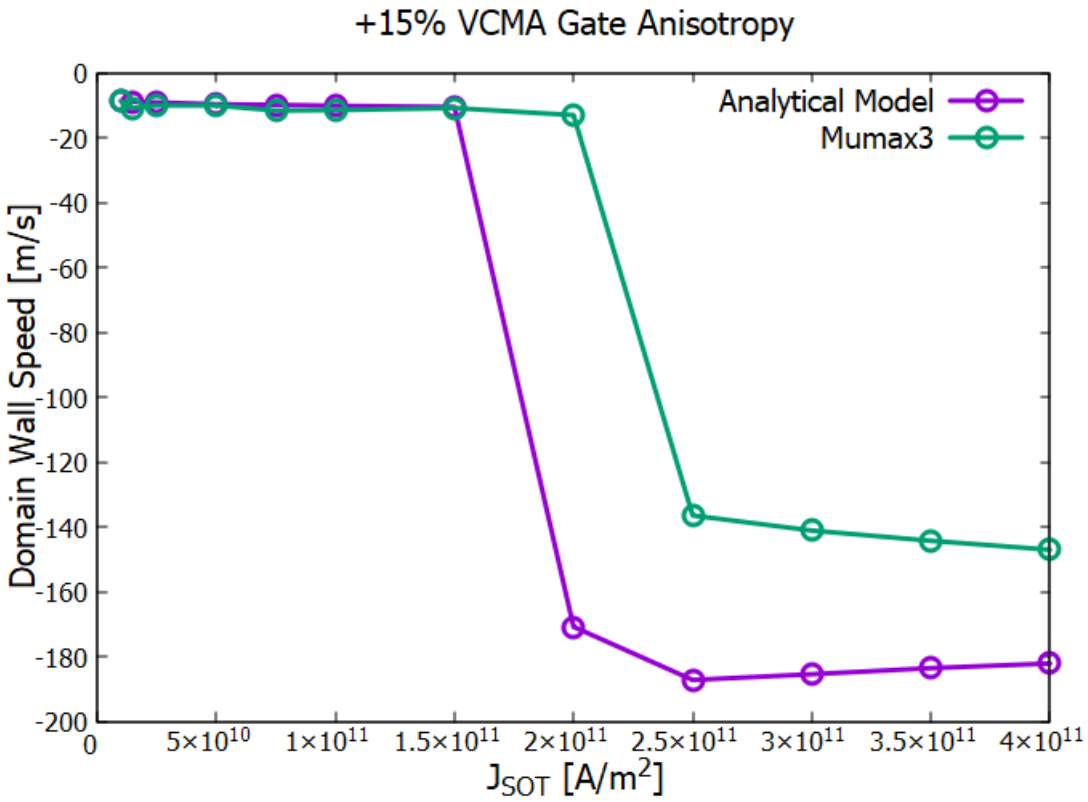

Figure 3.7: Average Speed of the Domain Wall in function of the applied current in the presence of a gate anisotropy 15% higher with respect to the anisotropy of the ferromagnetic layer

The analytical result discreetly fits with Mumax3 result, because the threshold current evaluated by the analytical model is more or less equal to $1.5e11\frac{A}{m^2}$ while the threshold current evaluated by Mumax3 is a bit higher, more or less equal to $2e11\frac{A}{m^2}$.

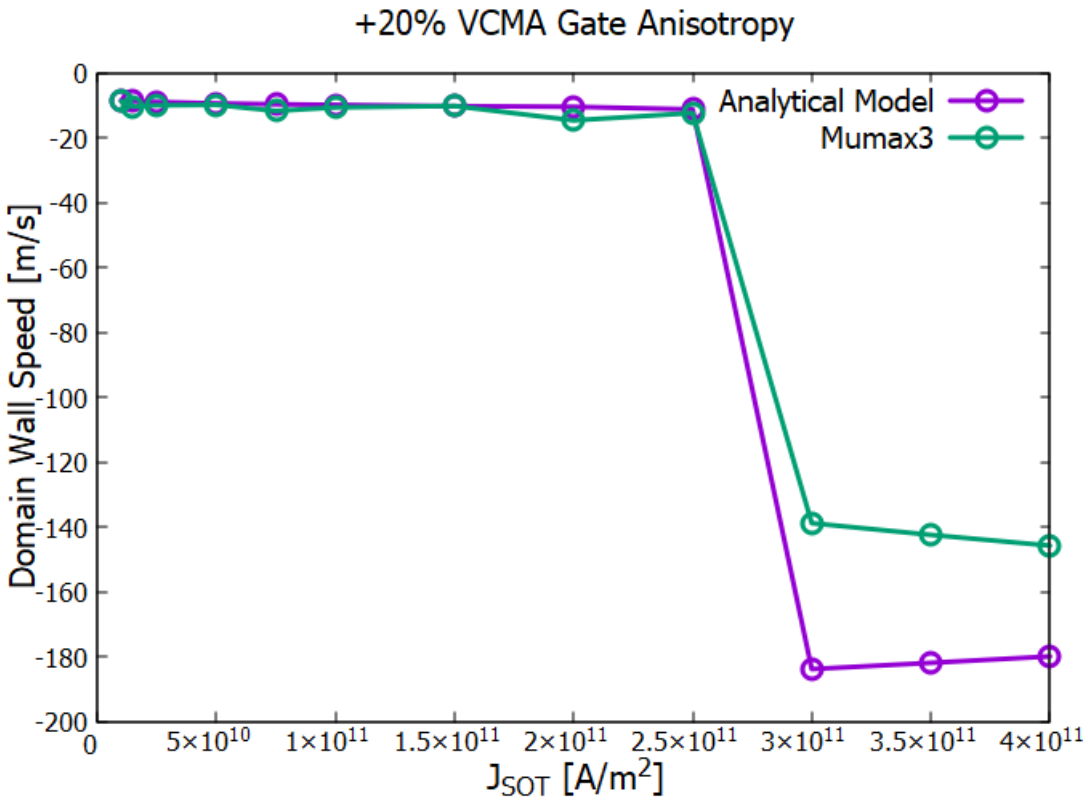

Figure 3.8: Average Speed of the Domain Wall in function of the applied current in the presence of a gate anisotropy 20% higher with respect to the anisotropy of the ferromagnetic layer

The analytical result is in agreement with Mumax3 result, because more or less the same threshold current is evaluated: $2.5e11\frac{A}{m^2}$. In other words, if the current is higher than $2.5e11\frac{A}{m^2}$ the domain wall crosses the VCMA gate. This last simulation will be chosen as a sample for the next section 3.4.1, in which the current steps will be thickened in order to obtain a more precise evaluation.

3.4.1 More accurate evaluation of the threshold current

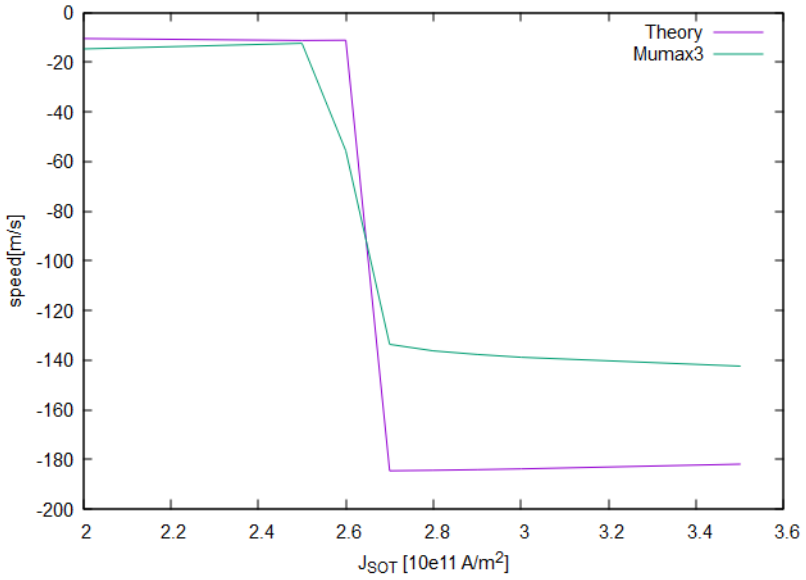

Figure 3.9: Average Speed of the domain wall in function of the applied current in the presence of a gate anisotropy 20% higher with respect to the anisotropy of the ferromagnetic layer

To be more precise in the evaluation of the threshold current, the simulation is thickened in the interval between $2.5 \cdot 10e11 \frac{A}{m^2}$ and $3 \cdot 10e11 \frac{A}{m^2}$, simulating in steps of $0.1 \cdot 10e11 \frac{A}{m^2}$. The analytical model foresees a threshold current equal to $2.7 \cdot 10e11 \frac{A}{m^2}$, in the same way Mumax3 foresees the same current beyond which the domain wall crosses the VCMA gate. When the current is equal to $2.6 \cdot 10e11 \frac{A}{m^2}$ the analytical model, however, provides for a complete locking of the domain wall while Mumax3 provides for a passage of the domain wall through the gate albeit very slow with a speed of about $-55 \frac{m}{s}$ against the $-11 \frac{m}{s}$ estimated by Matlab. In conclusion it is possible to state that the analytical predictions inherent to the threshold current above which the domain wall crosses the VCMA gate, are in agreement with those of Mumax3 with very low error.

Chapter 4

VCMA Gate Analysis

The parameters adopted in the Mumax3 simulation are reported in Table 3.1. For more detail about Mumax3 code implemented for all the simulations look at SOT code.

4.1 Choice of the VCMA constant

The two configurations of interest for the realization of the periodical gates along the Racetrack are:

- $Ta/CoFeB/MgO$;
- $W/CoFeB/MgO$;

The VCMA constant for the Ta stack is more or less equal to $30\frac{fJ}{Vm}$ [21] in the lowest case while the lowest VCMA constant for the W stack is equal to $40\frac{fJ}{Vm}$ about [21]. These two values are chosen for the simulations. The next pages concern the analysis of the passage of the domain wall through the gate. The gate width is varied from a minimum of 40 nm to a maximum of 80 nm while the anisotropy of the gate is varied from -20% up to $+20\%$ with respect to the anisotropy of the ferromagnetic track in steps of 5%. The following table shows the electric fields that must be applied across the gate in order to obtain the desired anisotropic variations.

Table 4.1: VCMA constant for Ta and W stacks

Material Stack	VCMA constant	Anisotropy Variation	Electric Field
$Ta/CoFeB/MgO$	$30\frac{fJ}{Vm}$	$\pm 20\%$	$\mp 5.33\frac{GV}{m}$
$Ta/CoFeB/MgO$	$30\frac{fJ}{Vm}$	$\pm 15\%$	$\mp 4\frac{GV}{m}$
$Ta/CoFeB/MgO$	$30\frac{fJ}{Vm}$	$\pm 10\%$	$\mp 2.66\frac{GV}{m}$
$Ta/CoFeB/MgO$	$30\frac{fJ}{Vm}$	$\pm 5\%$	$\mp 1.33\frac{GV}{m}$
$W/CoFeB/MgO$	$40\frac{fJ}{Vm}$	$\pm 20\%$	$\mp 4\frac{GV}{m}$
$W/CoFeB/MgO$	$40\frac{fJ}{Vm}$	$\pm 15\%$	$\mp 3\frac{GV}{m}$
$W/CoFeB/MgO$	$40\frac{fJ}{Vm}$	$\pm 10\%$	$\mp 2\frac{GV}{m}$
$W/CoFeB/MgO$	$40\frac{fJ}{Vm}$	$\pm 5\%$	$\mp 1\frac{GV}{m}$

4.2 Gate Width of 40nm

In Figure 4.1 the schematic of the ferromagnetic track is shown. The domain wall is initially centered in '0 nm' in the middle of the simulation window. The VCMA gate is centered in '-128 nm' and it is 40 nm wide.

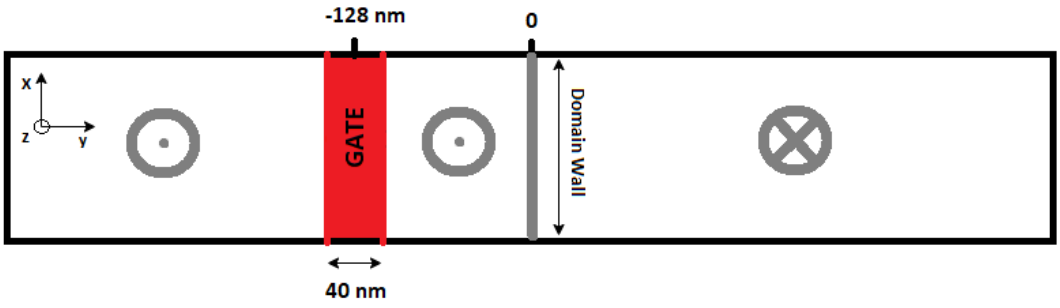

Figure 4.1: Schematic of the ferromagnetic layer with the initial state of the domain wall centered in '0 nm'. The VCMA gate is centered in -128 nm, and the gate width is equal to 40 nm. The magnetization in the left part of the ferromagnetic track is oriented up, while in the right part it is oriented down.

In all the following figures where the domain wall displacement is plotted

in function of time, the position of the VCMA gate will be indicated with two straight lines, one indicating the starting line of the gate, the other one indicating the ending line of the gate. Since the gate is centered in -128 nm and since it is 40 nm wide, the gate starts at 108 nm while the end of the gate is located at 148 nm. In the next pages the figures will show which is the current required for the domain wall to cross the gate when the gate itself is 40 nm wide and its anisotropy varies from -20% until $+20\%$ with respect to the anisotropy of the ferromagnetic track.

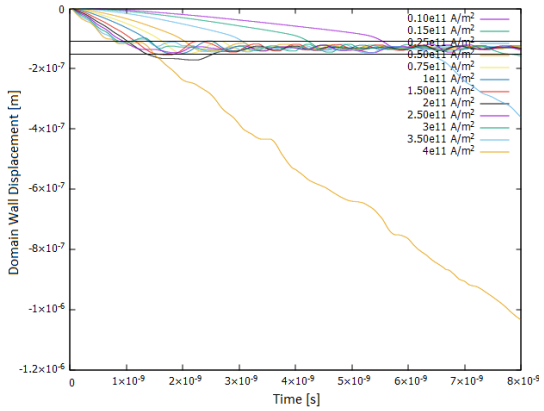

(a) Domain Wall Position with a gate's anisotropy of $0.64e6\frac{J}{m^3}$ and a variable SOT Current

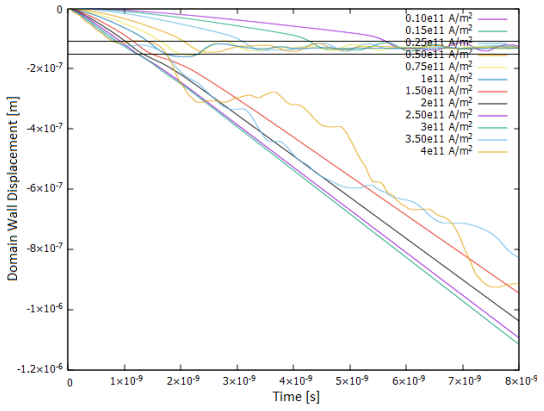

(b) Domain Wall Position with a gate's anisotropy of $0.68e6\frac{J}{m^3}$ and a variable SOT Current

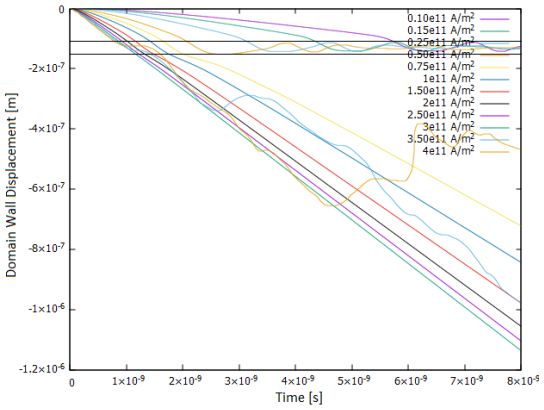

(c) Domain Wall Position with a gate's anisotropy of $0.72e6\frac{J}{m^3}$ and a variable SOT Current

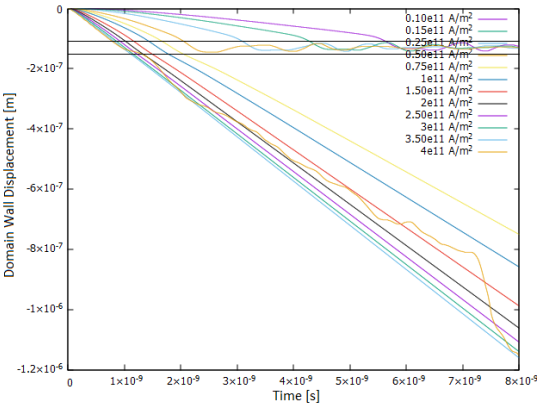

(d) Domain Wall Position with a gate's anisotropy of $0.76e6\frac{J}{m^3}$ and a variable SOT Current

Figure 4.2: Domain Wall Position with a gate centered in $-128nm$ and a gate's anisotropy from $0.64e6\frac{J}{m^3}$ until $0.76e6\frac{J}{m^3}$ in step of $0.04e6\frac{J}{m^3}$ and a variable SOT Current. The gate's width is equal to 40 nm while the anisotropy of the ferromagnetic track is equal to $0.8e6\frac{J}{m^3}$. The other paramaters are reported in Table 3.1

- If the gate anisotropy is equal to $0.64e6\frac{J}{m^3}$ as shown in Figure 4.2a the domain wall crosses the VCMA gate if the applied current through the heavy metal layer is more or less equal to $4e11\frac{A}{m^2}$ or higher. At this current level, different oscillations of the position of the domain wall are observable;

- If the gate anisotropy is equal to $0.68e6\frac{J}{m^3}$ as shown in Figure 4.2b the domain wall crosses the VCMA gate if the applied current through the heavy metal layer is more or less equal to $1.5e11\frac{A}{m^2}$ or higher. When the current is higher than $3.5e11\frac{A}{m^2}$ the domain wall exhibits tangible fluctuations;
- If the gate anisotropy is equal to $0.72e6\frac{J}{m^3}$ as shown in Figure 4.2c the domain wall crosses the VCMA gate if the applied current through the heavy metal layer is more or less equal to $0.75e11\frac{A}{m^2}$ or higher. When the current is higher than $3.5e11\frac{A}{m^2}$ the domain wall exhibits tangible fluctuations;
- If the gate anisotropy is equal to $0.76e6\frac{J}{m^3}$ as shown in Figure 4.2d the domain wall crosses the VCMA gate if the applied current through the heavy metal layer is more or less equal to $0.75e11\frac{A}{m^2}$ or higher. When the current is equal to $4e11\frac{A}{m^2}$ the domain wall exhibits tangible fluctuations;

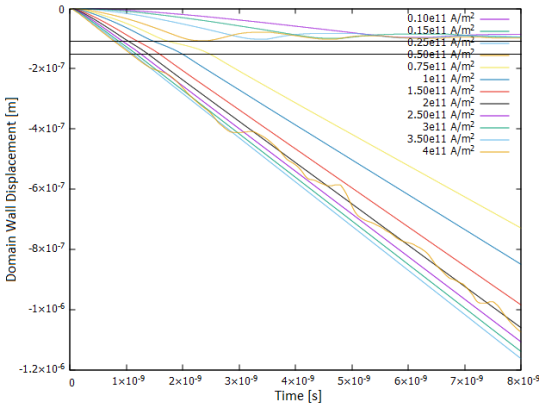

(a) Domain Wall Position with a gate's anisotropy of $0.84e6\frac{J}{m^3}$ and a variable SOT Current

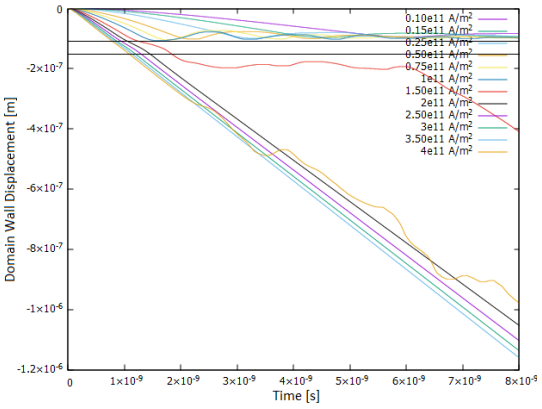

(b) Domain Wall Position with a gate's anisotropy of $0.88e6\frac{J}{m^3}$ and a variable SOT Current

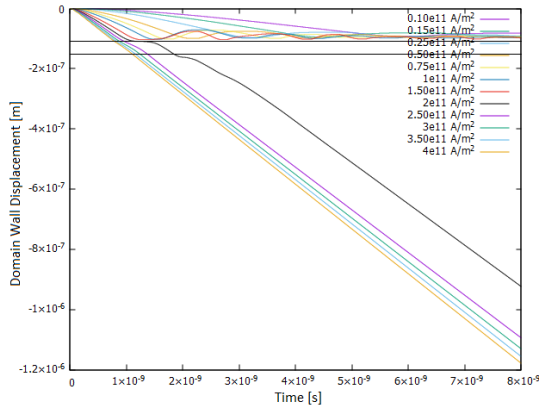

(c) Domain Wall Position with a gate's anisotropy of $0.92e6\frac{J}{m^3}$ and a variable SOT Current

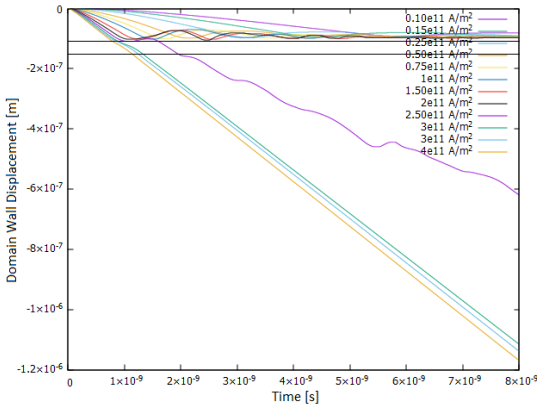

(d) Domain Wall Position with a gate's anisotropy of $0.96e6\frac{J}{m^3}$ and a variable SOT Current

Figure 4.3: Domain Wall Position with a gate centered in $-128nm$ and a gate's anisotropy from $0.84e6\frac{J}{m^3}$ until $0.96e6\frac{J}{m^3}$ in step of $0.04e6\frac{J}{m^3}$ and a variable SOT Current. The gate's width is equal to 40 nm while the anisotropy of the ferromagnetic track is equal to $0.8e6\frac{J}{m^3}$. The other paramaters are reported in Table 3.1

- If the gate anisotropy is equal to $0.84e6\frac{J}{m^3}$ as shown in Figure 4.3a the domain wall crosses the VCMA gate if the applied current through the heavy metal layer is more or less equal to $0.75e11\frac{A}{m^2}$ or higher. When the current is equal to $4e11\frac{A}{m^2}$ the domain wall exhibits tangible fluctuations;
- If the gate anisotropy is equal to $0.88e6\frac{J}{m^3}$ as shown in Figure 4.3b the

domain wall crosses the VCMA gate if the applied current through the heavy metal layer is more or less equal to $2e11\frac{A}{m^2}$ or higher. When the current is equal to $4e11\frac{A}{m^2}$ the domain wall exhibits tangible fluctuations;

- If the gate anisotropy is equal to $0.92e6\frac{J}{m^3}$ as shown in Figure 4.3c the domain wall crosses the VCMA gate if the applied current through the heavy metal layer is more or less equal to $2e11\frac{A}{m^2}$ or higher;
- If the gate anisotropy is equal to $0.96e6\frac{J}{m^3}$ as shown in Figure 4.3d the domain wall crosses the VCMA gate if the applied current through the heavy metal layer is more or less equal to $2.5e11\frac{A}{m^2}$ or higher. When the current is equal to $2.5e11\frac{A}{m^2}$ the domain wall exhibits tangible fluctuations;

4.3 Gate Width of 60nm

In Figure 4.4 the schematic of the ferromagnetic track is shown. The domain wall is initially centered in '0 nm' in the middle of the simulation window. The VCMA gate is centered in '-128 nm' and it is 60 nm wide.

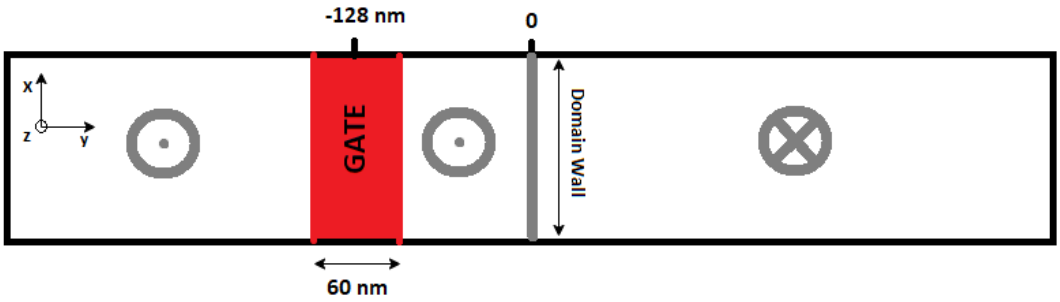

Figure 4.4: Schematic of the ferromagnetic layer with the initial state of the domain wall centered in '0 nm'. The VCMA gate is centered in -128 nm, and the gate width is equal to 60 nm. The magnetization in the left part of the ferromagnetic track is oriented up, while in the right part it is oriented up.

In all the following figures the position of the VCMA gate will be indicated with two straight lines, one indicating the starting line of the gate, the other one indicating the ending line of the gate. Since the gate is centered at -128 nm and since it is 60 nm wide, the starting line of the gate is located in 98

nm, while the ending line of the gate is located at 158 nm. The figures will show which is the current required for the domain wall to cross the gate when the gate itself is 60 nm wide.

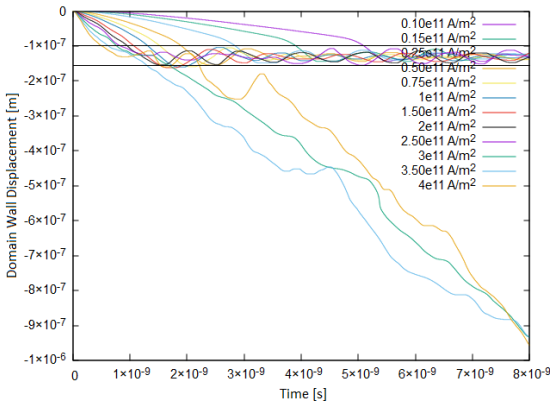

(a) Domain Wall Position with a gate's anisotropy of $0.64e6\frac{J}{m^3}$ and a variable SOT Current

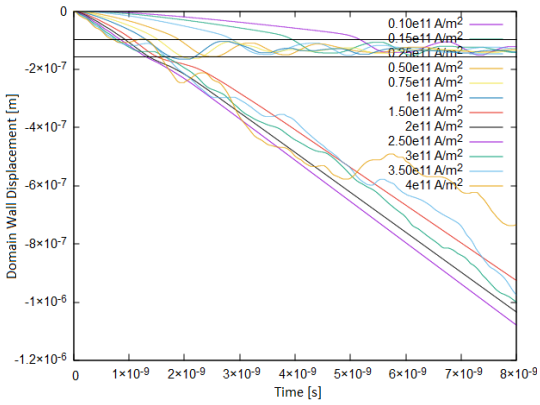

(b) Domain Wall Position with a gate's anisotropy of $0.68e6\frac{J}{m^3}$ and a variable SOT Current

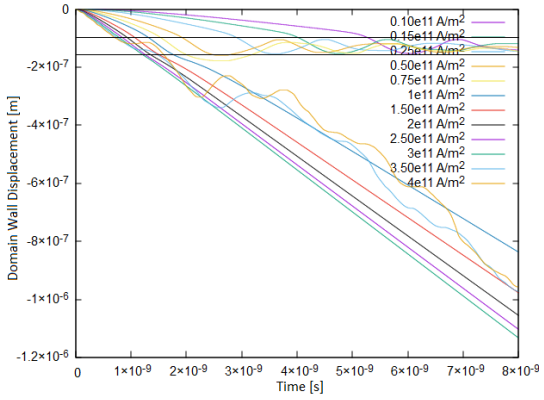

(c) Domain Wall Position with a gate's anisotropy of $0.72e6\frac{J}{m^3}$ and a variable SOT Current

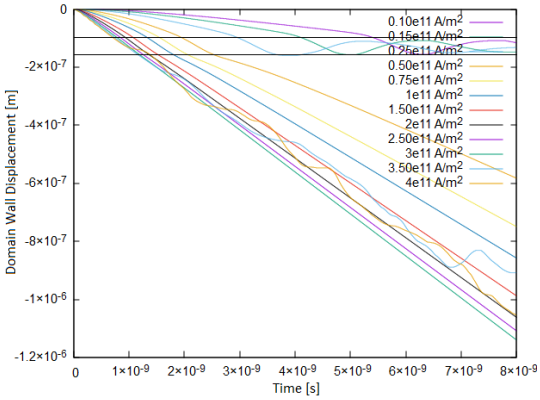

(d) Domain Wall Position with a gate's anisotropy of $0.76e6\frac{J}{m^3}$ and a variable SOT Current

Figure 4.5: Domain Wall Position with a gate centered in $-128nm$ and a gate's anisotropy from $0.64e6\frac{J}{m^3}$ until $0.76e6\frac{J}{m^3}$ in step of $0.04e6\frac{J}{m^3}$ and a variable SOT Current. The gate's width is equal to 60 nm while the anisotropy of the ferromagnetic track is equal to $0.8e6\frac{J}{m^3}$. The other paramaters are reported in Table 3.1

- If the gate anisotropy is equal to $0.64e6\frac{J}{m^3}$ as shown in Figure 4.5a the domain wall crosses the VCMA gate if the applied current through the

heavy metal layer is more or less equal to $3e11\frac{A}{m^2}$ or higher. When the current is higher than $3e11\frac{A}{m^2}$ the domain wall exhibits tangible fluctuations;

- If the gate anisotropy is equal to $0.68e6\frac{J}{m^3}$ as shown in Figure 4.5b the domain wall crosses the VCMA gate if the applied current through the heavy metal layer is more or less equal to $1.5e11\frac{A}{m^2}$ or higher. When the current is higher than $3e11\frac{A}{m^2}$ the domain wall exhibits tangible fluctuations;
- If the gate anisotropy is equal to $0.72e6\frac{J}{m^3}$ as shown in Figure 4.5c the domain wall crosses the VCMA gate if the applied current through the heavy metal layer is more or less equal to $1e11\frac{A}{m^2}$ or higher. When the current is higher than $3.5e11\frac{A}{m^2}$ the domain wall exhibits tangible fluctuations;
- If the gate anisotropy is equal to $0.76e6\frac{J}{m^3}$ as shown in Figure 4.5d the domain wall crosses the VCMA gate if the applied current through the heavy metal layer is more or less equal to $0.5e11\frac{A}{m^2}$ or higher. When the current is higher than $3.5e11\frac{A}{m^2}$ the domain wall exhibits tangible fluctuations;

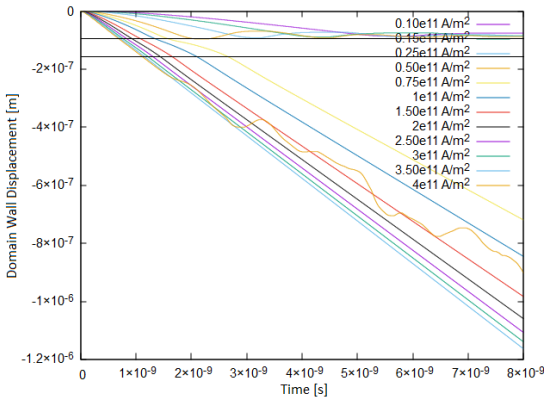

(a) Domain Wall Position with a gate's anisotropy of $0.84e6\frac{J}{m^3}$ and a variable SOT Current

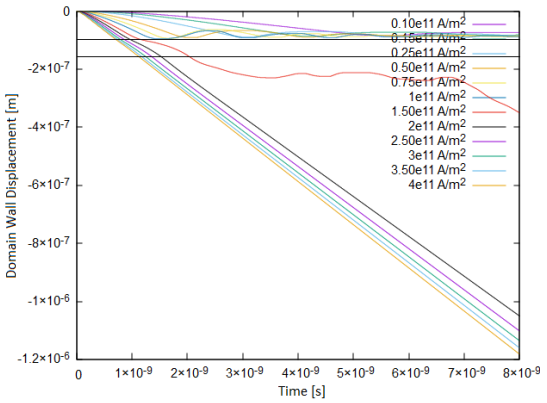

(b) Domain Wall Position with a gate's anisotropy of $0.88e6\frac{J}{m^3}$ and a variable SOT Current

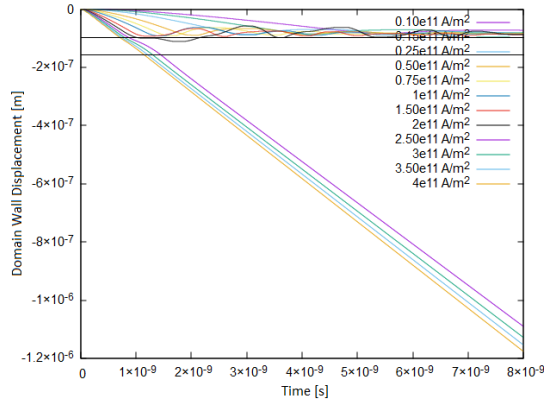

(c) Domain Wall Position with a gate's anisotropy of $0.92e6\frac{J}{m^3}$ and a variable SOT Current

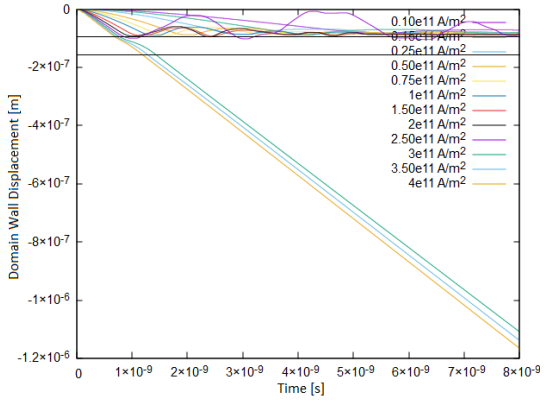

(d) Domain Wall Position with a gate's anisotropy of $0.96e6\frac{J}{m^3}$ and a variable SOT Current

Figure 4.6: Domain Wall Position with a gate centered in $-128nm$ and a gate's anisotropy from $0.84e6\frac{J}{m^3}$ until $0.96e6\frac{J}{m^3}$ in step of $0.04e6\frac{J}{m^3}$ and a variable SOT Current. The gate's width is equal to 60 nm while the anisotropy of the ferromagnetic track is equal to $0.8e6\frac{J}{m^3}$. The other paramaters are reported in Table 3.1

- If the gate anisotropy is equal to $0.84e6\frac{J}{m^3}$ as shown in Figure 4.6a the domain wall crosses the VCMA gate if the applied current through the heavy metal layer is more or less equal to $0.75e11\frac{A}{m^2}$ or higher. When the current is equal to $4e11\frac{A}{m^2}$ the domain wall exhibits tangible fluctuations;
- If the gate anisotropy is equal to $0.88e6\frac{J}{m^3}$ as shown in Figure 4.6b the

domain wall crosses the VCMA gate if the applied current through the heavy metal layer is more or less equal to $2e11\frac{A}{m^2}$ or higher. When the current is equal to $1.5e11\frac{A}{m^2}$ the domain wall exhibits tangible fluctuations;

- If the gate anisotropy is equal to $0.92e6\frac{J}{m^3}$ as shown in Figure 4.6c the domain wall crosses the VCMA gate if the applied current through the heavy metal layer is more or less equal to $2.5e11\frac{A}{m^2}$ or higher;
- If the gate anisotropy is equal to $0.96e6\frac{J}{m^3}$ as shown in Figure 4.6d the domain wall crosses the VCMA gate if the applied current through the heavy metal layer is more or less equal to $3e11\frac{A}{m^2}$ or higher;

4.4 Gate Width of 80nm

In Figure 4.7 the schematic of the ferromagnetic track is shown. The domain wall is initially centered in '0 nm' in the middle of the simulation window. The VCMA gate is centered in '-128 nm' and it is 80 nm wide.

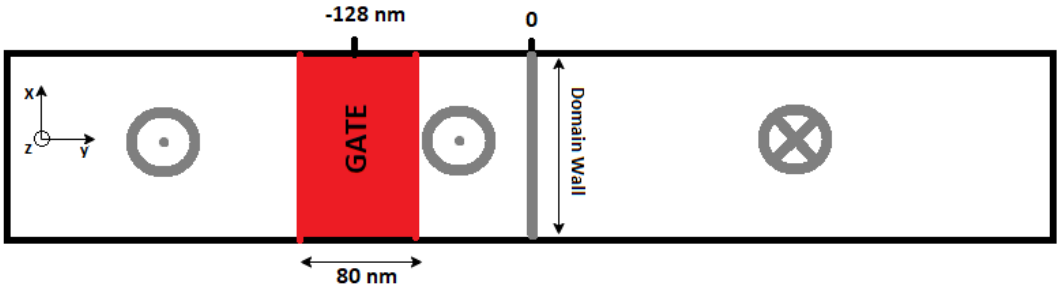

Figure 4.7: Schematic of the ferromagnetic layer with the initial state of the domain wall centered in '0 nm'. The VCMA gate is centered in -128 nm, and the gate width is equal to 80 nm. The magnetization in the left part of the ferromagnetic track is oriented up, while in the right part it is oriented up.

In all the following figures the position of the VCMA gate will be indicated with two straight lines, one indicating the starting line of the gate, the other one indicating the ending line of the gate. Since the gate is centered at -128 nm and since it is 80 nm wide, the starting line of the VCMA gate is located at 88 nm while the ending line of the gate is located at 168 nm. The figures

will show which is the current required for the domain wall to cross the gate when the gate itself is 80 nm wide.

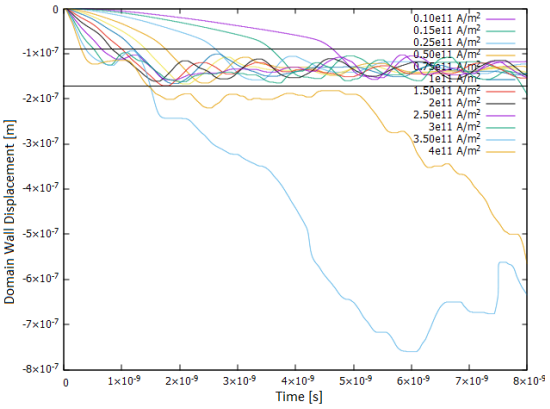

(a) Domain Wall Position with a gate's anisotropy of $0.64e6\frac{J}{m^3}$ and a variable SOT Current

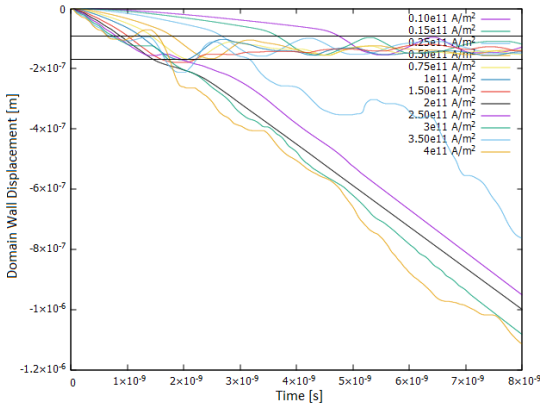

(b) Domain Wall Position with a gate's anisotropy of $0.68e6\frac{J}{m^3}$ and a variable SOT Current

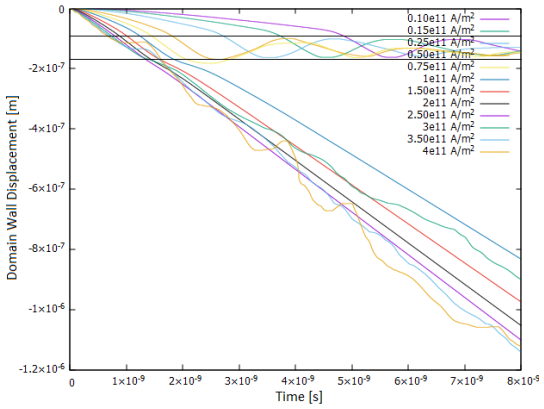

(c) Domain Wall Position with a gate's anisotropy of $0.72e6\frac{J}{m^3}$ and a variable SOT Current

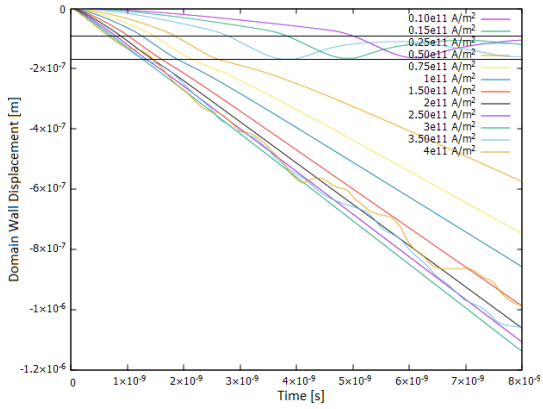

(d) Domain Wall Position with a gate's anisotropy of $0.76e6\frac{J}{m^3}$ and a variable SOT Current

Figure 4.8: Domain Wall Position with a gate centered in $-128nm$ and a gate's anisotropy from $0.64e6\frac{J}{m^3}$ until $0.76e6\frac{J}{m^3}$ in step of $0.04e6\frac{J}{m^3}$ and a variable SOT Current. The gate's width is equal to 80 nm while the anisotropy of the ferromagnetic track is equal to $0.8e6\frac{J}{m^3}$. The other paramaters are reported in Table 3.1

- If the gate anisotropy is equal to $0.64e6\frac{J}{m^3}$ as shown in Figure 4.8a the domain wall crosses the VCMA gate if the applied current through the heavy metal layer is more or less equal to $3.5e11\frac{A}{m^2}$ or higher. When

the current is higher than $3.5e11\frac{A}{m^2}$ the domain wall exhibits tangible fluctuations;

- If the gate anisotropy is equal to $0.68e6\frac{J}{m^3}$ as shown in Figure 4.8b the domain wall crosses the VCMA gate if the applied current through the heavy metal layer is more or less equal to $2e11\frac{A}{m^2}$ or higher. When the current is higher than $3e11\frac{A}{m^2}$ the domain wall exhibits tangible fluctuations;
- If the gate anisotropy is equal to $0.72e6\frac{J}{m^3}$ as shown in Figure 4.8c the domain wall crosses the VCMA gate if the applied current through the heavy metal layer is more or less equal to $1e11\frac{A}{m^2}$ or higher. When the current is higher than $3e11\frac{A}{m^2}$ the domain wall exhibits tangible fluctuations;
- If the gate anisotropy is equal to $0.76e6\frac{J}{m^3}$ as shown in Figure 4.8d the domain wall crosses the VCMA gate if the applied current through the heavy metal layer is more or less equal to $0.5e11\frac{A}{m^2}$ or higher. When the current is higher than $3.5e11\frac{A}{m^2}$ the domain wall exhibits tangible fluctuations;

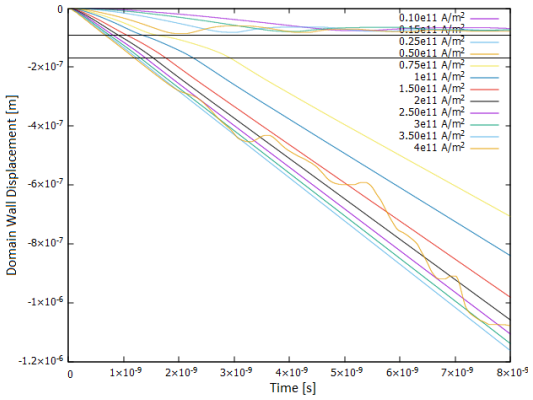

(a) Domain Wall Position with a gate's anisotropy of $0.84e6\frac{J}{m^3}$ and a variable SOT Current

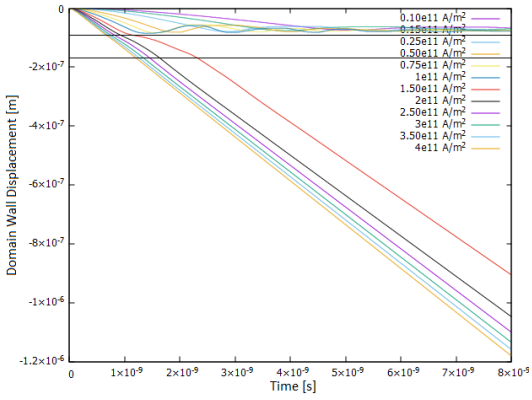

(b) Domain Wall Position with a gate's anisotropy of $0.88e6\frac{J}{m^3}$ and a variable SOT Current

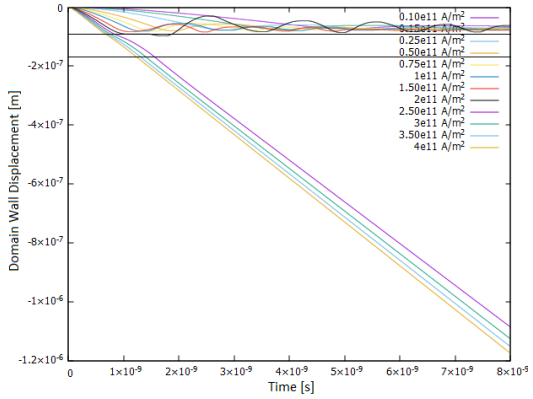

(c) Domain Wall Position with a gate's anisotropy of $0.92e6\frac{J}{m^3}$ and a variable SOT Current

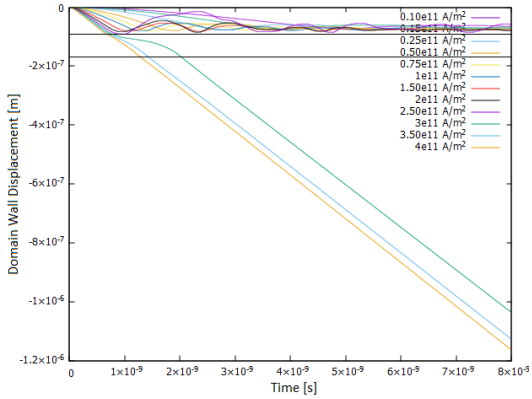

(d) Domain Wall Position with a gate's anisotropy of $0.96e6\frac{J}{m^3}$ and a variable SOT Current

Figure 4.9: Domain Wall Position with a gate centered in $-128nm$ and a gate's anisotropy from $0.84e6\frac{J}{m^3}$ until $0.96e6\frac{J}{m^3}$ in step of $0.04e6\frac{J}{m^3}$ and a variable SOT Current. The gate's width is equal to 80 nm while the anisotropy of the ferromagnetic track is equal to $0.8e6\frac{J}{m^3}$. The other paramaters are reported in Table 3.1

- If the gate anisotropy is equal to $0.84e6\frac{J}{m^3}$ as shown in Figure 4.9a the domain wall crosses the VCMA gate if the applied current through the heavy metal layer is more or less equal to $0.75e11\frac{A}{m^2}$ or higher. When the current is equal to $4e11\frac{A}{m^2}$ the domain wall exhibits tangible fluctuations;
- If the gate anisotropy is equal to $0.88e6\frac{J}{m^3}$ as shown in Figure 4.9b the

domain wall crosses the VCMA gate if the applied current through the heavy metal layer is more or less equal to $1.50e11\frac{A}{m^2}$ or higher;

- If the gate anisotropy is equal to $0.92e6\frac{J}{m^3}$ as shown in Figure 4.9c the domain wall crosses the VCMA gate if the applied current through the heavy metal layer is more or less equal to $2.5e11\frac{A}{m^2}$ or higher;
- If the gate anisotropy is equal to $0.96e6\frac{J}{m^3}$ as shown in Figure 4.9d the domain wall crosses the VCMA gate if the applied current through the heavy metal layer is more or less equal to $3e11\frac{A}{m^2}$ or higher;

4.5 Threshold Current

All the current threshold values shown in the sections 4.2, 4.3, 4.4 can be summarized with a single graph:

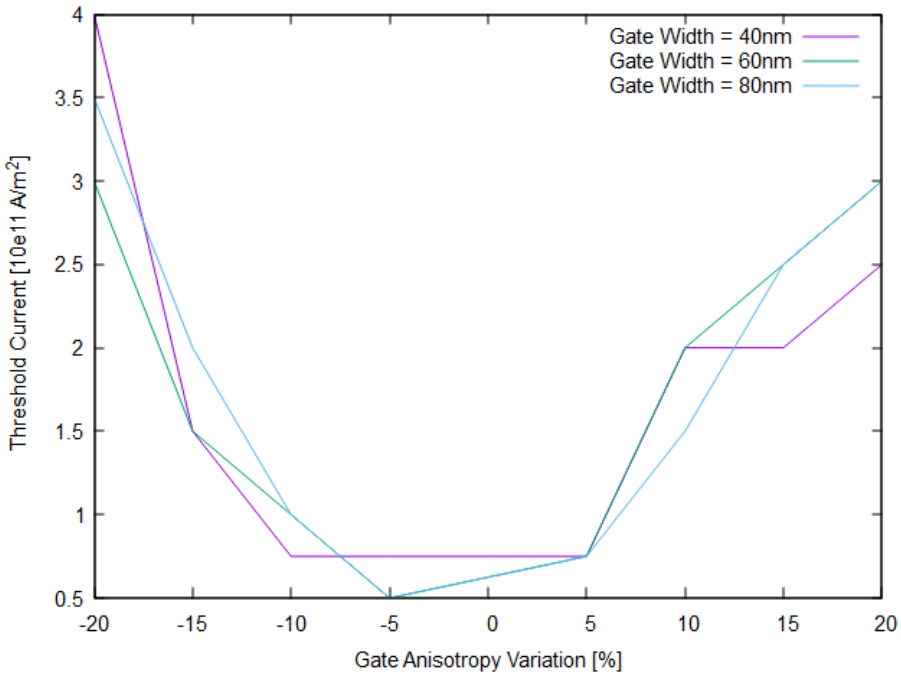

Figure 4.10: Threshold Current with different anisotropy levels of the VCMA gate, and with different gate width

For more details of the threshold current values, look at table A.1 in the Appendix, section A.
In figure 4.10 it can be observed that the threshold current as a function of

the anisotropic level of the gate maintains the same behaviour by varying the width of the gate. For anisotropic values of the VCMA gate lower with respect to that of the ferromagnetic track, the threshold current increases with a greater slope than for positive gate anisotropy values.

4.6 Memory optimization and evaluations of current, and speed

4.6.1 Functionality of a Racetrack Memory

The functionality of synchronization of a Racetrack memory with VCMA gates can be tested by comparing the time to reach the desired voltage across a VCMA gate, with the time required for a domain wall to travel from one gate to its successive. In other words, if the time to reach a certain "blocking" voltage at the gate is too long, the domain wall would escape the gate and it would not be possible to block the domain wall at the desired point. Therefore, if the time of reaching the desired voltage across the gate is compatible (lower) with the speed of the domain wall divided by the distance between two successive gates, it would be possible to block a domain wall just before a successive gate, so as to be able to scroll domain by domain along the ferromagnetic track.

4.6.2 Schematic of the VCMA gate structure and list of parameters

In Figure 4.11 a schematic of the VCMA gate structure is represented. The Aluminum layer is the top plate of the capacitor, the MgO layer is the oxide layer which determines the dielectric constant of the gate. $CoFeB$ layer is the ferromagnetic layer of the track while the Ta layer is the heavy metal layer through which is possible to exploit the SOT effect, and which works as the other plate of the capacitor. The $CoFeB$ layer should "shield" almost completely the other metal layers and the accumulation should take place practically all in the $CoFeB$. As a consequence only the MgO layer determines the dielectric constant of the gate and its thickness.

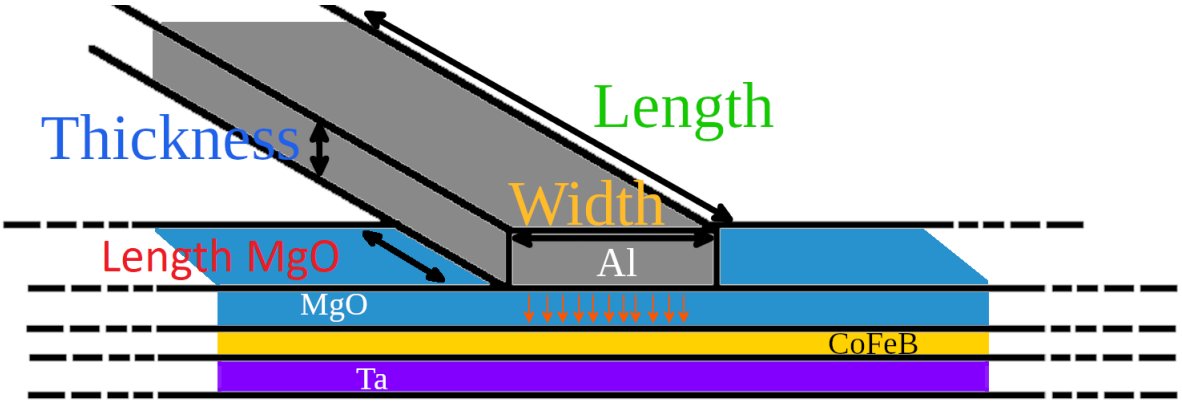

Figure 4.11: Schematic of the VCMA gate

In the table all the parameters of the structure are reported:

Table 4.2: VCMA gate parameters

Parameter	Value
ρ_{Al}	$2.7 \cdot 10^{-8} \Omega \cdot m$
$\epsilon_{r,MgO}$	9[47]
Length MgO	128 nm
Thickness Al	250 nm
Thickness MgO	1 nm
Width MgO	(40 nm, 60 nm, 80nm)
Width Al	(40 nm, 60 nm, 80nm)
Length Al	Variable [128 nm, 10 cm]

4.6.3 Charging/discharging time of a capacitor

When a voltage is applied across a VCMA gate, there is a charging period of the gate, which is nothing more than a capacitor. Likewise when the voltage is turned off, there will be a discharge phase of the VCMA gate. Therefore it is essential to evaluate the charging and discharging time of the gate. The

charging phase of a capacitor is described by the well-known equation:

$$V(t) = V_0(1 - e^{-\frac{t}{\tau}}) \tag{4.1}$$

while the discharging phase by:

$$V(t) = V_0 e^{-\frac{t}{\tau}} \tag{4.2}$$

Mathematically the desired voltage is reached in an infinite time, since the behaviour of the voltage is described by an exponential law, but in a good physical approximation, the voltage level is reached after a time equal to $\approx 5\tau$. τ is the defined in fact as the time constant and it is equal to:

$$\tau = RC \tag{4.3}$$

where R is the resistance of the circuit while C is the capacitance of the structure. Now it is fundamental to evaluate both the resistance and the capacitance of the gate, in order to determine the charging (discharging) time of the VCMA gate. Concerning the resistance of the gate, in good approximation, it is possible to equal the resistance of the structure only with the resistance of the Aluminum layer. To determine the resistance of the Aluminum layer, the resistivity formula must be exploited:

$$R_{gate} \approx R_{Al} = \rho_{Al} \frac{L_{Al}}{W_{Al} t_{Al}} \tag{4.4}$$

where L_{Al} is a variable, while the other parameters are well-known and they are reported in table 4.2. Concerning the capacitance of the structure, only the MgO layer is taken in consideration for the dielectric constant, and the well-known equation of a capacitor is exploited:

$$C_{gate} \approx \epsilon_{MgO} \frac{L_{MgO} W_{MgO}}{t_{MgO}} \tag{4.5}$$

Thus, the charging/discharging time of the gate is equal to:

$$t_g \approx 5\tau = 5 R_{Al} C_{gate} \tag{4.6}$$

Making explicit the equation:

$$t_g(L_{Al}) \approx 5 \rho_{Al} \epsilon_{MgO} \frac{L_{Al}}{W_{Al} t_{Al}} \frac{L_{MgO} W_{MgO}}{t_{MgO}} \tag{4.7}$$

t_g is a function of the Aluminum length. If the length of the Aluminum layer is increased, the charging/discharging time increases.
Obviously the width of the Al layer coincides with the width of the MgO layer, therefore:

$$t_g(L_{Al}) \approx 5\rho_{Al}\epsilon_{r,MgO}\epsilon_0\frac{L_{Al}L_{MgO}}{t_{Al}t_{MgO}} \tag{4.8}$$

As just explained before, all the parameters of the equation 4.8 are well-known, and they are reported in table 4.2. The charging/discharging time of the VCMA gate is independent from the width of the gate itself.
In Figure 4.12 the charging time t_g of the gate in function of the Aluminum length is shown.

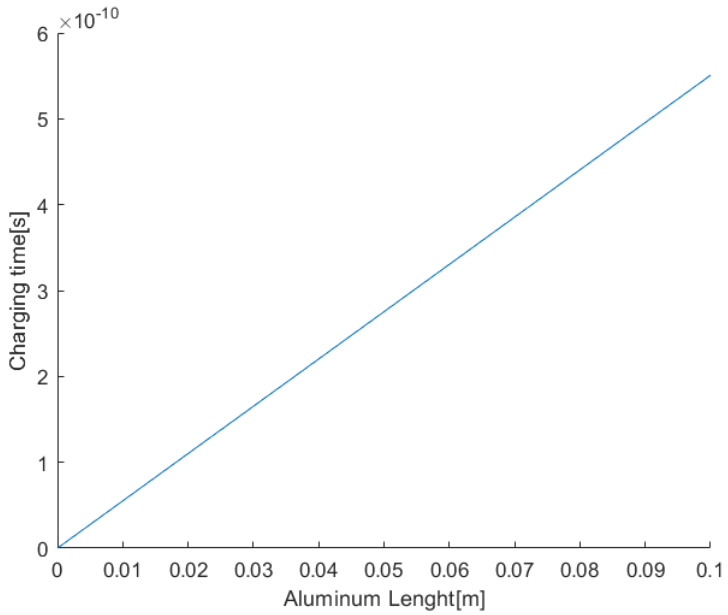

Figure 4.12: Charging time in function of the Aluminum layer length, Eq.4.8

The charging time of the gate in the worst case of long interconnection of Aluminum (equal to 10 cm) is equal to $\approx 0.55ns$. In the next subsection 4.6.4, the best combination of current and gate width is chosen, in order to reach the highest velocity with the thinnest gate.

4.6.4 Current Density and Gate Width

Looking at Figure 3.3 it is possible to notice that as the current increases the speed of the domain wall increases up to a value of $3.5e11\frac{A}{m^2}$. For current

values higher than $3.5e11\frac{A}{m^2}$, the speed of the domain wall tends to oscillate around a more or less constant value. Consequently, it is advisable to choose a gate width that blocks the highest current density, so that the Racetrack memory can run at higher speed. Suppose to choose a barrier configuration of the gate to block the passage of a domain wall, therefore suppose to choose values of anisotropy of the gate higher than those of the track. Looking at table A.1 and looking at positive percentage increment of the gate anisotropy with respect to the track's anisotropy, 60 nm of gate width is the best choice. For instance for +20% of gate anisotropy increasing, for a gate width of 40 nm the maximum current blocked by the gate is $\approx 2e11\frac{A}{m^2}$, for a gate width of 60 nm the maximum current blocked by the gate is $\approx 2.6e11\frac{A}{m^2}$, and more or less the same value is estimated for a gate width of 80 nm ($\approx 2.5e11\frac{A}{m^2}$). In conclusion for higher gate anisotropy values with respect to the track, the most reasonable choice as gate width for a faster memory with a thinner gate is 60 nm. Having a wider gate would imply having a wider domain so that successive gates are sufficiently distant, and at the same time a wider gate would require longer times of aluminum deposition, and therefore also greater area and more parassitic effect.
Looking again at Table A.1 for lower anisotropy value of the gate with respect to the track ("hole" anisotropy configuration) the best choice is a gate width of 40 nm. For instance when the anisotropy decreases of -20% or of -5% in the gate region with respect to the ferromagnetic track, the threshold current is higher when the gate width is equal to 40 nm. For values of the gate anisotropy equal to -10% or -15% with respect to the track anisotropy, the highest threshold current is obtained for a gate width of 80 nm, but taking into account the trade off between the speed of the domain wall and the gate size, the most reasonable choice for a gate configuration with lower anisotropy than the track is undoubtedly 40 nm as gate width. When the anisotropy of the gate is lowered by 20% and when the gate width is equal to 40 nm the highest current blocked by the gate is reached, equal to $\approx 3.5e11\frac{A}{m^2}$.
In conclusion to have the maximum velocity and at the same time the thinnest gate, the best choices are:

Table 4.3: Best choices of the VCMA gate

Gate width	Anisotropy	Max. Current	Domain Wall average speed
60 nm	+20%	$\approx 2.6e11\frac{A}{m^2}$	$\approx -139\frac{m}{s}$
40 nm	−20%	$\approx 3.5e11\frac{A}{m^2}$	$\approx -145\frac{m}{s}$

The average velocity of the domain wall as a function of the applied current is obtained from Figure 3.3.

4.6.5 Final verification of the functionality

The distance between two successive gates is equal to the width of a domain. The width of a domain could be assumed between 100 nm and 400 nm. Therefore it is sufficient to divide the distance that the domain wall would travel before being blocked by the next gate, by the average speed of the domain wall, to obtain the time taken by the domain wall to reach the subsequent gate. Thus, this time must be greater (or equal) than the time required to load the successive gate shown in Figure 4.12.

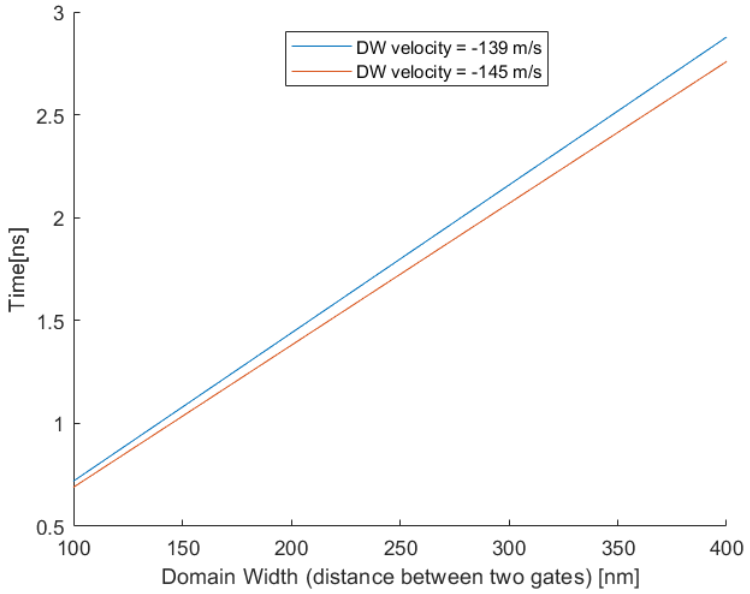

Figure 4.13: Time spent for a domain wall to travel from one gate to its successive in function of domain width

In the worst case of thinnest domain, the time spent for a domain wall to travel from one gate to its successive is equal to $\approx 0.69ns$.
The choice of the parameters of the structure, and therefore of the gate, the choice of the current density through the heavy metal and therefore of the speed of the domain wall match perfectly, or in other words, once a domain wall has been allowed to pass through a gate, it is possible to block it at the next gate since the "blocking" time is lower in the worst case than the time the domain wall itself takes to reach the next gate. In fact the worst time of gate charging is equal to $0.55ns$, which is lower with respect to $0.69ns$ which is the time spent for a domain wall to travel from one gate to its successive. In conclusion with these parameters, it is possible to obtain the best performance of the Racetrack Memory in terms of speed, and thinnest gate width. Obviously by choosing intermediate combinations of gate anisotropy $(\pm 5\%, \pm 10\%, \pm 15\%)$, lower current values must be applied through the heavy metal (Ta) so that the domain wall is blocked by the gate as shown in Table A.1. Consequently, for lower values of current, lower speed values of the domain wall would be obtained, and therefore even longer times for a domain wall to travel from one gate to the next one, therefore still compatible with the charging time of the gate. In conclusion, the VCMA gate synchronization

technology along the track would be compatible with Racetrack memories, and therefore a valid alternative to notches, or to geometric modifications 1.7.1 for blocking domain walls.

4.6.6 Energy Consumption

To charge a capacitor to a specific voltage it is necessary to have a battery that supplies an energy equal to $E = CV^2$. Half of the total energy is stored on the capacitor, while the other half is lost to heat, or to electromagnetic energy. In this section the energy required to charge a VCMA gate is evaluated. The gate capacitance is equal to:

$$C_{gate} \approx \epsilon_{MgO} \frac{L_{MgO} W_{MgO}}{t_{MgO}} \tag{4.9}$$

Depending on the material stack implemented for the VCMA gate, different voltages are needed to reach the desired anisotropy value of the gate. In Table 4.1 all the electric fields are reported. The voltages are equal to the product between the electric fields reported in Table 4.1 and the MgO thickness reported in table 4.2. In the following graph the energy consumption is plotted in function of the applied voltage for the three different values of gate width reported in Table 4.2:

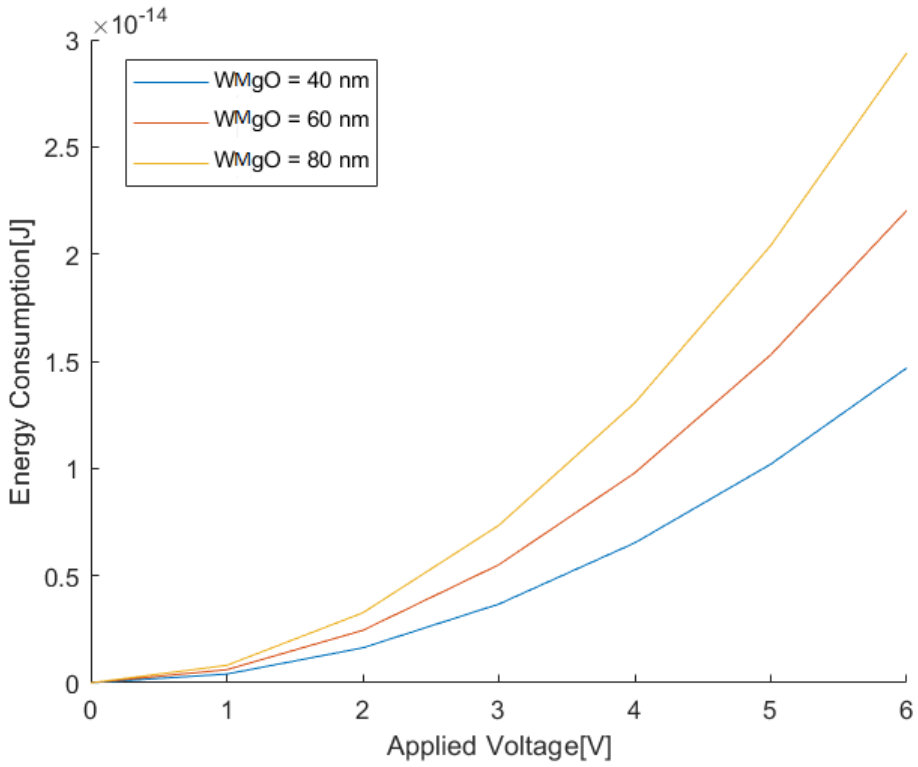

Figure 4.14: Energy Consumption in function of the applied voltage across the VCMA gate, evaluated for the three different values of gate width

The maximum consumption for an applied voltage of $6V$ in the case of wider gate ($80nm$), is equal to $\approx 30fJ$. Depending on the chosen stack (looking at table 4.1) the applied voltages needed to reach the desired anisotropy level of the gate change.
Looking at Table 4.3 the energy consumption for the 60 nm wide gate are equal to:

- $\approx 17.4fJ$ if a $Ta/CoFeB/MgO$ stack is chosen;
- $\approx 9.8fJ$ if a $W/CoFeB/MgO$ stack is chosen;

Looking at Table 4.3 the energy consumption for the 40 nm wide gate are equal to:

- $\approx 11.6fJ$ if a $Ta/CoFeB/MgO$ stack is chosen;
- $\approx 6.5fJ$ if a $W/CoFeB/MgO$ stack is chosen;

Therefore taking in consideration both the trade-off between the gate width and average velocity of the domain wall, and the lowest energy consumption, the best choice is to choose a $40nm$ wide gate, with $W/CoFeB/MgO$ stack with a VCMA gate anisotropy of 20% lower with respect to the anisotropy of the $CoFeB$ track.

Chapter 5

Conclusions

In summary, the thesis is aimed at demonstrating that the Voltage Controlled Magnetic Anisotropy (VCMA) technology is potentially applicable to a Racetrack memory because the time to reach a specific voltage level of a VCMA gate for blocking a domain wall is shorter than the time required for a domain wall to travel from one gate to its successive (deepen explanation in chapter 4.6). In addition to the compatibility of the operating times, also the relative consumption of the VCMA technology applied to a Racetrack memory is evaluated (look at section 4.6.6).
This analysis relating to the VCMA technology is carried out with the micromagnetic simulator Mumax3. At the same time, a two coordinates analytical model is developed, which allows to estimate the passage of a domain wall through a VCMA gate without the need to perform a micromagnetic study on the structure. In fact the two-coordinates analytical model reported in the equation 2.163 has been expanded with the addition of a pinning field related to the VCMA gate described by the equation 2.149 giving rise to the final differential system reported in equation 2.166. The analytical model predicts with a good approximation the current thresholds of the VCMA induced barriers.
For future works an improvement of the analytical model developed in the thesis would certainly consist in considering the effect of the external temperature, and of any grains present in the ferromagnetic material. In addition, possible defects in the material or in the track could also be taken in consideration. In the specific case of defects, they could be modeled as effective potentials, similarly to how a VCMA gate or a pinning site is modeled. There

are already some effective fields that allow to model these phenomena analytically but they have not been taken in consideration during the analysis carried out in the thesis. Moreover more materials could be analyzed, with different VCMA constants, or a more in-depth analysis could be done, varying as many parameters as possible during the timing analysis and during the energetic consumption evaluation. It would be interesting to study more complex systems, for instance an entire Racetrack memory: thus simulating several domains, and making an evaluation in terms of writing and reading times and consumption.

Appendix A

Appendix

Free electron tunneling model

The first theoretical approach to describe the behaviour of tunneling electron is a free electron model. Supposing that the potential barrier does not depend on time, and it is only a one-dimensional function of 'z':

$$\frac{-\hbar^2}{2m}\nabla^2\psi(x,y,z,t) + V(z)\psi(x,y,z,t) = i\hbar\frac{\partial\psi(x,y,z,t)}{\partial t} \tag{A.1}$$

Since $V(z)$ is a function of space and not a function of time, it can be made the assumption of factorizing the wave function separating the space component from the time component:

$$\frac{-\hbar^2}{2m}\nabla^2(\phi(x,y,z)\chi(t)) + V(z)\phi(x,y,z)\chi(t) = i\hbar\frac{\partial(\phi(x,y,z)\chi(t))}{\partial t} \tag{A.2}$$

$$\frac{-\hbar^2}{2m}\chi(t)\nabla^2\phi(x,y,z) + V(z)\phi(x,y,z)\chi(t) = i\hbar\phi(x,y,z)\frac{\partial\chi(t)}{\partial t} \tag{A.3}$$

Dividing both member of the equation by $\chi(t)\cdot\phi(x,y,z)$:

$$\frac{-\hbar^2}{2m\phi(x,y,z)}\nabla^2\phi(x,y,z) + V(z) = \frac{i\hbar}{\chi(t)}\frac{\partial\chi(t)}{\partial t} \tag{A.4}$$

The left side is a function of "z" while the right side is a function of time, so to be equal they must be equal to a constant:

$$\begin{cases} \frac{i\hbar}{\chi(t)}\frac{\partial\chi(t)}{\partial t} = E \\ \frac{-\hbar^2}{2m\phi(x,y,z)}\nabla^2\phi(x,y,z) + V(z) = E \end{cases} \tag{A.5}$$

Neglecting the time equation and focusing on the spatial part:

$$\frac{-\hbar^2}{2m}\nabla^2\phi(x,y,z) + V(z)\phi(x,y,z) = E\phi(x,y,z) \tag{A.6}$$

Being the potential only a function of "z" the spatial wave function could be factorized again:

$$\frac{-\hbar^2}{2m}\nabla^2(\Phi(x,y)\theta(z)) + V(z)\Phi(x,y)\theta(z) = E\Phi(x,y)\theta(z) \tag{A.7}$$

Making explicit ∇ and dividing both members by $\Phi(x,y)\theta(z)$:

$$\frac{-\hbar^2}{2m\Phi(x,y)}(\frac{\partial^2}{\partial x^2} + \frac{\partial^2}{\partial y^2})\Phi(x,y) - \frac{\hbar^2}{2m\theta(z)}\frac{\partial^2\theta(z)}{\partial z^2} + V(z) = E \tag{A.8}$$

In order to be equal to a constant, the two terms of the equation, one depending on x,y and one depending on z, must be equal to a constant:

$$\begin{cases} \frac{-\hbar^2}{2m\Phi(x,y)}(\frac{\partial^2}{\partial x^2} + \frac{\partial^2}{\partial y^2})\Phi(x,y) = E_{x,y} \\ -\frac{\hbar^2}{2m\theta(z)}\frac{\partial^2\theta(z)}{\partial z^2} + V(z) = E_z \end{cases} \tag{A.9}$$

from the first equation, it is easy to derive that:

$$k_{//} = \sqrt{\frac{2mE_{x,y}}{\hbar^2}} \tag{A.10}$$

Replacing in the three dimensional Schrodinger equation, it is trivial to obtain:

$$\frac{\partial^2\theta(z)}{\partial z^2} + (\frac{2mE_z}{\hbar^2} - \frac{2mV(z)}{\hbar^2} - k_{//}^2)\theta(z) = 0 \tag{A.11}$$

Since $V(z)$ is defined as follow:

$$\begin{cases} V_1 & z < 0 \\ V_B 0 < z < l \\ V_2 & z > l \end{cases} \tag{A.12}$$

As a consequence it is possible to define:

$$\begin{cases} k_1 = \sqrt{\frac{2m}{\hbar^2}(E_z - V_1) - k_{//}} \\ k_B = \sqrt{\frac{2m}{\hbar^2}(V_B - E_z) - k_{//}} \\ k_2 = \sqrt{\frac{2m}{\hbar^2}(E_z - V_2) - k_{//}} \end{cases} \tag{A.13}$$

Solutions of the Schrodinger equations are:

$$\begin{cases} \theta_1(z) = A \cdot e^{ik_1 z} + B \cdot e^{-ik_1 z} & z < 0 \\ \theta_B(z) = F \cdot e^{-k_B z} + G \cdot e^{k_B z} 0 < z < l \\ \theta_2(z) = C \cdot e^{ik_2 z} + D\dot{e}^{-ik_2 z} \end{cases} \tag{A.14}$$

Applying the boundary conditions:

$$\begin{cases} \theta_1(0) = \theta_B(0) \\ \theta_1^{'}(0) = \theta_B^{'}(0) \\ \theta_B(l) = \theta_2(l) \\ \theta_B^{'}(l) = \theta_2^{'}(l) \end{cases} \tag{A.15}$$

The system below is obtained:

$$\begin{cases} A + B = F + G \\ A - B = -\frac{k_B}{ik_1}(F - G) \\ F \cdot e^{-k_B l} + G \cdot e^{k_B l} = C \cdot e^{ik_2 l} \\ F \cdot e^{-k_B l} - G \cdot e^{k_B l} = -\frac{ik_2}{k_B} \cdot e^{ik_2 l} \end{cases} \tag{A.16}$$

Summing and subtracting the third and the fourth equation of the system above it is possible to obtain F and G, that could be replaced in the first and in the second equation, and subtracting and summing again it is possible to obtain a final expression for A and B:

$$\begin{cases} A = \frac{C}{2}\dot{e}^{ik_2 l}[(1 + \frac{k_2}{k_1})cosh(k_B l) + i(\frac{k_B}{k_1} - \frac{k_2}{k_B})sinh(k_{Bl})] \\ B = \frac{C}{2}e^{ik_2 l}[(1 - \frac{k_2}{k_1})cosh(k_B l) - i(\frac{k_B}{k_1} + \frac{k_2}{k_B})sinh(k_B l)] \end{cases} \tag{A.17}$$

Now, exploiting the definition of transmission probability:

$$T := |\frac{C}{A}|^2 = \frac{1}{\frac{1}{4}(1 + \frac{k_2}{k_1})^2 cosh(k_B l)^2 + \frac{1}{4}(\frac{k_B^2 - k_1 k_2}{k_1 k_B})^2 sinh(k_B l)^2} \tag{A.18}$$

Replacing $cosh(k_B l) = \frac{e^{k_B l} + e^{-k_B l}}{2}$ and $sinh(k_B l) = \frac{e^{k_B l} - e^{-k_B l}}{2}$, and after some trivial algebraic manipulation [48]:

$$T = \frac{16 k_1^2 k_B^2 e^{2k_B l}}{[k_B(k_1 + k_2)(1 + e^{2k_B l})]^2 + [(k_B^2 - k_1 k_2)(1 - e^{2k_B l})]^2} \tag{A.19}$$

Landauer Formula

To analyze the conduction of electrons moving from one ferromagnetic to the other through the tunneling barrier, the Landauer model is exploited. Under Landaur hypothesis the current corresponding to the k^+ states in one of the two ferromagnetic layer and for one 1D channel is given by [49]:

$$I_n^+ = -e \int_0^{+\infty} \frac{D(E)^{1D} v^+(E)}{2} f^+(E) dE \tag{A.20}$$

For simplicity $'x'$ and $'y'$ directions are neglected and taking in consideration only the $'z'$ direction[49].

$$\begin{cases} v(E) = \sqrt{\frac{2(E-E_n}{m^*}} \\ D(E) = \frac{1}{\pi\hbar}\sqrt{\frac{2m*}{E-E_n}} \\ f^+(E) = f(E - E_{FL}) \end{cases} \tag{A.21}$$

Replacing inside the equation of the current I^+[49]:

$$I_n^+ = -\frac{e}{\pi\hbar} \int_{E_n}^{+\infty} f(E - E_{FL}) dE \tag{A.22}$$

if E_n is higher than E_{FL} the conduction will not happen because the sub-band is empty. Defining a step function $\mu_n(E - E_n)$[49]:

$$\begin{cases} 0 E < E_n \\ 1 E > E_n \end{cases} \tag{A.23}$$

Summing the contribution of all the sub-bands[49]:

$$I^+ = \sum_n I_n^+ = -\frac{e}{\pi\hbar} \int_0^{+\infty} f(E - E_{FL}) \mu_n(E - E_n) dE \tag{A.24}$$

$$I^+ = -\frac{e}{\pi\hbar} \int_0^{+\infty} f(E - E_{FL}) \sum_n \mu_n(E - En) dE = -\frac{e}{\pi\hbar} \int_0^{+\infty} f(E - E_{FL}) M(E) dE \tag{A.25}$$

In the same way I^- could be defined[49]:

$$I^- = \frac{e}{\pi\hbar} \int_0^{+\infty} f(E - E_{FR}) M(E) dE \tag{A.26}$$

Summing the two current contributions, taking in consideration that at the oxide barrier there is a certain probability of reflection and a certain probability of tunneling, and supposing that the difference between the two Fermi distributions is unitary in the approximation of Fermi function as a step function (0K):

$$I = \frac{2e}{h} M(E_{FL} - E_{FR}) T_z = \frac{2e}{h} M(E_{FL} - E_{FR}) \int_{k_{//}} T(k_{//}) dk_{//} \tag{A.27}$$

Where M is an integer number depending on the function $M(E)$.
The conductance is defined as [49]:

$$G = \frac{|e|I}{(E_{FL} - E_{FR})} = \frac{2e^2 M}{h} \int_{k_{//}} T(k_{//}) dk_{//} \tag{A.28}$$

where $T(k_{//})$ is the function calculated with the free electron tunneling model.

$$G = \frac{|e|I}{(E_{FL} - E_{FR})} = \frac{2e^2 M}{h} \int_{k_{//}} \frac{16 k_1^2 k_B^2 e^{2k_B l}}{[k_B(k_1 + k_2)(1 + e^{-2k_B l})]^2 + [(k_B^2 - k_1 k_2)(1 - e^{-2k_B l})]^2} dk_{//} \tag{A.29}$$

remembering that k_1, k_2, k_B are function of $k_{//}$.

Julliere's model

It is a two current model based on the first assumption that the conductance is proportional to the product of the Fermi energy density of states in the electrodes on either side of the barrier:

$$\begin{cases} G_P = G^{\uparrow\uparrow} + G^{\downarrow\downarrow} \\ G_{AP} = G^{\uparrow\downarrow} + G^{\downarrow\uparrow} \end{cases} \tag{A.30}$$

where

$$\begin{cases} G^{\uparrow\uparrow} \propto N_L^{\uparrow} N_R^{\uparrow} \\ G^{\downarrow\downarrow} \propto N_L^{\downarrow} N_R^{\downarrow} \\ G^{\uparrow\downarrow} \propto N_L^{\uparrow} N_R^{\downarrow} \\ G^{\downarrow\uparrow} \propto N_L^{\downarrow} N_R^{\uparrow} \end{cases} \tag{A.31}$$

The tunnel magneto resistance is defined as follow:

$$TMR \equiv \frac{G_P - G_{AP}}{G_{AP}} = \frac{N_L^{\uparrow}N_R^{\uparrow} + N_L^{\downarrow}N_R^{\downarrow} - N_L^{\uparrow}N_R^{\downarrow} - N_L^{\downarrow}N_R^{\uparrow}}{N^{\uparrow}N^{\downarrow} + N_L^{\downarrow}N_R^{\uparrow}} = \frac{(N_L^{\uparrow} - N_L^{\downarrow}) \cdot (N_R^{\uparrow} - N_R^{\downarrow})}{N_L^{\uparrow}N_R^{\downarrow} + N_L^{\downarrow}N_R^{\uparrow}} \tag{A.32}$$

$$TMR \equiv \frac{\Delta N_L \Delta N_R}{N_L^{\uparrow}N_R^{\downarrow} + N_L^{\downarrow}N_R^{\uparrow}} \tag{A.33}$$

The denominator of the fraction can be rewritten as follow, with a trivial algebraic manipulation:

$$TMR \equiv \frac{\Delta N_L \Delta N_R}{\frac{1}{2}(N_L N_R - \Delta N_L \Delta N_R)} = \frac{2\frac{\Delta N_R \Delta N_L}{N_L N_R}}{1 - \frac{\Delta N_R \Delta N_L}{N_L N_R}} \tag{A.34}$$

Exploiting the definition of the polarization of the ferromagnetic layers (electrodes of the structure):

$$P_{L,R} \equiv \frac{N_{L,R}^{\uparrow} - N_{L,R}^{\downarrow}}{N_{L,R}^{\uparrow} + N_{L,R}^{\downarrow}} = \frac{\Delta N_{L,R}}{N_{L,R}} \tag{A.35}$$

Substituting inside the expression of the TMR:

$$TMR \equiv \frac{2P_L P_R}{1 - P_L P_R} \tag{A.36}$$

Slonczewski's model

Slonczewski started from the simplest free electron model. Combining the latter with the Julliere's result, he was able to find an effective polarization of the layer and to obtain a more exact equation for the TMR. The Hamiltonian of the free electron model is a bit modified, and then exploiting the charge current density, which is conserved throughout the junction, it is possible to obtain the Slonczewski's formula. The potential barrier is supposed to be a function of "x":

$$\begin{cases} H = \frac{\hbar^2 k_{\perp}^2}{2m} - \frac{1}{2}\vec{\Delta} \cdot \vec{\sigma} & x < 0 \cup x > l \\ H = \frac{\hbar^2 k_{\perp}^2}{2m^*} + U(x) & 0 \leq x \leq l \end{cases} \tag{A.37}$$

"m" is the effective mass inside the ferromagnetic layers while "m^*"is the effective mass inside the oxide barrier. $\vec{\Delta}$ is the exchange field while $\vec{\sigma}$ are

the Pauli matrices. Taking in consideration that the magnetization of the free layer is rotated for a certain angle θ, it is trivial to write the wave functions and the relative "k" in the three regions respectively [19]. Then exploiting the definition of the charge current density:

$$J_e = \frac{e\hbar}{2m^* i}[(\psi\uparrow^* \ \psi_\downarrow^*) \cdot \begin{pmatrix} \frac{d\psi_\uparrow}{dx} \\ \frac{d\psi_\downarrow}{dx} \end{pmatrix} - (\psi\uparrow \ \psi_\downarrow) \cdot \begin{pmatrix} \frac{d\psi_\uparrow^*}{dx} \\ \frac{d\psi_\downarrow^*}{dx} \end{pmatrix}] \tag{A.38}$$

and solving the equation for the leading order in $e^{-E_b(d)}$ [19], the Slonczewski equation is obtained:

$$J_e(E) = J_0(1 + P^2 cos(\theta)) \tag{A.39}$$

where "P" is the "effective polarization" which differs from the Julliere's polarization because this time it takes in consideration also the coupling between the spacer and the ferromagnetic contact.

$$P_i = \left(\frac{k_i^\uparrow - k_i^\downarrow}{k_i^\uparrow + k_i^\downarrow}\right) \cdot \left(\frac{k_B^2 - k_i^\uparrow k_i^\downarrow}{k_B^2 + k_i^\uparrow k_i^\downarrow}\right) \tag{A.40}$$

Defining the polarization in this new way, Slonczewski was able to define the Tunnel Magneto Resistance (TMR) with the same mathematical formulation of Julliere:

$$TMR \equiv \frac{I_P - I_{AP}}{I_{AP}} \propto \frac{2P_L P_R}{1 - P_L P_R} \tag{A.41}$$

with P_i the "new effective polarization" defined just above.

Four-Collective Coordinates system

In this section, just to add more detail to the thesis, the Four-Collective Coordinates system obtained through the Lagrangian approach is reported

[36]:

$$\begin{cases} \frac{cos(\Gamma)}{\Delta}\dot{q} = \frac{w}{2\Delta cos(\Gamma)}\dot{\Gamma} + \frac{\pi\gamma D_0}{2M_s\Delta}sin(\phi-\Gamma) - \frac{\gamma K_d}{M_s}sin(2(\phi-\Gamma)) + \alpha\dot{\phi} + \\ \qquad + \frac{u\cdot cos(\Gamma)}{\Delta} + \gamma\frac{\pi}{2}a_{FL}cos(\phi) \\ \dot{\phi} = -\mu_0\gamma H_{ext} - \alpha\frac{cos(\Gamma)}{\Delta}\dot{q} + \alpha\frac{w}{2\Delta cos(\Gamma)}\dot{\Gamma} + \frac{\beta u\cdot cos(\Gamma)}{\Delta} - \gamma\frac{\pi}{2}b_{DL}cos(\phi) \\ \alpha\frac{\pi^2}{12}[\frac{\dot{\Delta}}{\Delta} - \frac{\dot{\Gamma}}{cos(\Gamma)}] = \frac{\gamma}{M_s}[\frac{A}{\Delta^2}(1+sin(2\Gamma)) - K_u - k_d sin^2(\phi-\Gamma)] - \frac{\pi}{2}\gamma a_{FL}sin(\phi) \\ \alpha\frac{\pi^2}{12}[\frac{\dot{\Delta}}{\Delta} - \frac{\dot{\Gamma}}{\Gamma}((\frac{w}{\pi\Delta})^2 + \frac{sin^2(\Gamma)}{2})] = \frac{\gamma}{M_s}[\frac{A}{\Delta^2}(2cos^3(\Gamma)+sin(\Gamma)) + \\ \qquad + sin(\Gamma)(K_u + k_d sin^2(\phi-\Gamma)) + \\ \qquad - cos(\Gamma)k_d sin(2(\phi-\Gamma))] + \\ \qquad + \frac{\pi D_0\gamma}{2\Delta M_s}sin(\phi) - \frac{\pi}{2}\gamma sin(\Gamma)a_{FL}sin(\phi) \end{cases} \tag{A.42}$$

Implementing this differential equation system, the domain wall motion could be described more accurately with respect to the differential system 2.162. To make the system 2.162 more accurate, the domain wall width is considered as a piecewise function in the case of the presence of gates that modify the local anisotropy during the resolution of the differential system with Matlab. At the same time the average of the tilting angle is evaluated using Mumax3 as explained in the section 2.1. For more details about the four coordinate model, its limitations and its innovativeness look at [36].

Threshold Current

In the following table all the threshold current values, for different anisotropy levels of the VCMA gate, and for different gate width are reported:

Table A.1: Threshold Current

Gate width	Anisotropy Variation	Threshold Current
40 nm	-20%	$\approx 4e11\frac{A}{m^2}$
40 nm	-15%	$\approx 1.5e11\frac{A}{m^2}$
40 nm	-10%	$\approx 0.75e11\frac{A}{m^2}$
40 nm	-5%	$\approx 0.75e11\frac{A}{m^2}$
40 nm	$+5\%$	$\approx 0.75e11\frac{A}{m^2}$
40 nm	$+10\%$	$\approx 2e11\frac{A}{m^2}$
40 nm	$+15\%$	$\approx 2e11\frac{A}{m^2}$
40 nm	$+20\%$	$\approx 2.5e11\frac{A}{m^2}$
60 nm	-20%	$\approx 3e11\frac{A}{m^2}$
60 nm	-15%	$\approx 1.5e11\frac{A}{m^2}$
60 nm	-10%	$\approx 1e11\frac{A}{m^2}$
60 nm	-5%	$\approx 0.5e11\frac{A}{m^2}$
60 nm	$+5\%$	$\approx 0.75e11\frac{A}{m^2}$
60 nm	$+10\%$	$\approx 2e11\frac{A}{m^2}$
60 nm	$+15\%$	$\approx 2.5e11\frac{A}{m^2}$
60 nm	$+20\%$	$\approx 3e11\frac{A}{m^2}$
80 nm	-20%	$\approx 3.5e11\frac{A}{m^2}$
80 nm	-15%	$\approx 2e11\frac{A}{m^2}$
80 nm	-10%	$\approx 1e11\frac{A}{m^2}$
80 nm	-5%	$\approx 0.5e11\frac{A}{m^2}$
80 nm	$+5\%$	$\approx 0.75e11\frac{A}{m^2}$
80 nm	$+10\%$	$\approx 1.5e11\frac{A}{m^2}$
80 nm	$+15\%$	$\approx 2.5e11\frac{A}{m^2}$
80 nm	$+20\%$	$\approx 3e11\frac{A}{m^2}$

Mumax3 Code

STT code

```
//Dimension of the material and its discretization
Nx := 768
Ny := 128
Nz := 1
setGridSize(Nx, Ny, Nz)
setCellSize(1e-9, 1e-9, 1e-9)
//Period Boundary Condition (PBC). PBC must be canceled out to evaluate the position, the speed, and the tilting angle of the Domain Wall through ext_dwpos, ext_dwspeed, ext_dwtilt respectively
//setPBC(4,0,0)


//Tilting angle of anisotropy vector
angle := 0.05 //between 0.01 and 1
py := sin(angle * pi/180)
pz := cos(angle * pi/180)

//Parameters
Msat = 1e6 //Saturation Magnetization
Aex = 10e-12 // Exchange stiffness interaction
anisU = vector(0, py, pz) //Anisotropy Vector
Ku1 = 0.8e6 //Anisotropy constant
alpha = 0.04 //max = 0.04 min = 0.015, Damping factor
Xi = 0.2 //Non-adiabatic parameter
pol = 1 //Current Polarization
//Dind = 0.6e-3 //DMI interaction J/m^3
w := 60e-9 //VCMA gate width
n := 1 //Number of Domain Walls in the piece of material
p :=-Nx*1e-9/2+Nx*1e-9/(2*n) //Parameter necessary for the evaluation of the magnetization domains and for the VCMA gate position


//Magnetization Domain Definition
for i := n; i>0; i-=1
defregion(i, rect(Nx*1e-9/n,Ny).transl(p+(n-i)*(Nx*1e-9/n),0,0)) m.setRegion(i,
```

twoDomain(0,0,-pow(-1,i), 0,1,0, 0,0, pow(-1,i)).transl(p+(n-i)*(Nx*1e-9/n),0,0))

minimize() //Energy Minimization

//Region of different anisotropy definition
for k := n; k>0; k-=1 {
defregion(n+k, rect(w,Ny).transl(p+(n-k)*(Nx*1e-9/n)+64e-9,0,0)) Ku1.setRegion(n+k, 1.1*Ku1.GetRegion(0)) }

ext_centerWall(2)//Centering of the simulation window to evaluate position, speed and tilting angle of the DW

// Schedule output
autosave(m, 10e-12) //Magnetization autosave
tableadd(*ext_dwpos*) //Domain Wall Position
tableadd(*ext_dwspeed*) //Domain Wall Speed
tableadd(*ext_dwtilt*) //Domain Wall Tilting Angle
tableautosave(10e-16) //Really dense autosaving to have good fitting of the DW Tilting Angle

j = vector(0.75e12, 0, 0) //STT Current in 'x' direction
// Run for 8ns with current through the sample
run(8e-9)

SOT code

//Dimension of the material and its discretization
Nx := 768
Ny := 128
Nz := 1
setGridSize(Nx, Ny, Nz)
setCellSize(1e-9, 1e-9, 1e-9)
//Period Boundary Condition (PBC). PBC must be canceled out to evaluate the position, the speed, and the tilting angle of the Domain Wall through

ext_dwpos, *ext_dwspeed*, *ext_dwtilt* respectively
//setPBC(4,0,0)

//Tilting angle of anisotropy vector angle := 0.05 //between 0.01 and 1 rad
py := sin(angle * pi/180)
pz := cos(angle * pi/180)

//Parameters
Msat = 1e6 //Saturation Magnetization
Aex = 10e-12 // Exchange stiffness interaction
anisU = vector(0, py, pz) //Anisotropy Vector
Ku1 = 0.8e6 //Anisotropy constant
alpha = 0.04 //max = 0.04 min = 0.015, Damping factor
Xi = 0.2 //Non-adiabatic parameter
pol = 1 //Current Polarization
Dind = 0.6e-3 //DMI interaction $\frac{J}{m^3}$
w := 60e-9 //VCMA gate width
n := 1 //Number of Domain Walls in the piece of material
p :=-Nx*1e-9/2+Nx*1e-9/(2*n) //Parameter necessary for the evaluation of the magnetization domains and for the VCMA gate position

//Magnetization Domain Definition
for i := n; i>0; i-=1 {
defregion(i, rect(Nx*1e-9/n,Ny).transl(p+(n-i)*(Nx*1e-9/n),0,0)) m.setRegion(i, twoDomain(0,0,-pow(-1,i), pow(-1,i),0,0, 0,0, pow(-1,i)).transl(p+(n-i)*(Nx*1e-9/n),0,0)) }

minimize() //Energy Minimization

//Define constants for SOT
AlphaH := 0.15 //Parameter of the Damping like SOT
e := 1.6021766e-19 //Electron charge
d := 1e-9 //oxide thickness
Ms := 1e6 //Saturation Magnetization
hbar := 1.0545718e-34 //Reduced Planck constant
zi := ConstVector(0, 1, 0) //Direction Perpendicular to the Spin Current

and to the Underlayer Current
SOTxi := -2.0 //Ratio between Field Like SOT and Damping SOT
J_SOT := abs(-0.5e11) //Underlayer Current

//Define Damping Like SOT and Field Like SOT prefactors
aj := Const(J_SOT*(hbar/2.*alphaH/e/d/Ms)) //Damping Like factor
bj := Mul(aj,Const(SOTxi)) //Field Like Factor

//Add damping-like SOT term
dampinglike := Mul(aj, Cross(m,zi))
AddFieldTerm(dampinglike)
AddEdensTerm(Mul(Const(-0.5),Dot(dampinglike,M_full)))

//Add field-like SOT term
fieldlike := Mul(bj,zi)
AddFieldTerm(fieldlike)
AddEdensTerm(Mul(Const(-0.5),Dot(fieldlike,M_full)))

//Region of different anisotropy definition
for k := n; k>0; k-=1 {
defregion(n+k, rect(w,Ny).transl(p+(n-k)*(Nx*1e-9/n)-128e-9,0,0)) Ku1.setRegion(n+k,
1*Ku1.GetRegion(0))
}

$ext\_centerWall$(2) //Centering of the simulation window to evaluate position, speed and tilting angle of the DW

// Schedule output
autosave(m, 10e-12) //Magnetization autosave
tableadd(ext_dwpos) //Domain Wall Position
tableadd($ext\_dwspeed$) //Domain Wall Speed
tableadd(ext_dwtilt) //Domain Wall Tilting Angle
tableautosave(10e-16) //Really dense autosaving to have good fitting of the DW Tilting Angle

// Run for 8ns with current through the sample
run(8e-9)

Descriptive images of the code

In order to better understand the following piece of the code: for i := n; i>0; i-=1 {
defregion(i, rect(Nx*1e-9/n,Ny).transl(p+(n-i)*(Nx*1e-9/n),0,0)) m.setRegion(i, twoDomain(0,0,-pow(-1,i), pow(-1,i),0,0, 0,0, pow(-1,i)).transl(p+(n-i)*(Nx*1e-9/n),0,0)) }
the following images are reported:

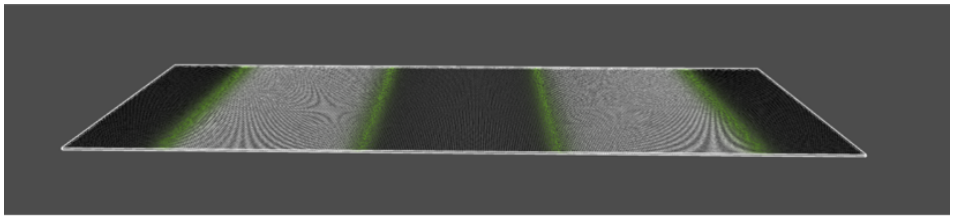

Figure A.1: Four Domain Walls (DWs) $n = 4$

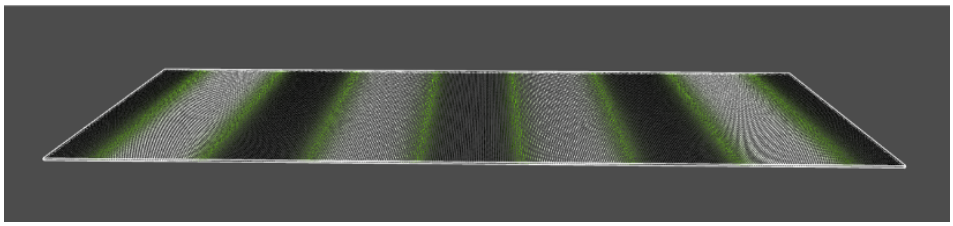

Figure A.2: Eight Domain Walls (DWs) $n = 8$

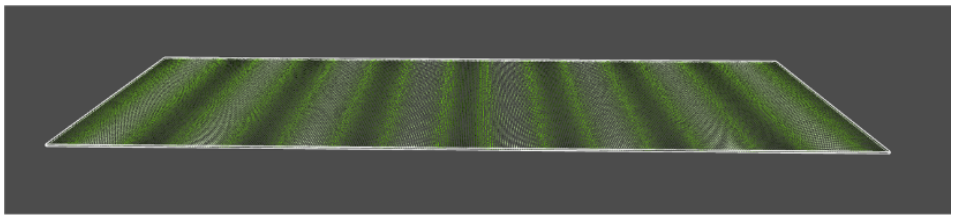

Figure A.3: Sixteen Domain Walls (DWs) $n = 16$

Matlab Code

```
clear all
clc

%Mumax_section
load tiltMumax.txt %Mumax3 simulation file
mum = tiltMumax(:,:);

angle_mum = mum (:,7); %tilting angle vector of the Domain Wall
velocity = mum (:,6); %velocity vector of the Domain Wall
pos = mum (:,5); %position vector of the Domain Wall
t = mum(:,1); %time vector of Mumax3 simulation
time = 0:8e-9/(length(angle_mum)-1):8e-9;
M = length(time);

%polynomial approximation of the tilting angle of the Domain Wall
[p, S, mu] = polyfit(t, angle_mum, 35);
%polynomial approximation of the tilting angle of the Domain Wall
[angle, delta_p] = polyval(p,t,S,mu);
%time derivative of the tilting angle polynomial function of the Domain Wall
dangle = zeros(1,length(angle));

%average tilting angle of the Domain Wall
sum_angle = 0;
for i = 1:length(angle)
    sum_angle = sum_angle + angle_mum(i);
end
%average tilting angle of the Domain Wall
angle_average = sum_angle/length(angle);

%Parameters
A = 10*10^-12; %Exchange stiffness [j/m]
M_s = 10^6; %Saturation magnetization [A/m]
N_x = 0; %Demagnetizing Tensor
N_y = 0; %Demagnetizing Tensor
N_z = 1; %Demagentizing Tensor
mu_0 = 4*pi*10^-7; %Magnetic permeability [Henry/m]
t_FM = 10^-9; %ferromagnetic layer thickness
H = 0; %external field along 'z' axis
alpha = 0.04; %damping factor
Q = -1.602176634*10^-19; %electron charge
```

```
m = 9.109*10^-31; %electron mass [kg]
gamma = -1.7595e11; %gyromagnetic ratio [rad/(s*T)]
hbar = 1.0545718*10^-34; %reduced Planck constant
J_SOT = 1.5*10^11; %SOT current density [A/m^2]
mu_b = 9.274*10^-24; %Bohr Magneton [J/tesla]
tau_fl = hbar*J_SOT*0.3/(2*Q*t_FM*M_s*mu_0); %SOT Field-like
tau_dl = -hbar*J_SOT*0.15/(2*Q*t_FM*M_s*mu_0); %SOT Damping-like
D_dmi = 0.6e-3; %Dzyaloshinskii-Moriya interaction
G = 2; %Landé Factor
P = 1; %Polarization of the STT current density
J = 1*10^12; %STT current density [A/m^2]
beta = 0.2; %Non-Adiabaticity STT factor
u = G*mu_b*P*J/(2*Q*M_s*(1+beta^2)); %Adiabaticity STT factor
w = 128e-9; %width of the ferromagnetic material
k_u = 0.8e6; %anisotropy constant of the ferromagnetic layer
delta = sqrt((A)/(k_u+0.5*mu_0*M_s^2*(-N_z))); %Initial Domain Wall width
%Sharpness of the anisotropy profile of the VCMA gate
delta_1 = sqrt((A)/(k_u+0.5*mu_0*M_s^2*(-N_z)));
k_d = (d*log(2)/(pi*delta))*mu_0*M_s*M_s/2; %Transverse Shape Anisotropy

%VCMA Gate Parameters
anisotropy_var = 0.16e6; %Anisotropy variation of the VCMA Gate
%'c' = position of the center of the VCMA gate
%positive value of 'c' implies a shifting of the gate to the left
%with respect to center of the track ('0' position)
c = 128e-9; %[m]
w_gate = 60e-9; %width of the VCMA Gate [m]

%Initialization vector
phi = zeros(length(dangle),1);
q = 0*ones(1,length(time));

for i = 1:length(dangle)
%First alternative for the evaluation of the tilting profile
% of the Domain Wall: this approach could create instability
%of the results due to non-precise polynomial approximations.
%The tilting angle of the Domain Wall is given to the differential system
%point by point
tilt = angle_mum(i);
%the time derivative of the tilting angle of the Domain Wall
%is given to the differential system point by point
dtilt = dangle(i);
```

```
%Second alternative for the evaluation of the tilting profile
%of the Domain Wall: this approach gives stable results,
%and it is still valid because usually the Domain Wall after a while
%reaches an almost constant tilting angle
tilt = angle_average(i);
dtilt = 0;

%Diffential equation system

%'fq' = time derivative of 'q' which is the center of the Domain Wall

fq{i} = @(t, q, phi, delta, k_d) (dtilt.*w.*(1+alpha.^2)./(cos(tilt).*2.*delta)
- gamma.*k_d.*sin(2.*(phi-tilt))./M_s
+ pi.*D_dmi.*gamma.*sin(phi-tilt)./(2.*delta.*M_s) + u.*cos(tilt)./delta
+ mu_0.*gamma.*pi.*tau_fl.*cos(phi)./2 + alpha.*beta.*u.*cos(tilt)./(delta)
-alpha.*gamma.*(anisotropy_var./2).*(4.*(csch((c-w_gate./2+q)./delta_1)).^2
.*(coth((c-w_gate./2+q)./delta_1).*((c-w_gate./2+q)./delta_1)-1)
- 4.*(csch((c+w_gate./2+q)./delta_1)).^2.*(coth((c+w_gate./2+q)./delta_1)
.*((c+w_gate./2+q)./delta_1)-1))./(2.*M_s) - alpha.*mu_0.*gamma.*H
- alpha.*mu_0.*gamma.*tau_dl.*cos(phi).*pi./2)./(cos(tilt).*(1+alpha.^2)./delta);

%'fphi' = time derivative of 'phi' which is the precession angle of the
%magnetization of the Domain Wall

fphi{i} = @(t, q, phi, delta, k_d) - gamma.*(anisotropy_var./2)
.*(4.*(csch((c-w_gate./2+q)./delta_1)).^2.*(coth((c-w_gate./2+q)./delta_1)
.*((c-w_gate./2+q)./delta_1)-1) - 4.*(csch((c+w_gate./2+q)./delta_1)).^2
.*(coth((c+w_gate./2+q)./delta_1).*((c+w_gate./2+q)./delta_1)-1))./(2.*M_s)
+ alpha.*dtilt.*w./(cos(tilt).*2.*delta) + beta.*u.*cos(tilt)./(delta)
- mu_0.*gamma.*H - mu_0.*gamma.*tau_dl.*cos(phi).*pi./2
- alpha.*(cos(tilt)./(delta)).*(dtilt.*w.*(1+alpha.^2)./(cos(tilt).*2.*delta)
- gamma.*k_d.*sin(2.*(phi-tilt))./M_s +
pi.*D_dmi.*gamma.*sin(phi-tilt)./(2.*delta.*M_s) + u.*cos(tilt)./delta
+ mu_0.*gamma.*pi.*tau_fl.*cos(phi)./2 + alpha.*beta.*u.*cos(tilt)./(delta)
- alpha.*gamma.*(anisotropy_var./2).*(4.*(csch((c-w_gate./2+q)./delta_1)).^2
.*(coth((c-w_gate./2+q)./delta_1).*((c-w_gate./2+q)./delta_1)-1)
- 4.*(csch((c+w_gate./2+q)./delta_1)).^2.*(coth((c+w_gate./2+q)./delta_1)
.*((c+w_gate./2+q)./delta_1)-1))./(2.*M_s) - alpha.*mu_0.*gamma.*H
- alpha.*mu_0.*gamma.*tau_dl.*cos(phi).*pi./2)./(cos(tilt).*(1+alpha.^2)./delta);

end
```

```
%Initial conditions
t(1) = 0;
q(1) = 0;
phi(1) = pi/2;
%If phi(1) = n*pi/2 with 'n' an integer, the Domain Wall starting profile
%is a Bloch Domain Wall configuration
%If phi(1) = n*pi with 'n' an integer, the Domain Wall starting profile
%is a Néel Domain Wall configuration

%Step size
tfinal = 8e-9; %Duration of the simulation
N = length(dangle);
h = tfinal/N;

%update loop
for i=1:N
 %Update time
 t(i+1) = t(i) + h;

 %Update q, phi

 k1q = fq{i}(t(i),q(i),phi(i), delta, k_d);
 k1phi = fphi{i}(t(i),q(i),phi(i), delta, k_d);

 k2q = fq{i}(t(i)+h/2,q(i)+h/2*k1q,phi(i)+h/2*k1phi, delta, k_d);
 k2phi = fphi{i}(t(i)+h/2,q(i)+h/2*k1q,phi(i)+h/2*k1phi, delta, k_d);

 k3q = fq{i}(t(i)+h/2,q(i)+h/2*k2q,phi(i)+h/2*k2phi, delta, k_d);
 k3phi = fphi{i}(t(i)+h/2,q(i)+h/2*k2q,phi(i)+h/2*k2phi, delta, k_d);

 k4q = fq{i}(t(i)+h/2,q(i)+h*k3q,phi(i)+h*k3phi, delta, k_d);
 k4phi = fphi{i}(t(i)+h/2,q(i)+h*k3q,phi(i)+h*k3phi, delta, k_d);


 q(i+1) = q(i)+h/6*(k1q + 2*k2q + 2*k3q + k4q);
 phi(i+1) = phi(i)+h/6*(k1phi + 2*k2phi + 2*k3phi + k4phi);

 %If there is a VCMA gate, the local anisotropy constant changes at the gate,
 %therefore the Domain Wall width 'delta' changes

 if ((c-w_gate/2) <= abs(q(i))) & (abs(q(i)) < (c+w_gate/2))
```

```
        k_u = 0.8e6 + anisotropy_var; %VCMA Gate region
        delta = sqrt((A)/(k_u+0.5*mu_0*M_s^2*(-N_z)));
 end

if (0 < abs(q(i))) & (abs(q(i)) < (c-w_gate/2))
        k_u = 0.8e6;
        delta = sqrt((A)/(k_u+0.5*mu_0*M_s^2*(-N_z)));
 end
if (c+w_gate/2) <= abs(q(i))
        k_u = 0.8e6;
        delta = sqrt((A)/(k_u+0.5*mu_0*M_s^2*(-N_z)));
 end

end

%Velocity of the Domain Wall
speed = 0*ones(1,length(time));
for i = 2:N
    speed(i) = fq{i}(t(i),q(i),phi(i), delta, k_d);
end

%Comparison of the average speed of the Domain Wall
%evaluated by Mumax3 and by the Analytical model
sum_th = 0;
sum_mu = 0;

for i = 1:length(speed)
    sum_th = sum_th + speed(i);
    sum_mu = sum_mu + velocity(i);
end

%Average speed of the the Domain Wall evaluate by the Analytical model
speed_theory_av = sum_th/(length(speed));
%Average speed of the the Domain Wall evaluate by Mumax3
speed_mumax_av = sum_mu/(length(speed));

%Plots
%Plot of the Domain Wall's position evaluated by Mumax3
%and by the Analytical model
hold on
xlabel ('time')
ylabel ('DW position')
```

```
plot(time,q(1:end-1))
plot(time, pos)
hold off
figure
%Plot of the Domain Wall's average speed evaluated by Mumax3
%and by the Analytical model
hold on
xlabel ('time')
ylabel ('DW speed')
plot(time,speed)
plot(time, velocity)
hold off
figure
%Plot of the tilting angle of the Domain Wall evaluated
%by Mumax3 and its polynomial approximation
hold on
plot(time, angle_mum)
plot(time, angle)
hold off
figure
%Plot of the time derivative of the tilting angle of the Domain Wall
plot(time, dangle)
```

Bibliography

[1] P. Kusch and H. Foley, "The magnetic moment of the electron," *Physical Review*, vol. 74, no. 3, p. 250, 1948.

[2] "Magnetic moment," https://it.wikipedia.org/wiki/Momento_magnetico, accessed: 2010-09-30.

[3] J. D. Jackson, "Classical electrodynamics," 1999.

[4] S. Chikazumi and C. D. Graham, *Physics of Ferromagnetism 2e*. Oxford University Press on Demand, 2009, no. 94.

[5] D. J. Griffiths and D. F. Schroeter, *Introduction to quantum mechanics*. Cambridge University Press, 2018.

[6] "Exchange interaction," https://www.magnet-shop.com/lexikon/exchange-interaction, accessed: 2010-09-30.

[7] T. Moriya, "Anisotropic superexchange interaction and weak ferromagnetism," *Physical review*, vol. 120, no. 1, p. 91, 1960.

[8] M. Darby and E. Isaac, "Magnetocrystalline anisotropy of ferro-and ferrimagnetics," *IEEE Transactions on Magnetics*, vol. 10, no. 2, pp. 259–304, 1974.

[9] "Demagnetizing field," http://mriquestions.com/object-shape.html, accessed: 2010-09-30.

[10] S. S. Parkin, M. Hayashi, and L. Thomas, "Magnetic domain-wall racetrack memory," *Science*, vol. 320, no. 5873, pp. 190–194, 2008.

[11] S. Parkin and S.-H. Yang, "Memory on the racetrack," *Nature nanotechnology*, vol. 10, no. 3, pp. 195–198, 2015.

[12] R. Bläsing, A. A. Khan, P. C. Filippou, C. Garg, F. Hameed, J. Castrillon, and S. S. Parkin, "Magnetic racetrack memory: From physics to the cusp of applications within a decade," *Proceedings of the IEEE*, vol. 108, no. 8, pp. 1303–1321, 2020.

[13] S. S. Parkin, "Shiftable magnetic shift register and method of using the same," Dec. 21 2004, uS Patent 6,834,005.

[14] S. Parkin, "Magnetic race-track memory: Current induced domain wall motion," *IBM Research*, 2006.

[15] A. D. West, T. J. Hayward, K. J. Weatherill, T. Schrefl, D. A. Allwood, and I. G. Hughes, "A simple model for calculating magnetic nanowire domain wall fringing fields," *Journal of Physics D: Applied Physics*, vol. 45, no. 9, p. 095002, 2012.

[16] D. Kumar, T. Jin, S. Al Risi, R. Sbiaa, W. S. Lew, and S. Piramanayagam, "Domain wall motion control for racetrack memory applications," *IEEE Transactions on Magnetics*, vol. 55, no. 3, pp. 1–8, 2018.

[17] M. Julliere, "Tunneling between ferromagnetic films," *Physics letters A*, vol. 54, no. 3, pp. 225–226, 1975.

[18] X. Zhang, "Theory of spin-dependent tunneling."

[19] Y. Xie, I. Rungger, K. Munira, M. Stamenova, S. Sanvito, and A. W. Ghosh, "Spin transfer torque: A multiscale picture," *Nanomagnetic and Spintronic Devices for Energy-Efficient Memory and Computing*, p. 91, 2016.

[20] Y. Zhang, S. Luo, X. Yang, and C. Yang, "Spin-orbit-torque-induced magnetic domain wall motion in ta/cofe nanowires with sloped perpendicular magnetic anisotropy," *Scientific reports*, vol. 7, no. 1, pp. 1–10, 2017.

[21] X. Li, G. Yu, H. Wu, P. Ong, K. Wong, Q. Hu, F. Ebrahimi, P. Upadhyaya, M. Akyol, N. Kioussis *et al.*, "Thermally stable voltage-controlled perpendicular magnetic anisotropy in mo| cofeb| mgo structures," *Applied Physics Letters*, vol. 107, no. 14, p. 142403, 2015.

[22] Y.-W. Oh, K.-W. Park, and B.-G. Park, "Underlayer dependence of electric field effect on magnetic anisotropy and its volatility in cofeb/mgo structures," *Current Applied Physics*, vol. 19, no. 1, pp. 50–54, 2019.

[23] F. Xue, N. Sato, C. Bi, J. Hu, J. He, and S. X. Wang, "Large voltage control of magnetic anisotropy in cofeb/mgo/ox structures at room temperature," *APL Materials*, vol. 7, no. 10, p. 101112, 2019.

[24] X. Li, K. Fitzell, D. Wu, C. T. Karaba, A. Buditama, G. Yu, K. L. Wong, N. Altieri, C. Grezes, N. Kioussis *et al.*, "Enhancement of voltage-controlled magnetic anisotropy through precise control of mg insertion thickness at cofeb| mgo interface," *Applied Physics Letters*, vol. 110, no. 5, p. 052401, 2017.

[25] Z. Li and S. Zhang, "Domain-wall dynamics driven by adiabatic spin-transfer torques," *Physical Review B*, vol. 70, no. 2, p. 024417, 2004.

[26] S.-W. Jung, W. Kim, T.-D. Lee, K.-J. Lee, and H.-W. Lee, "Current-induced domain wall motion in a nanowire with perpendicular magnetic anisotropy," *Applied Physics Letters*, vol. 92, no. 20, p. 202508, 2008.

[27] S.-M. Seo, K.-W. Kim, J. Ryu, H.-W. Lee, and K.-J. Lee, "Current-induced motion of a transverse magnetic domain wall in the presence of spin hall effect," *Applied Physics Letters*, vol. 101, no. 2, p. 022405, 2012.

[28] G. Consolo, C. Currò, E. Martinez, and G. Valenti, "Mathematical modeling and numerical simulation of domain wall motion in magnetic nanostrips with crystallographic defects," *Applied Mathematical Modelling*, vol. 36, no. 10, pp. 4876–4886, 2012.

[29] J. Franken, "Domain-wall pinning by a local electric-field in a pt/co/alox/pt microwire yuxiang yin august, 2013," 2013.

[30] O. Boulle, G. Malinowski, and M. Kläui, "Current-induced domain wall motion in nanoscale ferromagnetic elements," *Materials Science and Engineering: R: Reports*, vol. 72, no. 9, pp. 159–187, 2011.

[31] E. Martinez, S. Emori, and G. S. Beach, "Current-driven domain wall motion along high perpendicular anisotropy multilayers: The role of the rashba field, the spin hall effect, and the dzyaloshinskii-moriya interaction," *Applied Physics Letters*, vol. 103, no. 7, p. 072406, 2013.

[32] S. A. Nasseri, "Magnetic domain wall motion: Numerical simulation and collective coordinate modeling," 2018.

[33] A. Thiaville, Y. Nakatani, J. Miltat, and N. Vernier, "Domain wall motion by spin-polarized current: a micromagnetic study," *Journal of Applied Physics*, vol. 95, no. 11, pp. 7049–7051, 2004.

[34] A. Thiaville, J. Garcıa, and J. Miltat, "Domain wall dynamics in nanowires," *Journal of Magnetism and Magnetic Materials*, vol. 242, pp. 1061–1063, 2002.

[35] A. Thiaville and Y. Nakatani, "Domain-wall dynamics in nanowiresand nanostrips," *Spin dynamics in confined magnetic structures III*, pp. 161–205, 2006.

[36] S. A. Nasseri, B. Sarma, G. Durin, and C. Serpico, "Analytical modelling of magnetic dw motion," *Physics Procedia*, vol. 75, pp. 974–985, 2015.

[37] A. Mougin, M. Cormier, J. Adam, P. Metaxas, and J. Ferré, "Domain wall mobility, stability and walker breakdown in magnetic nanowires," *EPL (Europhysics Letters)*, vol. 78, no. 5, p. 57007, 2007.

[38] "Magnetic domains," https://ocw.mit.edu/courses/materials-science-and-engineering/3-024-electronic-optical-and-magnetic-properties-of-materials-spring-2013/

lecture-notes/MIT3_024S13_2012lec26.pdf, accessed: 2010-09-30.
[39] "Exchange stiffness," https://journals.aps.org/pr/abstract/10.1103/PhysRev.120.353, accessed: 2010-09-30.
[40] K.-J. Kim, Y. Yoshimura, and T. Ono, "Current-driven magnetic domain wall motion and its real-time detection," *Japanese Journal of Applied Physics*, vol. 56, no. 8, p. 0802A4, 2017.
[41] S.-W. Lee and K.-J. Lee, "Magnetization dynamics driven by angle-dependent spin-orbit spin-transfer torque," *Journal of the Korean Physical Society*, vol. 67, no. 10, pp. 1848–1852, 2015.
[42] E. Martinez, S. Emori, and G. S. Beach, "Current-driven domain wall motion along high perpendicular anisotropy multilayers: The role of the rashba field, the spin hall effect, and the dzyaloshinskii-moriya interaction," *Applied Physics Letters*, vol. 103, no. 7, p. 072406, 2013.
[43] E. Martinez, S. Emori, N. Perez, L. Torres, and G. S. Beach, "Current-driven dynamics of dzyaloshinskii domain walls in the presence of in-plane fields: Full micromagnetic and one-dimensional analysis," *Journal of Applied Physics*, vol. 115, no. 21, p. 213909, 2014.
[44] O. Boulle, S. Rohart, L. Buda-Prejbeanu, E. Jué, I. Miron, S. Pizzini, J. Vogel, G. Gaudin, and A. Thiaville, "Domain wall tilting in the presence of the dzyaloshinskii-moriya interaction in out-of-plane magnetized magnetic nanotracks," *Physical review letters*, vol. 111, no. 21, p. 217203, 2013.
[45] "Mumax3," https://mumax.ugent.be/mumax3-workshop/tutorial4.pdf, accessed: 2010-09-30.
[46] "Runge-kutta(4,5)," https://it.mathworks.com/help/matlab/ref/ode45.html#References, accessed: 2010-09-30.
[47] D. Bhattacharya, S. A. Razavi, H. Wu, B. Dai, K. L. Wang, and J. Atulasimha, "Creation and annihilation of non-volatile fixed magnetic skyrmions using voltage control of magnetic anisotropy," *Nature Electronics*, vol. 3, no. 9, pp. 539–545, 2020.
[48] J. MacLaren, X.-G. Zhang, and W. Butler, "Validity of the julliere model of spin-dependent tunneling," *Physical Review B*, vol. 56, no. 18, p. 11827, 1997.
[49] T. Ouisse, *Electron transport in nanostructures and mesoscopic devices: an introduction*. John Wiley & Sons, 2013.